공학박사 학위논문

Mesenchymal Stem Cell-derived Therapeutic Nanovesicles for Treatment of Central Nervous System Injuries

중간엽 줄기세포 유래 치료용 나노베지클을
이용한 중추신경계 손상 치료

2019년 8월

서울대학교 대학원
화학생물공학부
김 한 영

Abstract

Mesenchymal Stem Cell-derived Therapeutic Nanovesicles for Treatment of Central Nervous System Injuries

Han Young Kim

School of Chemical and Biological Engineering

The Graduate School

Seoul National University

Central nervous system (CNS) injuries such as ischemic stroke, hemorrhage, traumatic brain injury, and spinal cord injury (SCI) are leading cause of long-term disability or death. As a novel tissue regenerative strategy, application of mesenchymal stem cell-derived exosomes (MSC-exosomes) for treatment of CNS injuries has drawn much attention. Owing to their unique properties, MSC-exosomes have been actively studied for treatment of wide variety of diseases including CNS injuries. However, it still remains challenging to

improve the therapeutic outcomes of using exosomes to treat CNS injuries. Very small quantities of exosomes are released from MSC, and MSC-exosomes poorly accumulate in target tissue after systemic administration. Thus, iron oxide nanoparticles (IONP) were introduced to MSC and exosome-mimetic nanovesicles were isolated from those IONP-treated MSC. Treatment of IONP contribute to enhanced expression of therapeutic growth factors in MSC, which are attributed to IONP that are slowly ionized to iron ions which activate the JNK and c-Jun signaling cascades in MSC. Isolated nanovesicles incorporate not only IONP which act as magnet-navigating tool, but also large amount of therapeutic growth factors. In this thesis, *in vivo* systemic delivery of IONP-harboring nanovesicles and their therapeutic effects in CNS lesions are presented.

First, IONP-haboring nanovesicles (NV-IONP) were fabricated by serial extrusion of IONP-treated MSC (MSC-IONP), and systemically delivered to injured spinal cord in mouse SCI model with help of external magnetic field (MF). While intravenous injection of MSC-IONP resulted in severe lung accumulation due to their large size, nano-sized NV-IONP evaded lung entrapment and significantly accumulated in injured spinal cord in presence of MF. NV-IONP accumulated in SCI lesion contributed to blood vessel reconstruction, polarized inflammatory M1 macrophages to anti-inflammatory M2 subtype, attenuated astrogliosis, inhibited neuronal death. Consequently, increased amount of NV-IONP accumulated in injured spinal cord exerted therapeutic effects and improved the spinal cord function, as evaluated by Basso Mouse Scale (BMS) behavioral test.

Second, IONP-incorporated magnetic nanovesicles (MNV) derived from MSC were intravenously administered to rat ischemic stroke models. Animals received middle cerebral artery occlusion (MCAO) to induce ischemic stroke. *In vitro*, MNV exerted enhanced angiogenic, anti-apoptotic, and anti-inflammatory effect in various types of cells, as

compared to control nanovesicles (NV). *In vivo*, we applied magnet helmet which act as an external MF, to rat MCAO models immediately after intravenous injection of MNV. Fluorescence imaging showed successful accumulation of MNV specifically in left hemisphere of brain (ischemic lesion). Quantification of infarcted area at 3 days after treatment revealed that administration of MNV in presence of MF resulted in significant reduction of infarcted area compared to control group. Limb placement test (LPT) also demonstrated that treatment of MNV (MF+) improves the functional behavior of MCAO-received animals.

Thus, we observed that the nanovesicles synthesized from IONP-laden MSC contain both greater amounts of reparative growth factors and IONP which act as a magnet-guided navigation tool toward injured spinal cord or cerebral lesion. These IONP-harboring nanovesicles derived from MSC can serve as excellent therapeutic agent for treatment of CNS injuries, and can be a preferable replacement of conventional MSC or MSC-exosome therapy. This technology can be used in the future for successful therapy of CNS injuries.

Keywords: mesenchymal stem cells, exosomes, nanovesicles, iron oxide nanoparticles, spinal cord injury, ischemic stroke, central nervous system injury

Student Number: 2015-31024

Table of Contents

List of Figures

Abbreviations

hMSC	human mesenchymal stem cells
EVs	extracellular vesicles
ESCRT	endosomal sorting complex required for transport
ILVs	intraluminal vesicles
HUVECs	human umbilical vein endothelial cells
CNS	central nervous system
SCI	spinal cord injury
MSC-exosomes	MSC-derived exosomes
IONP	iron oxide nanoparticles
MSC-IONP	IONP-treated MSC
NV	nanovesicles
NV-IONP	IONP-harboring nanovesicles
MNV	magnetic nanovesicles
CCK-8	cell counting kit-8
RITC	rhodamine-B-isocyanate
TEM	transmission electron microscopy
Ang-1	angiopoietin-1
FGF2	fibroblast growth factor-2
HGF	hepatocyte growth factor
VEGF	vascular endothelial growth factor
TGF-β	transforming growth factor beta
BDNF	brain-derived neurotrophic factor

ICP-MS	inductively coupled plasma mass spectrometry
NTA	nanoparticle tracking analysis
DiO	3,3´-dioctadecyloxacarbocyanine perchlorate
qRT-PCR	quantitative real-time polymerase chain reaction
RT-PCR	reverse transcription polymerase chain reaction
LPS	lipopolysaccharide
FDA	fluorescein diacetate
EB	ethidium bromide
IL	interleukin
MMP	matrix metalloproteinase
PDGF	platelet-derived growth factor
ELISA	enzyme-linked immunosorbent assay
TNF	tumor necrosis factor
Arg-1	arginase-1
MAP2	microtubule Associated Protein 2
GFAP	glial fibrillary acidic protein
NF	neurofilament
vWF	Von Willebrand factor
TUNEL	terminal deoxynucleotidyl transferase dUTP nick end labeling
BMS	Basso mouse scale
LPT	limb placement test
IHC	immunohistochemistry
DAPI	4′,6-diamidino-2-phenylindole
SD rat	Sprague Dawley rat

MCAO	middle cerebral artery occlusion
PBS	phosphate buffered saline
C-Cas-3	cleaved caspase-3
BSA	bovine serum albumin
PFA	paraformaldehyde
GDNF	glial cell-derived neurotrophic factor
NGF	nerve growth factor
NT	Neurotrophin
TTC	triphenyltetrazolium chloride
ANOVA	analysis of variance
rBMDM	rat bone marrow-derived macrophages
MF	magnetic field
ECM	extracellular matrix
RES	reticuloendothelial system

Chapter 1. Research background and objectives

1.1. Challenges and limitations of MSC-based therapeutics

Application of mesenchymal stem cells (MSC) for treatment of wide variety of diseases has gained great attention for recent decades. Owing to its unique properties, a lot of clinical trials using MSC have been accomplished with corresponding clinical outcomes. More than two thousand patients received autologous or allogeneic transplantation of MSC.[1] However, in spite of numerous studies reporting obvious therapeutic effect of MSC in various diseases, growing evidence strongly suggest that MSC do not differentiate to damaged cells and replace them in the lesion. Recent studies support the notion that paracrine factors from MSC including growth factors and extracellular vesicles such as exosomes, play the major role in their therapeutic mechanism of action.[2] Poor survival and fast clearance of transplanted MSC show that the major therapeutic effects of MSC in injured tissue are attributed to secreted factors from MSC. In addition, there are many potential risks of MSC therapy (Figure 1.1) such as possible tumorigenesis, immune response, poor survival, and the route of cell administration. Particularly, challenge associated with MSC-based therapeutic approach is the route of administration for efficient delivery. Local transplantation of MSC increase the risk and side effects such as bleeding and tissue injury due to direct tissue injection.[3] Notably in CNS, direct administration of MSC pose a severe risk of further damage of neurons. The brain is highly susceptible for damage emerging from surgical manipulation.

As an alternative method, intravenous administration can be performed. They are relatively easy to perform and less invasive than local cell delivery approaches. However, there are also serious concerns about systemic administration of stem cells. For instance, non-autologous systemic stem cell transplantation can ignite an instant immune response against the cells causing a loss of the graft or its functional impairment.[4] Importantly, following

intravenous infusion, the majority of MSC are trapped inside the lungs.[5] Pulmonary passage is a major obstacle for systemic intravenous stem cell administration with smaller number of stem cells crossing over to the arterial system and the majority of cells being trapped inside the pulmonary vasculature. Because the main cause of this event is the relatively large diameter of MSC from 10 to 50 μm exceeding the size of pulmonary vessels, recently the extracellular vesicles are introduced to replace MSC for treatment of various diseases.

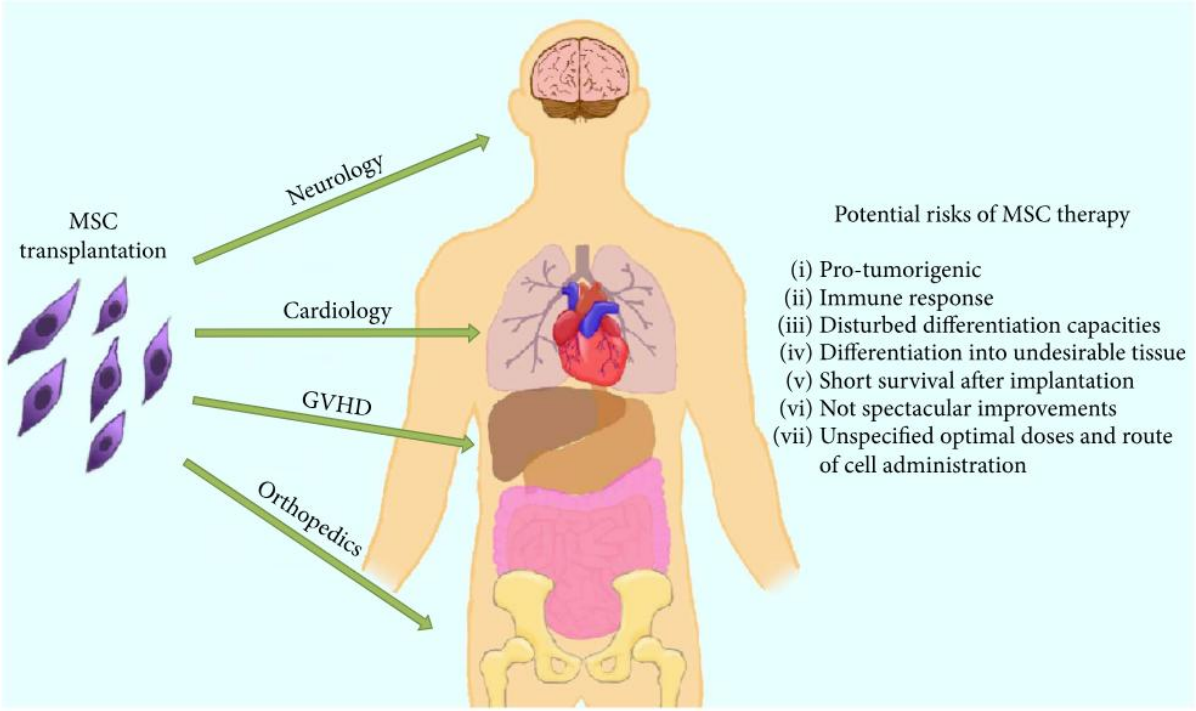

Figure 1.1. The scheme of potential risks of adverse events during MSC transplantation[6]

1.2. Extracellular vesicles

Extracellular vesicles (EVs) are group of cell-derived membrane structures, namely exosomes and microvesicles (Figure 1.2).[7] EVs are produced in donor cell by a budding process, and are involved in various physiological processes including communications between cells. EVs can transmit biological information by directly activating cell surface receptors the recipient cells. They allow cells to exchange mRNAs, miRNAs, proteins, and lipids, and act as signaling vehicles.[8, 9] Therefore, they can regulate recipient cells at a post-transcriptional level. They mainly participate in the homeostasis such as stem cell maintenance, tissue repair, and immune surveillance. Also they have been implicated in tumor progression.[10] EVs can be classified to two main categories, exosomes and microvesicles. Exosomes are membrane vesicles with size of 30-100 nm in diameter.[11] Secretion of exosomes can be differed in various cell types, however their pathological processes are well reported. Exosomes are functional, and can circulate in the whole body and can pass through the body's interstitial space.[12] For biogenesis of exosomes, several mechanisms have been described. One of the reported mechanisms, endosomal sorting complex required for transport (ESCRT) is the best-characterized mechanism. Four protein complexes along with accessory proteins bind future exosome cargoes and for intraluminal vesicles (ILVs). Microvesicles are in size of 50-1000 nm in diameter, or even larger up to 10 μm. In contrast to exosomes, they are generated by outward budding and released to extracellular space.[13] Their surface markers are largely dependent on the composition of the membrane of origin. These EVs including exosomes and microvesicles have been proposed as a means of "cell-free regenerative medicine" for various types of diseases such as cancer, immune disorder, cardiovascular disease, and CNS diseases.[14] Their unique properties of stability, biocompatibility and low immunogenicity have prompted research into their

potential as therapeutic delivery agents.

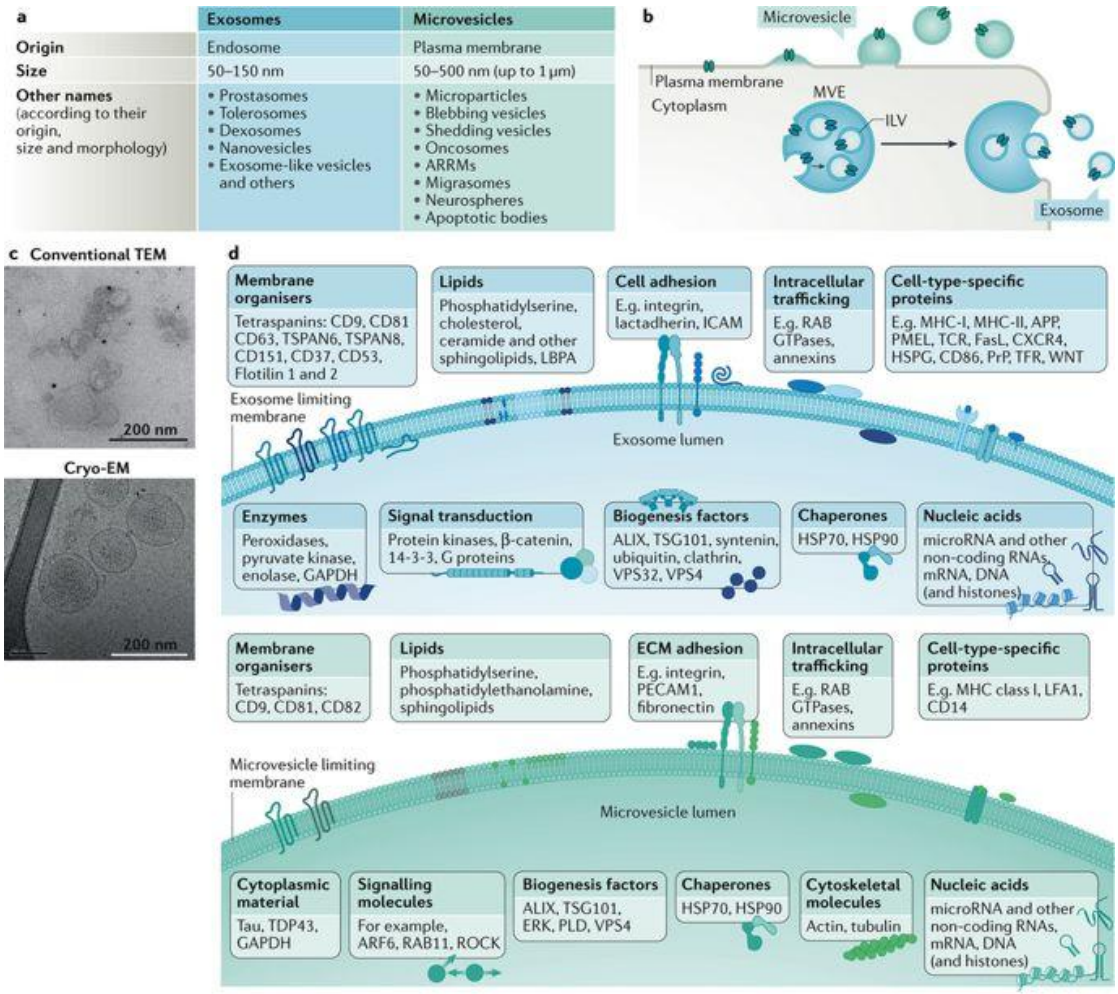

Figure 1.2. Main features of extracellular vesicles[7]

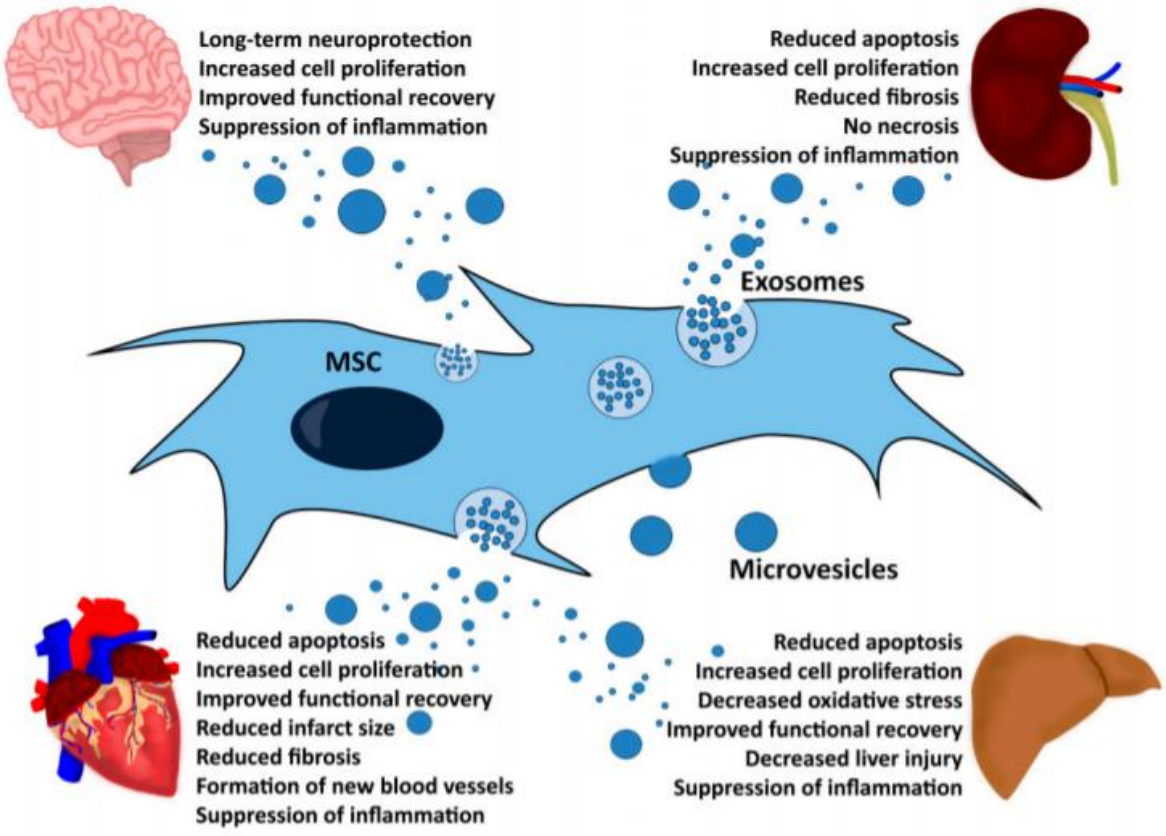

Figure 1.3. Overview of the MSC-EV-mediated therapeutic effects observed in animal models for kidney, heart, liver and brain injuries.[15]

1.3. Therapeutic potency of MSC-derived EVs.

1.3.1. *In vitro* effects on target cells

Previous studies report that exosomes from MSC stimulate proliferation, migration, and angiogenesis of endothelial cells.[16] Treatment of MSC-exosomes stimulated the tube formation of HUVECs. They stimulate Wnt4/β-Catenin pathway which is critically involved in angiogenesis through the modulation of endothelial cell proliferation, migration, vascular sprouting, remodeling, and vascular system maturation.[17] MSC-exosomes also show neuro-protective effect against apoptosis in neuronal-like cells,[18] and prevent cardiomyocyte apoptosis induced by oxidative stress.[19] They inhibit calcification of vascular smooth muscle cells[20] and activation of astrocytes.[21]

In various immune cells, MSC-exosomes exert immunosuppressive effect by eliciting polarization of immune cells from pro-inflammatory to anti-inflammatory subtypes. For instance, MSC-exosomes polarize macrophage from M1 (inflammatory) type to M2 (regenerative) type.[22-24] Maturation of dendritic cells can boost the body's immune response by secreting various inflammatory cytokine, however, treatment of MSC-exosomes can attenuate the dendritic cell maturation and their function.[25] Among various types of T cells, regulatory T cells contribute to tissue regeneration, and MSC-exosomes enhance regulatory T cells production *in vitro*. They increased the polarization of CD4+ T cells to CD4+CD25+FoxP3+ regulatory T cells in the presence of allogeneic dendritic cells.[26]

1.3.2. Pre-clinical studies in various disease models

Recently, MSC-derived exosomes are being examined for their role in MSC-based cellular therapy. First, various groups have confirmed that MSC-derived exosomes exhibit cardio-protective activity.[27-30] Purified exosomes reduced infarct size in a mouse model of myocardial ischemia/reperfusion injury. Also, MSC-exosomes attenuated limb ischemia by promoting angiogenesis in mice.[31] They ameliorated carbon tetrachloride-induced liver fibrosis.[32, 33] In lung studies, the mouse MSC exosomes were effective in improving pulmonary hypertension[34] and edema[35] MSC-exosomes also promoted muscles regeneration[36], and showed immunosuppressive effects on inflammatory arthritis[37] and osteoarthritis[38]

In case of central nervous system (CNS) injuries or diseases, MSC-exosomes showed surprising therapeutic outcomes. In spinal cord injury (SCI), MSC-exosomes successfully suppressed the activation of neurotoxic astrocytes[21], and targeted M2 macrophages[39]. Systemic administration of miR-133b-modifed MSC-exosomes in spinal cord-injured rats preserved neurons, promoted the regeneration of axons, and improved the recovery of hindlimb locomotor function following SCI.[40] In ischemic stroke, intravenous infusion of MSC-exosomes in rat MCAO model resulted in neurogenesis, neurite remodeling, angiogenesis, and improved functional recovery.[41] In subcortical infarct model, MSC-exosomes showed enhanced fiber tract integrity, axonal sprouting, white matter repair markers, and restored white matter integrity.[42] Moreover, intra-arterial administration of MSC-exosomes improved neurite remodeling and brain plasticity.[43] MSC-exosomes also showed their therapeutic effects on traumatic brain injury.[44, 45] In addition to CNS injuries, MSC-exosomes can be potential therapeutic agents for CNS disorders such as Alzheimer's disease[46, 47] and Parkinson's disease.[48] Together, MSC-exosome or furtherly MSC-derived

EVs are multifaceted therapeutic agent for treating wide variety of diseases including CNS diseases (Figure 1.3).[15]

1.4. Exosome-mimetic nanovesicles

Although MSC-exosomes have great potency for treatment of various diseases, their poor production yield is critical hurdle for their further application. Most mammalian cells release relatively low quantities of exosomes and purification of exosomes is cumbersome, which results in a relatively low yield.[49, 50] Particularly for MSC, exosomes are secreted only 1-4 μg from one million cells per day, which indicates that extremely large scale of cell culture is required to sufficiently supply the MSC-exosomes for pre-clinical and clinical studies.[51]

Therefore, bioengineered and bioinspired cell-derived nanocarriers, coined as exosome-mimetic nanovesicles are introduced.[52] By subjecting cells of different origin to serial extrusion through filters with diminishing pore sizes, exosome-mimetic nanovesicles can be fabricated with precise control of their hydrodynamic size. During the extrusion, the lipid bilayer fragments would be planar immediately after membrane fragmentation, but would immediately self-assemble spontaneously into spheres due to the amphiphilic properties of lipids in aqueous solution (Figure 1.4). Because this technology does not require ultracentrifugation of conditioned medium which are used for isolation of natural exosome, production yield of exosome-mimetic nanovesicles are significantly higher than natural exosomes (~100-fold higher).[53] Also, these nanovesicles contain intracellular contents such as cytosolic proteins, RNAs and membrane proteins which are similar to natural exosomes. Furthermore, because the concentrations of intracellular contents in the nanovesicles are higher than natural exosomes, nanovesicles have great therapeutic potency. Thus, therapeutic application of exosome-mimetic nanovesicles were recently reported. Hepatocyte-derived

nanovesicles promoted hepatocyte proliferation and regenerated injured liver *in vivo*,[54] and long nonconding RNA H19-carrying nanovesicles accelerated the healing process of diabetic wounds.[55]

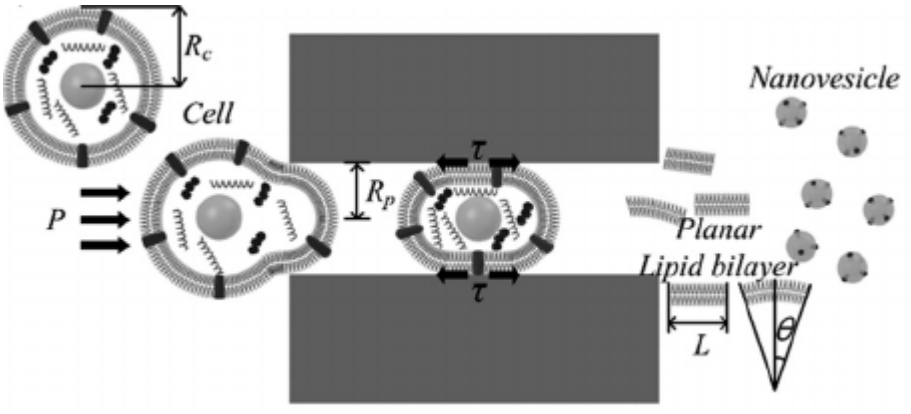

Figure 1.4. Schematic of nanovesicle generation.[53] When a cell passes through a pore, the area of the lipid bilayer is extended by the tension caused by adhesion. The tension makes the lipid bilayer elongate, undergo plastic deformation and possibly fail. The lipid bilayers would be a planar form right after the failure, but should spontaneously self-assemble into hollow spheres.

1.5. Magnetic drug delivery

Despite intensive research endeavors, specific and efficient delivery of nano-sized materials including exosomes to target tissue remain challenging. Uptake of nanoparticles from reticuloendothelial system (RES) causes most on administered nanoparticles to accumulate in liver and spleen.[56] This body's immune system impedes the accumulation of nanoparticles in target tissue. Thus, novel strategies to improve targeting efficacy of intravenously infused nanoparticles should be developed. One promising approach in this context is magnetic delivery. The concept is to tag drug carriers with magnetic nanoparticles such as iron oxide nanoparticles (IONP), after which the drugs can be summoned preferably to target tissues by applying an external MF at the sites. Because IONP are ferromagnetic/superparamagnetic, they can be manipulated by an external MF which can drive them to the target organs. Magnetic modulation of particle movement has proven to be feasible with IONP-incorporated nanoparticles such as silica nanoparticles,[57] graphene oxide,[58] oleosome,[59] RBC membranes,[60] and exosomes.[61] For treatment of stroke, MSC were labeled with IONP and delivered to ischemic lesion with a help of external magnetic field.[62] Application of magnetic field not only increase the accumulation of nanoparticles in the target site, but also enhance the retention of nanoparticles and prevent the wash out by body fluid.[58] In the above-mentioned researches, IONP were incorporated to delivery vehicle by chemical conjugation, which requires multiple chemical reaction steps. Those chemical reactions cannot be applied to MSC-exosomes because its harsh condition (e.g. low pH, high temperature) may denature exosomal proteins. Hence, easier and biocompatible method for incorporating IONP to MSC-exosomes should be developed.

1.6. Research objectives of the thesis

MSC-exosome therapy has emerged as a novel strategy for treatment of CNS injuries. MSC-exosomes have attracted much attention because they are nano-sized, independent to cell viability, and have less possibility of immune rejection. Importantly, MSC-exosomes exert diverse therapeutic effects which are similar or equivalent to their parent cell, MSC. However, their poor production yield from MSC and insufficient organ targeting efficiency are leading cause of therapeutic failure.

In this thesis, we propose the therapeutic application of MSC-derived exosome-mimetic nanovesicles endowed with magnetic properties by introducing IONP. Simple treatment of IONP to MSC significantly enhance the gene and protein expressions of therapeutic growth factors that contribute to reconstruction of blood vessels, protect injured neurons, and polarize inflammatory macrophages to anti-inflammatory subtype. By subjecting IONP-treated MSC to micro- and nano-sized pores, IONP-incorporated exosome-mimetic nanovesicles can be fabricated. The research objectives of this thesis are summarized as follows: 1) Fabrication of IONP-incorporated exosome-mimetic nanovesicles from MSC. 2) Evaluation of angiogenesis, neuro-protection, anti-apoptosis, and anti-inflammatory effect of those nanovesicles in various cells. 3) Enhancing the targeting efficacy of nanovesicles to injured CNS tissue by applying external MF. 4) Ultimately, improving the motor function in CNS-injured animal model

In chapter 3, therapeutic effect of IONP-incorporated nanovesicles (NV-IONP) in SCI mouse model was reported. We investigated the IONP treatment significantly increase

the expressions of therapeutic growth factors in MSC and their derivative NV-IONP can carry those growth factors to target cells. Intravenously *in vivo*, NV-IONP successfully targeted injured spinal cord with help of external MF. As previously reported, MSC were entrapped in lung and failed to target injured spinal cord. Injection of NV-IONP (MF+) resulted in preservation of spinal cord structure. Consequently, recovery of spinal cord function was demonstrated.

In chapter 4, magnetic nanovesicles (MNV), exosome-mimetic nanovesicles loaded with IONP were applied to rat MCAO models of ischemic stroke. *In vitro*, MNV showed significantly enhanced angiogenic effect in endothelial cells, anti-apoptotic and neuro-protective effect in neuron-like cells, and anti-inflammatory effect in LPS-activated macrophages, as compared to control nanovesicles (NV). *In vivo*, intravenously infused MNV (MF+) specifically accumulated in left hemisphere of brain where ischemic stroke was occurred. Accumulated MNV promoted angiogenesis, inhibited neuronal loss, and polarized macrophages to M2 subtype, attenuating inflammatory cytokines. Ultimately, infarcted area of brain markedly decreased in MNV (MF+) injected group.

Chapter 2. Experimental procedures

2.1. Cell culture

Human bone marrow-derived MSCs (Lonza, Switzerland) with passage number from 4 to 6, rat brain cortex astrocytes (Lonza), and Raw 264.7 cells (Korea Cell Line Bank, South Korea) were cultured with high-glucose Dulbecco's Modified Eagle's Medium (DMEM, Gibco, NY) supplemented with 10% (v/v) fetal bovine serum (FBS), penicillin (100 units/mL), and streptomycin (100 μg/mL). HUVECs (Lonza) were cultured in 200PRF (Gibco) supplemented with low serum growth supplement (LSGS, Gibco) consisting of FBS 2% (v/v), hydrocortisone (1 μg/mL), human epidermal growth factor (10 ng/mL), FGF2 (3 ng/mL), and heparin (10 μg/mL). PC12 cells (Paragon Biotech, Baltimore, MD) were cultured in RPMI 1640 (Gibco) supplemented with 7.5% (v/v) FBS, 7.5% (v/v) horse serum, and 1% (v/v) penicillin/streptomycin.

2.2. Preparation and characterization of materials

2.2.1. IONP synthesis

IONP, which were 12 nm in size, were synthesized *via* thermal decomposition of iron oleate complex using a previously reported method.[1] Briefly, the iron oleate complex was prepared by mixing 40 mmol of iron chloride and 120 mmol of sodium oleate into a solution containing 80 ml ethanol, 60 ml distilled water, and 140 ml hexane. The resulting solution was heated up to 70°C for 4 h. The upper organic layer was separated and washed several times with distilled water. After evaporation of the organic solvent, iron oleate complex was obtained for the synthesis of IONP. To synthesize 12 nm-sized IONP, 40 mmol of as-prepared iron oleate complex and 20 mmol of oleic acid was dissolved in 200 g of 1-octadecene. After degassing under vacuum, the mixture was heated up to 320°C with heating rate of 3.3°C/min and aged for 30 min. The resulting product was cooled down to room temperature and washed with ethanol several times.

2.2.2. Fabrication of NV-IONP derived from hMSC-IONP

Forty-eight h after IONP treatment, hMSC-IONP were thoroughly washed 5 times with PBS to remove non-internalized IONPs. After washing, hMSC-IONP were detached from dishes by a cell scraper and centrifuged at 300 g for 5 min. Cell pellet was collected, and the cells were resuspended in PBS at a concentration of 2×10^6 cells/mL. Next, the cell resuspension was sequentially extruded 5 times through 10 μm, 5 μm, 1 μm, and 400 nm pore-sized membrane filters (Whatman, UK) using a mini-extruder (Avanti Polar Lipids, AL). For density-gradient ultracentrifugation, step gradient was formed using iodoxanol (OptiPrep, Axis-shield, UK). Iodoxanol (10% (v/v)) was carefully overlaid on top of 50% (v/v) iodoxanol. Sequentially extruded hMSC-IONP were ultracentrifuged at 100,000 g for 2 h. Subsequently, the brown-colored layer between 50% and 10% iodoxanol was harvested and ultracentrifuged again at 100,000 g for 2 h. After formation of the brown-colored pellet by ultracentrifugation, the pellet was resuspended in PBS, and neodymium magnet (diameter: 5 mm, thickness: 2 mm) was applied at the bottom of the tube to isolate NV-IONP. Synthesized NV-IONP were finally filtered through 0.22 μm syringe-filter (Merck Millipore). Meanwhile, NV were fabricated from untreated hMSC with the same protocol except for the magnetic separation. The protein and iron content in each fraction obtained after the ultracentrifugation and magnetic separation was determined by the Bradford assay using the Bradford reagent (Sigma, MO), and ICP-MS (ICPS8100, Shimadzu, Japan), respectively. Isolated NV and NV-IONP were aliquoted and stored in -70°C until needed.

2.2.3. Characterziation of NV-IONP

The morphology of NV and NV-IONP was visualized using TEM. Iron content was quantified by ICP-MS. To confirm the incorporation of IONP within NV-IONP, RITC-labeled IONPs and DiO-labeled NV were visualized using confocal fluorescence microscopy (LSM710, Carl Zeiss) installed at the National Center for Inter-university Research Facilities (NCIRF) at Seoul National University. In addition, Raw 264.7 cells treated with NV and NV-IONP were visualized after 16 h of treatment. The size distribution of NV and NV-IONP was determined by Nanoparticle Tracking Analysis (NTA) system using Nanosight (LM10, Malvern, UK). RNA or proteins carried by NV and NV-IONP were extracted with either TRIzol® (Life Technologies, CA) or Cell Lysis Buffer® (Cell Signaling Technology, MA) according to the manufacturer's instructions. To evaluate the expression of genes encoding hMSC surface markers (i.e., $CD29^{+}$, $CD34^{-}$, $CD44^{+}$) in NV and NV-IONP, RT-PCR was carried out. The primers used for RT-PCR are listed in Table S1. Amplified cDNA was mixed with loading buffer and loaded on 1.5% agarose gel, followed by gel electrophoresis under 75V for 30 min. To detect exosome markers (i.e., CD9 and CD63) in NV and NV-IONP, extracted proteins were analyzed with western blot analysis using primary antibodies against CD9 and CD63 (Abcam, UK).

2.3. *In vitro* assays

2.3.1. IONP uptake by hMSC

To evaluate the cytotoxicity of IONP against hMSC, IONPs were added to the culture medium at concentrations of 5, 10, 20, 40, and 80 μg/mL. The cell viability of IONP-treated hMSC was determined by the cell counting kit-8 (CCK-8) assay. Based on the result from the CCK-8 assay, hMSCs were treated with IONPs at a concentration of 40 μg/mL in the following experiments. After 16 h of IONP treatment, hMSCs were extensively washed 3 times with PBS. For detection of internalized IONPs, hMSC-IONP were visualized using TEM (LIBRA 120, Carl Zeiss, Germany). Internalization of RITC-labeled IONPs was observed with confocal fluorescence microscopy (SP8X, Leica, Germany). For the assessment of time-dependent gene expression, after internalization of IONPs by hMSCs, RNA was isolated from hMSC-IONP at 24 h and 48 h after the IONP treatment. Proteins were extracted from the cell lysate 48 h after IONP treatment for western blot analysis.

2.3.2. Angiogenic effect of NV-IONP

To investigate the angiogenic effect of NV-IONP, tube formation assay, proliferation assay, and cell migration assay were carried out using HUVECs treated with IONP (0.68 μg/mL, iron content equal to that of NV-IONP), NV (40 μg/mL), or NV-IONP (40 μg/mL). For tube formation assay, HUVECs were stained with DiI for 30 min, washed 3 times with PBS, and seeded on Matrigel (Corning, NY)-coated 24-well plates. IONP, NV, or NV-IONP were added into the culture. After 8 h of incubation, the capillary tube formation of HUVECs was examined with fluorescence microscopy. The number of tubes and tube junctions formed were quantified from more than 5 images taken from each well (n = 3 well per group). Cell proliferation assay was carried out by determining relative cell number in culture for 72 h after treatment of IONP, NV, or NV-IONP. Relative cell number was determined by CCK-8 assay. For cell migration assay, HUVECs seeded on 6-well plates were scratched with a plastic pipette tip and incubated with IONP, NV, or NV-IONP in LSGS-free 200PRF medium. Microscopic images were captured at 0 h and 24 h, and analyzed using ImageJ software (n = 3 well per group). For western blot analysis of signaling cascades in HUVECs, proteins were extracted from cells at 16 h after treatment of IONP, NV, or NV-IONP.

2.3.3. Evaluation of anti-apoptosis in neuronal cells.

To investigate the neuroprotective and anti-apoptotic effects of NV-IONP, PC12 cells were treated with IONP (680 ng/mL), NV (40 μg/mL), or NV-IONP (40 μg/mL) for 16 h. After PBS washing, LPS (1 μg /mL) was added, and subsequently the PC12 cells were incubated under hypoxic condition (2% O_2) for 24 h. Next, cells were stained with fluorescein diacetate (FDA) and ethidium bromide (EB) to detect live cells and dead cells. The cell viability was quantified through the CCK-8 assay, and RNA was extracted for further analysis. The expression of genes encoding Bcl-2 and Bax were evaluated using qRT-PCR.

2.3.4. Assessment of astrocyte modulation

Rat brain cortex-derived astrocytes were seeded on 6-well plates and treated with IONP (680 ng/mL), NV (40 μg/mL), or NV-IONP (40 μg/mL) for 16 h. Astrocytes were extensively washed with PBS, and fresh DMEM was added. After 48 h, the conditioned medium was collected and RNA from astrocytes was isolated for further analysis. Gene expression and growth factors (Ang-1, FGF2, HGF, VEGF, BDNF) secreted from astrocytes were evaluated using qRT-PCR and ELISA, respectively.

2.3.5. Macrophage polarization

2.3.5.1 Preparation of rBMDM

To isolate rat bone marrow-derived macrophages (BMDMs), bone marrow was collected from the femurs of five-week-old male Sprague Dawley (SD) rat (Koatech., Gyunggi-do, Korea), as described previously.[63] First, hind limbs of animals were collected and muscle tissue was removed to expose femur bones. Bones were then flushed with PBS using syringes to isolate bone marrow cells. After centrifugation, collected bone marrow cells were differentiated to macrophages for 4 days in differentiation medium composed of high-glucose DMEM supplemented with 30% (v/v) L929 cell-conditioned medium, 15% (v/v) FBS, 5% (v/v) horse serum, and 1% (v/v) penicillin/streptomycin. Conditioned medium from L929 cells was prepared by growing cells in high-glucose DMEM containing 10% (v/v) FBS, and 1% (v/v) penicillin/streptomycin. After 4 days of incubation, macrophage differentiation medium was discarded and adherent BMDMs were harvested using cell scrapers.

2.3.5.2 Evaluation of macrophage phenotype

To evaluate the macrophage polarization, rBMDM or Raw 264.7 cells were seeded on 6-well plates, and treated with LPS (200 ng/mL) for 24 h. After removal of LPS, cells were treated with IONP (680 ng/mL), NV (40 μg/mL), or NV-IONP (40 μg/mL) for 16 h, followed by extensive washing with PBS and addition of fresh DMEM. After 48 h, the conditioned medium was collected and RNA was isolated from rBMDM or Raw 264.7 cells. Expression of pro-inflammatory cytokines (M1), anti-inflammatory cytokines (M2), and angiogenesis-related factors, and that of the respective genes were quantified using qRT-PCR, ELISA, and protein array.

2.3.6. qRT-PCR, western Blot, ELISA, and protein array assay

Gene expression was assessed using FAST SYBR Green PCR master mix (Applied Biosystems) in StepOnePlus real-time PCR system (Applied Biosystems, CA) with amplification with 40 cycles at 94℃ for 3 s and at 60℃ for 30 s. For western blot analysis, total protein concentration of cells or NV lysates were determined by Bradford assay. Lysates were mixed with NuPAGE® LDS sample buffer (Life Technologies, CA) and loaded on 10% (w/v) SDS-polyacrylamide gel. After 100 min of electrophoresis at 80V, proteins were transferred to Immobilon-P membrane (Millipore Corp., Bedford, MA) using Trans-Blot® SD Semi-Dry Electrophoretic Transfer Cell (Bio-Rad, CA) for 50 min at 20V. Subsequently, the membrane was blocked with 5% skim milk for 2 h, and probed with primary antibodies for 16 h at 4℃. Next, captured proteins were conjugated with horseradish peroxidase-conjugated secondary antibodies (Abcam, Cambridge, UK) for 1 h in room temperature. Blots were developed using chemiluminescence detection system (GE healthcare, Buckinghamshire, UK). To detect proteins or cytokines secreted by cells in conditioned medium, ELISA was performed according to the manufacturer's instructions, and protein array assay was performed using Proteome Profiler® (R&D systems, MN).

2.4. *In vivo* studies

2.4.1. Experimental animal models

2.4.1.1. SCI models

Eight-week-old C57BL/6 (20 ~ 25 g, Orient Bio Inc, Korea) mice were used in this study. Animals were anesthetized with a mixture of Zoletil® (50 mg/kg, Virbac Laboratories, France) and Rompun® (10 mg/kg, Bayer, Korea). A laminectomy was performed to expose a T10 ~ T11 thoracic area of spinal cord under a surgical microscope. Allis clamps were used to stabilize the vertebral column at T8 and T12 spinous processes. A 20 G metal impounder was then gently placed on T10 ~ T11 dura for 1 min. Following compression injury for 1 min, the injury site was closed by suturing the muscle, fascia, and skin. Animals were kept on a heating pad. Bladders were emptied manually twice daily till the bladder reflex returned to normal. All animal experiments were carried out according to the approved protocol by the Institutional Animal Care and Use Committee (IACUC) of CHA University (IACUC170096).

2.4.1.2. MCAO ischemia-reperfusion models

Nine-week-old SD rats (male, 250-300 g) purchased from Koatech, were used in all the experiments. All the experimental procedures were performed according to the guidelines and with the approval of the Institutional Animal Care and Use Committee of the Biomedical Research Institute of Seoul National University Hospital. The focal ischemia-reperfusion model of SD rats was developed using left transient middle cerebral artery occlusion (MCAO) with the intra-arterial thread occlusion method as described in previous studies. After 60 minutes of left MCAO, the thread was carefully removed for reperfusion, and the wound was sutured.[64-67] Body temperature was maintained at 37±0.5 °C during procedures using a heating blanket while rectally monitoring the temperature.

2.4.2. *In vivo* biodistribution

2.4.2.1. Biodistribution of MSC-IONP and NV-IONP in SCI mouse model

To investigate the biodistribution of intravenously injected hMSC-IONP and NV-IONP, *ex vivo* fluorescence imaging was carried out. hMSC-IONP and NV-IONP were fluorescently-labeled with VivoTrack 680 (Perkin Elmer, MA). Next, hMSC-IONP (5×10^5 cells) and NV-IONP (40 μg) were dispersed in 100 μL PBS and intravenously injected into the right retro-orbital sinus of mice with or without a neodymium magnet (3 mice per group). The injection was performed 1 h after SCI. For magnetic guidance, neodymium magnet was strapped above the skin of SCI region using Tegaderm® and Coban® self-adherent strap (3M, MN). Each mouse was kept in a separated animal cage to avoid the interference by the magnet on other animals. After 24 h, mice were sacrificed and major organs including spinal cord were removed. Collected organs were observed and analyzed using eXplore Optix System (Advanced Research Technologies Inc., Canada). For the histological analysis, isolated spinal cord tissues were embedded in paraffin, and longitudinal sections of 10 μm thickness were prepared. Spinal cord tissue sections were counter-stained with DAPI and visualized by confocal fluorescence microscopy. For iron detection, Prussian blue staining was carried out and nuclear fast red solution was used for counter-staining.

2.4.2.2. MNV biodistribution in MCAO rat model

MCAO-induced rats (n=3 for each group) were sacrificed at 24 h after intravenous injection of VivoTrack 680-labeled NV-IONP (200 μg). The distribution of the injected MNV in brain, liver, lung, spleen, and kidney were evaluated using epi-illumination fluorescence imaging system (IVIS Lumina II, PerkinElmer, MA, USA). For the histological analysis, isolated ischemic brain tissues were embedded in paraffin, and coronal sections of 10 μm thickness were prepared. Prussian blue staining was carried out to visualize irons, and nuclear fast red solution was used for counter-staining.

2.4.3. Animal group assignment

2.4.3.1. SCI mouse model

The spinal cord-injured mice were randomly assigned into five groups. In the sham group, mice were subjected to only laminotomy. In the PBS group, SCI was induced in mice, and they were injected with 100 μL PBS. In the NV group, SCI was induced in mice, and they were injected with 40 μg of NV in 100 μL PBS. In the NV-IONP group, SCI was induced in mice, and they were injected with 40 μg of NV-IONP in 100 μL PBS, in the presence or absence of a magnet strapped on the mice. The injury area was well defined after injury and neodymium magnet was placed on the injury site with the help of Tegaderm® film, followed by addition of one layer of Coban® self-adherent strap. To avoid the interference by the magnet on other animals, each mouse was kept in a separated animal cage. The injection was performed 1 h after injury. After 24 hours, the position of magnet was confirmed before removal.

2.4.3.2. MCAO rat model

The experimental models were categorized into three groups: transient MCAO with phosphate-buffered saline (PBS), transient MCAO with NV-IONP injection [NV-IONP (MF-)], and magnet helmeted transient MCAO with NV-IONP injection [NV-IONP (MF+)]. Immediately after the reperfusion, NV-IONP (200 μg in 300 uL PBS) or 300 uL PBS were injected into the tail vein. In NV-IONP (MF+) group, magnet helmet was applied for 3 days after injection of NV-IONP to evaluate the effect of the targeted delivery. The magnet helmet was made from ProJet using a 3D printer embedded with a neodymium magnet (5 × 10 × 2 mm, 0.32T) on the left.

2.4.4. Therapeutic mechanism of NV-IONP

2.4.4.1. Evaluation of apoptosis and fibrotic scar formation in SCI model

For evaluation of apoptotic cells, TUNEL assay was performed with tissue sections from injured spinal cord 7 days after injury. To assess the spinal cord structure and fibrotic tissue after injections, spinal cord tissue was extracted at 28 days after injury. Digital images of isolated spinal cord tissue were captured, and the tissues were embedded in paraffin. Transverse sections of the lesion core was prepared, and fibrotic tissue area was evaluated by Masson's trichrome staining.

2.4.4.2. Immunohistochemistry and western blot analysis of extracted spinal cord

At 1, 7, 14 and 28 days after SCI, mice were sacrificed. For immunohistochemistry, the spinal cord at the compression site was retrieved, immersed in 4% paraformaldehyde for one day, embedded in paraffin, sectioned at 5 or 10 μm thickness, dewaxed, and stained with primary antibodies against vWF, Arg-1, CD68, TNF-α, GFAP, NF, laminin, and BDNF. Secondary antibodies used were goat anti-rabbit Alexa Fluor® 568 and goat anti-mouse Alexa Fluor® 568 (Abcam). Sections were counterstained with DAPI, fixed, and examined using a fluorescence microscope. For quantification of vWF-positive vascular density, vWF-positive area relative to DAPI-positive area was measured using ImageJ software. For western blot analysis, retrieved spinal cord tissues were homogenized (D1000, Benchmark Scientific, NJ) in the presence of 300 μL lysis buffer, incubated on ice for 1 h, and centrifuged at 14,000 g for 30 min. After centrifugation, the protein concentration of the isolated supernatant was measured by the Bradford assay, and western blot was performed as previously described for *in vitro* analysis, with primary antibodies for Ang-1, VEGF, IL-6, IL-1β, TNF-α, C-Cas-3, GFAP, and MAP-2.

2.4.4.3. Western blot and IHC analysis of extracted brain tissue of MCAO model

SD rats (n = 3 for each group) were sacrificed and transcardially perfused 3 days after the transient MCAO. For western blot analysis, retrieved brain tissues were homogenized (D1000, Benchmark Scientific, NJ) in the presence of 300 μL lysis buffer, incubated on ice for 1 h, and centrifuged at 14,000 g for 30 min. After centrifugation, the protein concentration of the isolated supernatant was measured by the Bradford assay, and western blot was performed with primary antibodies against iNOS, nNOS, Arg-1, and MAP2 (Abcam, CA). For IHC, the coronal cryosections (30-um thickness) were obtained from the brain tissue and mounted onto silane-coated slides (Dako, Glostrup, Denmark). The sections were blocked by incubating with 0.5% bovine serum albumin/0.3% Triton-X and 10% normal serum in PBS for 1 h. Additionally, they were incubated with primary antibody at 4 ℃ for 16 h. After washing, the sections were incubated with a fluorescent-dye conjugated secondary antibody, including monoclonal antibody against IL-1β, Arg-1, vWF, MAP2 (Abcam, CA), Ox-6, and MPO (Santa Cruz Biotech, Santa Cruz, CA). The primary antibody was omitted as a negative control of staining. The microscopic analyses were performed using a Leica DM5500B microscope (Leica Microsystems) and LAS-AF image acquisition software (Leica Microsystems, Rijswijk, Netherlands).

2.4.5. Evaluation of therapeutic effects from accumulated NV-IONP

2.4.5.1. Hindlimb locomotor score of SCI model

Hindlimb motor functions of 50 mice were evaluated on 1, 7, 14, 21 and 28 days following SCI and treatment, by scoring according to the open-field BMS (10 mice per group). The scores range from 0 point (no ankle movement) to 9 points (complete functional recovery).[2] The hindlimb locomotor score was evaluated by two experienced investigators who were blinded to the experimental animal groups.

2.4.5.2. Measurement of cerebral infarct volume of MCAO model

The rats were sacrificed 3 days after transient left MCAO by cardiac perfusion with saline, followed by 4% paraformaldehyde in 0.1 M PBS. The brains were removed and cut into 30-μm thickness coronal sections and mounted on glass slides. Infarct volume was evaluated on eight sections collected for TTC (2,3,5-triphenyltetrazolium chloride) staining (n = 11 for each group), which covered the entire region treated with MCAO. To measure the infarct volume, the ImageJ program (National Institutes of Health, Bethesda, MD) was employed to analyze images of TTC stained sections.

2.4.5.3. Functional behavior test of MCAO model

For evaluating functional recovery after MNV administration, a forelimb placing test was conducted at 1 , 3, 7, 14, 21, and 28 days after transient MCAO by two investigators blinded to the groups (n = 6 for each group).[64, 68] It consisted of two limb-placing tasks for assessing the sensorimotor integration of the forelimb and hindlimb by responses to tactile and proprioceptive stimulation of rats. The following scores were used to detect impairment of the forelimb and hindlimb: 0 points, when the rat performed normally; 1 point, if the rat performed with a delay of more than 2 s and/or incompletely; and 2 points, if the rat did not perform the task. Both sides of the body were tested. Rats having a score of 8 indicated the most severe neurological symptom, and conversely, rats with 0 points were normal.

2.5. Statistical analysis

In vitro and *in vivo* data are quantitatively shown as mean ± SD. *p*-values were calculated by one-way analysis of variance (ANOVA) or two-way ANOVA with the Tukey's significant difference post hoc test using the GraphPad Prism software. A value of $p < 0.05$ was considered as statistically significant.

Chapter 3. Therapeutic efficacy-potentiated and diseased organ-targeting nanovesicles derived from mesenchymal stem cells for spinal cord injury treatment

3.1. Introduction

In spite of numerous studies reporting on human mesenchymal stem cell (hMSC)-based therapies, the therapeutic mechanism has not been clear until recently. An increasing number of reports has revealed that the therapeutic effects of hMSCs are not by the replacement of damaged cells or differentiation of implanted hMSCs. Majority of injected cells were washed out or showed poor survival rate in the lesion. Thus, ascending evidence supports the notion that hMSC plays role in a paracrine manner,[69, 70] in which hMSC-derived exosomes (hMSC-exosomes) are major component.[71, 72] As a type of extracellular vesicles, exosomes contain various proteins, DNAs, mRNAs, and microRNAs that have originated from the parent cells.[73] Exosomes are involved in cell-to-cell communication during physiological processes, and they transmit specific information from parent cells to recipient cells, thereby influencing the genotype or phenotype of recipient cells.[74] Based on therapeutic effects of hMSCs, hMSC-exosomes have recently emerged as a new therapeutic platform for cell-free therapeutics and currently being tested in animal studies[75, 76] and human clinical trials[77] for treatment of various diseases. In animal studies, hMSC-exosomes improved cardiac function in animal models of myocardial infarction,[27, 78] and promoted angiogenesis, attenuated fibrosis, and enhanced muscle regeneration in mouse model of muscle injury.[36] hMSC-exosomes can also exert anti-inflammatory effects by inducing macrophage polarization.[22] These reports demonstrate that hMSC-exosomes exert similar or equivalent therapeutic functions compared to hMSCs. Furthermore, hMSC-exosomes provide several advantages over hMSCs in that hMSC-exosomes do not have a low grafting efficiency as possessed by implanted hMSCs, they have a lower possibility of immune-rejection, and they can avoid the entrapment in pulmonary capillaries which is the major barrier for systemic administration of hMSCs.[5]

The complexity of pathology in spinal cord injury (SCI), including axonal loss, inflammation, glial scar formation, and blood vessel disruption, suggests that mono-therapy may be inadequate for the treatment of SCI.[79, 80] Recently, hMSC therapy has been suggested as a favored approach for the treatment of SCI,[81, 82] as hMSCs can secrete multifactorial therapeutic factors for neuroprotection, angiogenesis, and immunomodulation. However, the direct implantation of hMSCs to an injured spinal cord is more invasive as compared to systemic administration, and thus it limits clinical translation for the treatment of SCI.[83] Moreover, implanted hMSCs show poor survival rate, and hMSCs do not differentiate into neurons in injured spinal cord.[84] These issues suggest that hMSC-exosomes may be an adequate therapeutic agent for the treatment of SCI. As various therapeutic growth factors and their mRNAs are present in hMSC-exosomes,[85-87] they have an outstanding ability to repair tissue as compared to exosomes derived from other cell types such as fibroblasts.[88, 89] Additionally, several recent studies reported that hMSC-exosomes also show therapeutic effects for central nervous system (CNS) diseases[90, 91] including SCI.[92]

Although hMSC-exosome therapy has advantages over hMSC therapy, hMSC-exosome technology should be further improved for clinical application. hMSCs form only a small amount of exosomes (1–4 μg exosome proteins from 10^6 cells per day).[51] Therefore, long-term cell culture and large number of hMSCs are required to produce sufficient amount of hMSC-exosomes for clinical applications. However, the MSCs at the late passage exhibit significantly reduced gene and protein expression of growth factors,[93] which would reduce the quantity of therapeutic growth factors and their mRNAs in the secreted exosomes. Therefore in this study, rather than using naturally secreted hMSC-exosomes, we utilized exosome-mimetic nanovesicles derived from hMSCs for treatment of SCI. Extracellular nanovesicles that mimic exosomes, can be generated by subjecting cells to serial extrusion.[52] The extracellular nanovesicles show significantly higher production yield and contain a

greater amount of mRNAs and proteins than exosomes.[53] Also, the nanovesicles can deliver the contained mRNAs and proteins to target cells, which is identical to the characteristics of exosomes. However, despite those several advantages of nanovesicles over exosomes, both exosomes and nanovesicles show poor accumulation in target organ after systemic administration *in vivo*.[94-96] In this context, to increase the *in vivo* targeting efficiency of hMSC-derived nanovesicles, we fabricated iron oxide nanoparticle (IONP)-harboring exosome-mimetic nanovesicles (NV-IONP, ~150 nm) through extrusion of IONP-treated hMSC (hMSC-IONP). The IONP, which is ionized and assimilated *in vivo* over a long period of time[97, 98] and thus FDA-approved for clinical usage (e.g. ferumoxytol), was used as a navigation tool for NV-IONP *via* external magnetic guidance (Figure 3.1A). Importantly, we found the IONP treatment significantly enhanced the gene and protein expression of therapeutic growth factors in hMSCs. Thus, NV-IONP that are derived from hMSC-IONP, contained both IONPs and augmented amounts of therapeutic growth factors as compared to nanovesicles (NV) that are derived from untreated hMSCs. Moreover, NV-IONP could efficiently deliver those increased amounts of growth factors to injured spinal cord with the help of magnetic guidance for SCI therapy. In addition, we evaluated the therapeutic mechanisms of NV-IONP for SCI therapy (Figure 3.1B), including angiogenesis of endothelial cells, anti-apoptosis of neuronal cells, stimulation of therapeutic growth factor secretion from astrocytes, and anti-inflammation by polarization of macrophages from inflammatory M1 to tissue-reparative M2 phenotype. Finally, we observed that the intravenous injection of NV-IONP with magnetic guidance has successfully improved the tissue repair and functional recovery in spinal cord-injured mice.

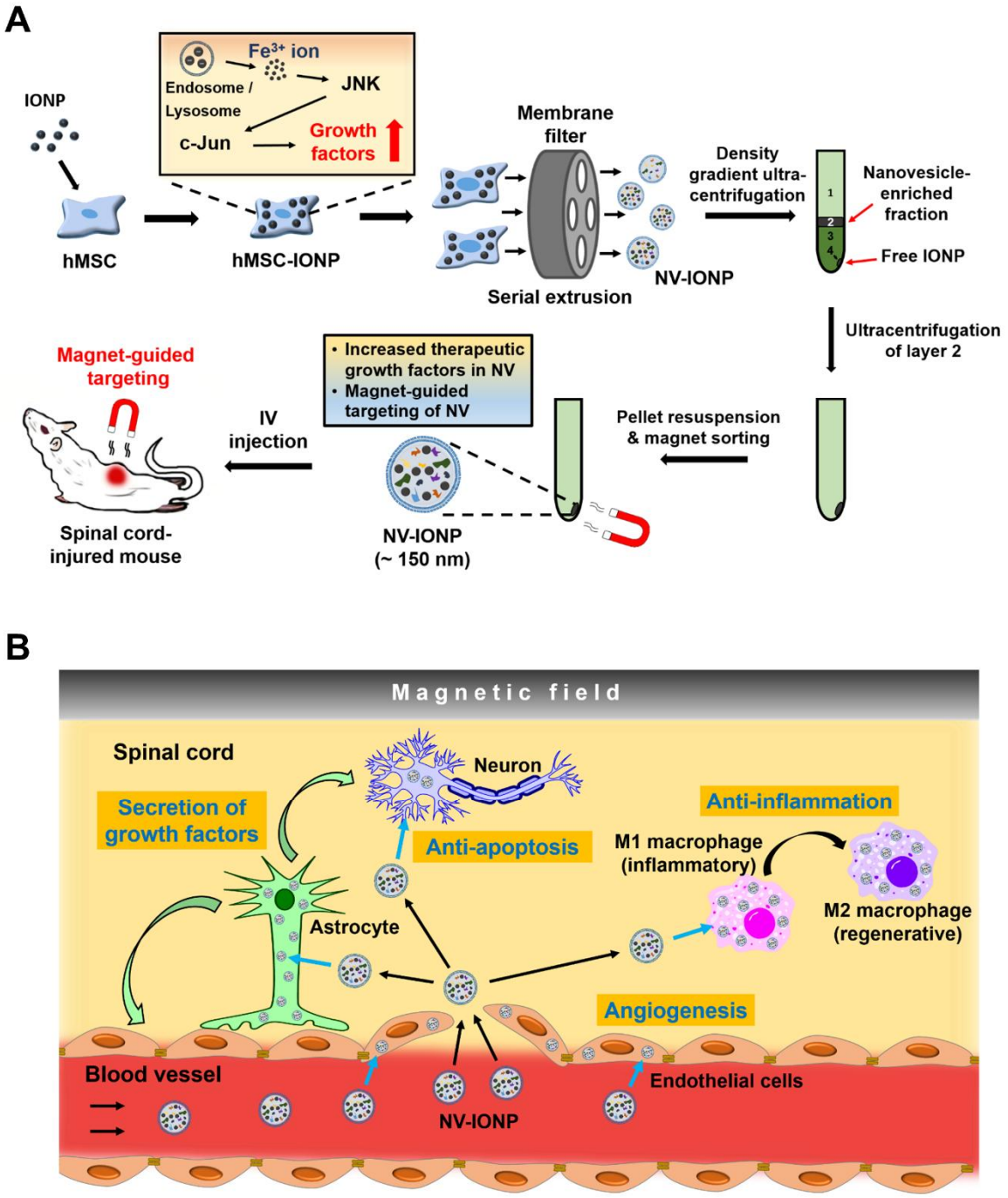

Figure 3.1. Schematic illustration of the preparation of IONP-incorporated exosome-mimetic nanovesicle followed by magnet-guided targeting of spinal cord, and therapeutic effects on various cells in injured spinal cord

3.1. Result and discussion

3.2.1. IONP internalization into hMSCs and up-regulation of growth factors

We initially investigated the effects of IONP internalization on the expression of angiogenic, anti-apoptotic, anti-inflammatory, and neurotrophic factors in hMSCs (Figure 3.2). Despite the high responsiveness to the external magnetic field, IONPs with large hydrodynamic size show low colloidal stability in the presence of serum and therefore easily form aggregates.[99] The resulting aggregates are hardly internalized into hMSCs. Therefore, PEG-ylated superparamagnetic IONPs with a spherical shape and a size of approximately 12 nm were utilized in this study to maximize the magnetization and maintain their colloidal stability in serum. Transmission electron microscopy (TEM) revealed the spherical shape and colloidal stability of the dispersed IONPs in the serum containing culture medium, and their internalization into hMSCs (Figure 3.2A). IONPs showed no aggregation after dispersion in serum-containing culture medium. After internalization, agglomerated IONP clusters (red arrows) were observed in hMSC endosomes, revealing the nanoparticle uptake mechanism[100] and indicating that IONPs will be encapsulated in nanovesicles with a clustered conformation. To examine the cytotoxicity of IONPs against hMSCs, hMSCs were treated with increasing doses of IONPs for 16 h. The CCK-8 assay results showed that up to 80 μg/mL dose treatment showed no observable cytotoxicity of IONPs on hMSCs (Figure 3.2B). IONPs were labeled with rhodamine-B-isothiocyanate (RITC) to visualize internalized IONPs in hMSCs using fluorescence microscopy. IONP-treated hMSCs (hMSC-IONP) emitted strong fluorescence signal from cell cytosol, while untreated hMSCs showed no signal (Figure 3.2C). Next, we examined whether the internalized IONPs influenced the expression of growth factors and their genes in hMSC-IONP. Quantitative reverse transcription-polymerase chain

reaction (qRT-PCR) assay was carried out to evaluate the expression of angiogenic (Ang-1, FGF2, HGF, and VEGF), anti-apoptotic (FGF2, HGF, and VEGF), neurotrophic (BDNF), and anti-inflammatory (TGF-β1) factors in hMSC-IONP at 24 h and 48 h after removal of the IONP-containing culture medium (Figure 3.2D). Importantly, it was observed that the respective genes encoding these factors were significantly up-regulated in a time-dependent manner compared to those in untreated hMSCs. Next, we investigated the intracellular signaling mechanisms underlying the growth factor up-regulation. Our previous report showed that internalized IONPs can be slowly ionized to iron ions and these ions activate JNK and c-Jun signaling cascades.[101] In brief, relatively low pH in the intracellular endosome, where internalized IONPs localize, induces partial ionization of the IONPs into iron ions. These iron ions induce phosphorylation of JNK and c-Jun, a pathway that is strongly associated with the expression of growth factors[102-104] (Figure 3.2E). Based on the qRT-PCR data shown in Figure 2D, hMSC-IONP at 48 h post-treatment were selected for western blot analysis (Figure 3.2F). The results revealed a significant up-regulation in phosphorylated forms of both JNK (p-JNK) and c-Jun (p-c-Jun) relative to the non-phosphorylated form in hMSC-IONP. Therefore, the stimulation of p-JNK and p-c-Jun by iron ions released into the cytoplasm through IONP ionization provides a plausible mechanism by which the therapeutic growth factor expression was significantly enhanced in hMSC-IONP.

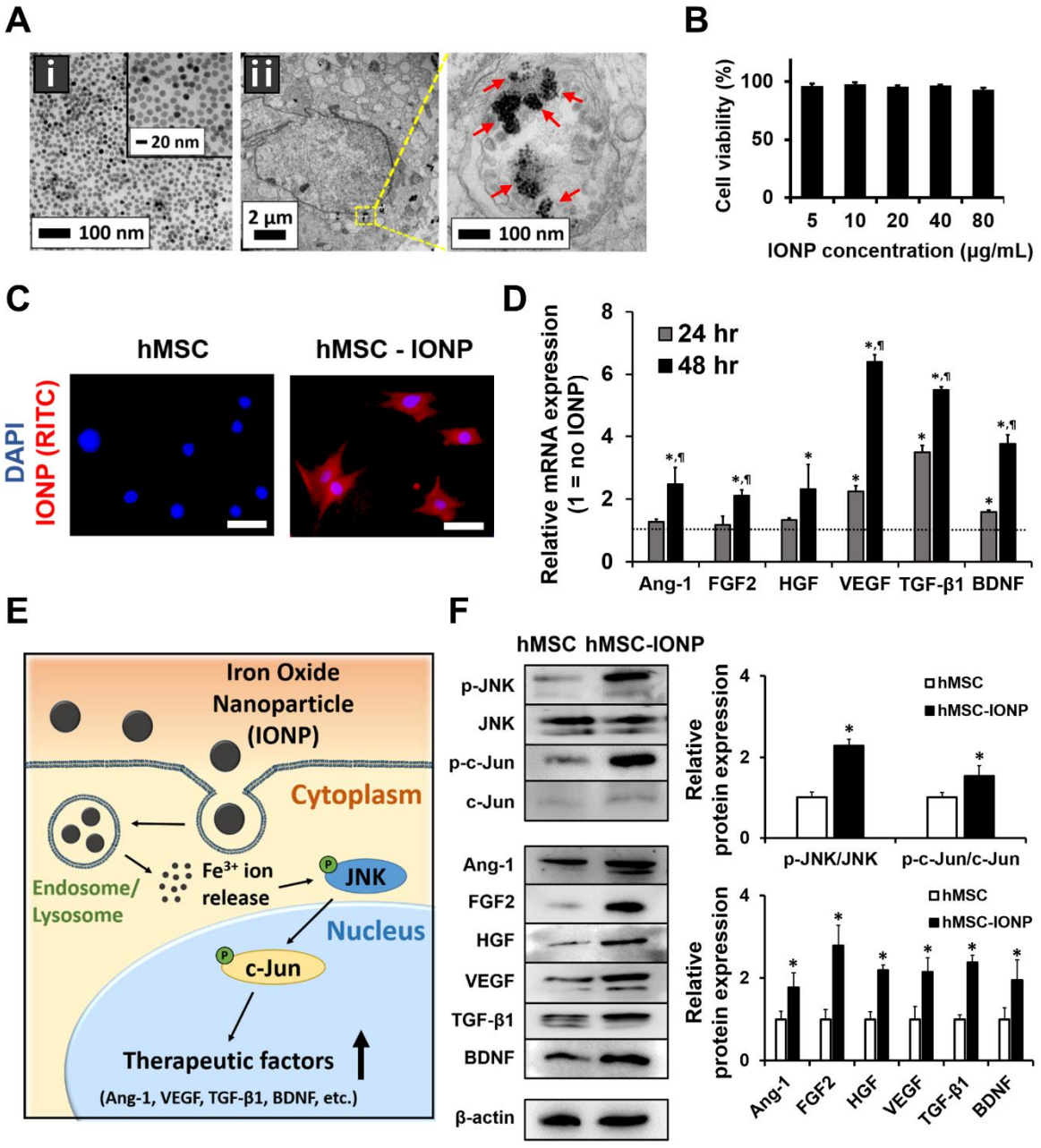

Figure 3.2. Up-regulation of angiogenic, anti-apoptotic, anti-inflammatory, and neurotrophic factors in hMSC by IONP incorporation. (A) TEM images of (i) IONP and (ii) hMSC-IONP. The red arrows indicate IONP. (B) The viability of hMSCs treated with various concentrations of IONP for 16 h, as evaluated by CCK-8 assay. n = 3 per concentration. (C) Fluorescence microscopy images of hMSCs before and after treatment with RITC(red)-IONP (40 μg/mL). The cell nuclei were stained with DAPI. (D) qRT-PCR

analysis for mRNA expression of angiogenic (Ang-1, FGF2, HGF, and VEGF), anti-apoptotic (FGF2, HGF, and VEGF), neurotrophic (BDNF), and anti-inflammatory (TGF-β1) factors in hMSC-IONP at 24 h and 48 h. The values were normalized to those of hMSCs without IONP treatment. n = 3, *$p < 0.05$ versus no IONP, and ¶$p < 0.05$ versus 24 h. (E) Schematic illustration of IONP-mediated signaling pathways for therapeutic factor up-regulation in hMSC-IONP. (F) Western blot analysis and the quantification of expression of intracellular signaling-associated molecules and therapeutic factors in hMSC and hMSC-IONP at 48 h. n = 3, *$p < 0.05$ versus hMSC.

3.2.2. Characterization of nanovesicles isolated from hMSC-IONP

As hMSC-IONP contains both, IONPs and increased amounts of therapeutic growth factors and their mRNAs, we hypothesized that NV-IONP prepared from hMSC-IONP can carry both IONPs and increased levels of therapeutic growth factors compared to NV prepared from untreated hMSC. Forty-eight hours after removal of IONP-containing medium from hMSC culture, hMSC-IONP were collected. Subsequently, NV-IONP were prepared by serial extrusion of hMSC-IONP, followed by density-gradient ultracentrifugation to harvest NV-enriched fraction, and finally magnetic sorting to isolate NV-IONP (Figure 3.1A). During the serial extrusion, the cell membrane of hMSCs undergoes deformation, the components (e.g., mRNA and proteins) in hMSCs start to leak out, and the lipid bilayer fragments immediately self-assemble and partially encapsulate the components. The density-gradient ultracentrifugation of the extruded hMSC-IONP resulted in the separation of layers according to the difference in density of the components. The protein and iron content in each fraction was analyzed by protein measurement and inductively coupled plasma mass spectrometry (ICP-MS), respectively (Figure 3.3). Cellular organelles and proteins with a low density were localized in the upper layer (fraction 1), while free IONPs with a high density were accumulated as a pellet in the bottom of the tube (fraction 4). After ultracentrifugation and magnetic separation of fraction 2, protein and ICP-MS analysis revealed that NV-IONP were accumulated in fraction 6. To examine whether the prepared products are actually NV harboring IONPs in its inner space, the morphology was examined by TEM (Figure 3.4A). NV-IONP contained IONPs (red arrow). To determine the IONP content within NV-IONP, ICP-MS analysis was carried out (Figure 3.4B). By normalization to the protein amount, NV-IONP contained approximately 17 ng of iron in 1 μg of NV protein. To evaluate the feasibility of NV-IONP as a magnet-guided delivery tool, dispersed NV-IONP were magnetized with a neodymium magnet (Figure 3.4C). The magnetization resulted in NV-

IONP pellet formation near the neodymium magnet. The size of NV and NV-IONP was determined with nanoparticle tracking analysis (NTA; Figure 3.4D). NV and NV-IONP showed the mean size of 151.4 ± 32.5 nm and 158.7 ± 40.7 nm, respectively. Both NV and NV-IONP contained CD9 and CD63 (Figure 3.4E), which are exosome markers, indicating that NV and NV-IONP are exosome-like. We also investigated whether NV expressed MSC-specific markers. Agarose gel electrophoresis of RT-PCR products showed that both, NV and NV-IONP contained MSC-specific markers ($CD29^+$, $CD34^-$, $CD44^+$) with quantities equivalent to those in hMSC and hMSC-IONP (Figure 3.5). The IONP treatment did not alter the hMSC-marker expression. These results indicate that both NV and NV-IONP were exosome-mimetic and contained MSC-specific markers. Next, IONPs inside NV were further visualized by confocal fluorescence microscopy (Figure 3.4F). RITC-labeled IONPs were used for NV-IONP preparation. 3,3′-dioctadecyloxacarbocyanine perchlorate (DiO), which anchors the lipid bilayer and emits green fluorescence, was utilized to label NV. Green (NV) and red (IONP) fluorescence signals were perfectly overlapped in NV-IONP, while red fluorescent signal was not observed in NV, indicating the successful IONP encapsulation in NV-IONP. To confirm the stable incorporation of IONPs inside NV after the NV-IONP is internalized into cells, Raw 264.7 cells were treated with DiO- and RITC- labeled NV-IONP (Figure 3.4G). The cells treated with NV-IONP were double-positive for green fluorescence (NV) and red fluorescence (IONP).

Next, we investigated whether the NV-IONP contain higher levels of therapeutic growth factors than NV. As expected, from that hMSC-IONP contained a higher level of therapeutic growth factors than hMSCs; qRT-PCR analysis showed that NV-IONP contained a significantly higher mRNA level of therapeutic growth factors than NV (Figure 3.4H). Furthermore, western blot analysis showed that NV-IONP contained a significantly higher protein level of therapeutic growth factors than NV (Figure 3.4I). Together, these data

indicate that IONP can be utilized in NV-IONP not only for magnet navigation tool, but also for increasing the loading amount of various therapeutic growth factors and their mRNAs inside NV-IONP.

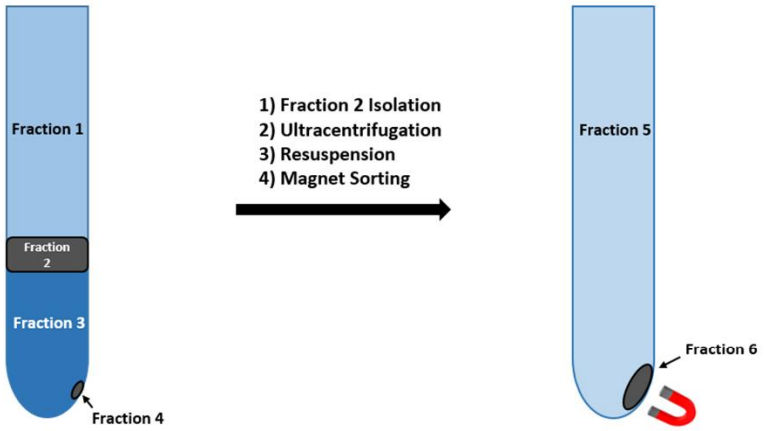

	Protein Percentage (%)	Iron Oxide Percentage (%)
Fraction 1	74.6 ± 2.1	3.4 ± 0.2
Fraction 2	21.6 ± 0.9	63.9 ± 3.8
Fraction 3	4.5 ± 0.1	8.5 ± 0.7
Fraction 4	1.8 ± 0.4	24.1 ± 1.5

	Protein Percentage (%)	Iron Oxide Percentage (%)
Fraction 5	7.4 ± 1.7	2.7 ± 0.2
Fraction 6	93.8 ± 4.5	97.2 ± 3.3

Figure 3.3. Quantification of protein and iron content in each fraction obtained during the NV-IONP isolation process. The protein and iron content in each fraction are shown as percentage of total protein content or total iron content in the tube, respectively.

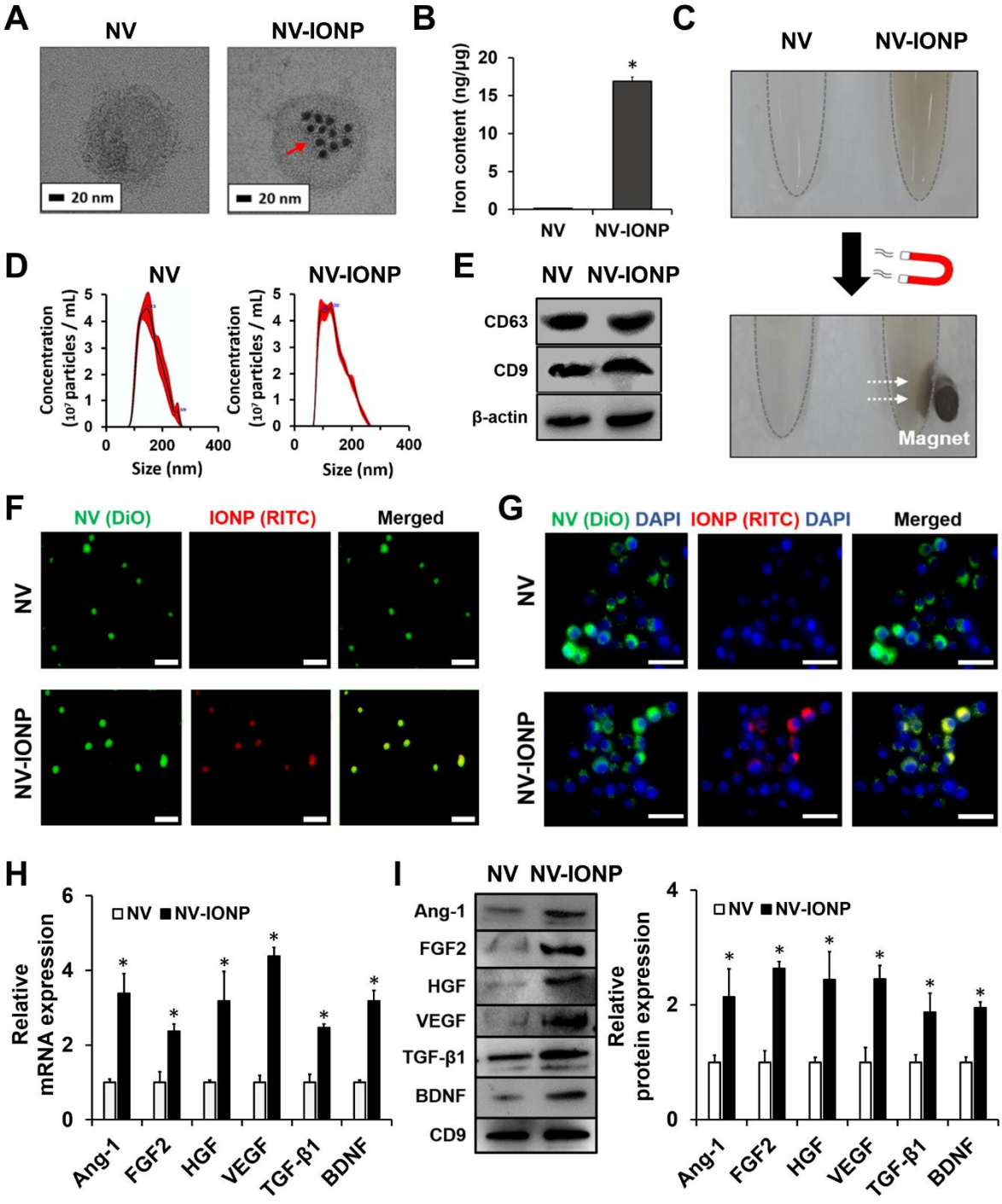

Figure 3.4. Charaterization of NV (prepared from hMSC) and NV-IONP (prepared from hMSC-IONP). (A) TEM images of NV and NV-IONP. The red arrow indicates IONP. (B) Iron content in NV and NV-IONP, as evaluated by ICP-MS analysis. *$p < 0.05$ versus NV. (C) Demonstration of magnetic guidance of NV-IONP. (D) Size distribution of NV and NV-

IONP, as evaluated by NTA analysis. (E) Western blot analysis for exosome markers (CD9 and CD63) in NV and NV-IONP. (F) Confocal microscopy images showing IONP incorporation in NV-IONP. NV and IONP were labeled with DiO lipophilic dye (green) and RITC (red), respectively. NV is visualized as $DiO^{+}/RITC^{-}$, while NV-IONP is visualized as $DiO^{+}/RITC^{+}$. Bars = 1 μm. (G) Fluorescence microscopy images showing incorporation of NV (green) and NV-IONP (green-red) in Raw264.7 macrophages. Blue indicates DAPI (nucleus). Bars = 50 μm. (H) qRT-PCR analysis for angiogenic, anti-apoptotic, neurotrophic, and anti-inflammatory factor mRNAs inside NV and NV-IONP. n = 3, $*p < 0.05$ versus NV. (I) Western blot analysis for angiogenic, anti-apoptotic, neurotrophic, and anti-inflammatory factors inside NV and NV-IONP. CD9, an exosome-specific marker, was used for the loading control. n = 3, $*p < 0.05$ versus NV.

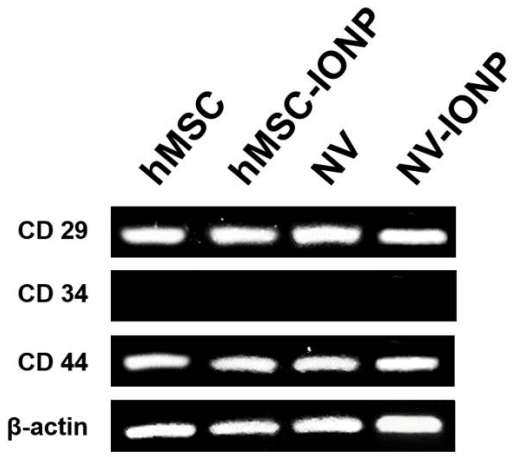

Figure 3.5. The expression of MSC marker (CD29+, CD34-, and CD44+) genes in hMSC, hMSC-IONP, NV, and NV-IONP

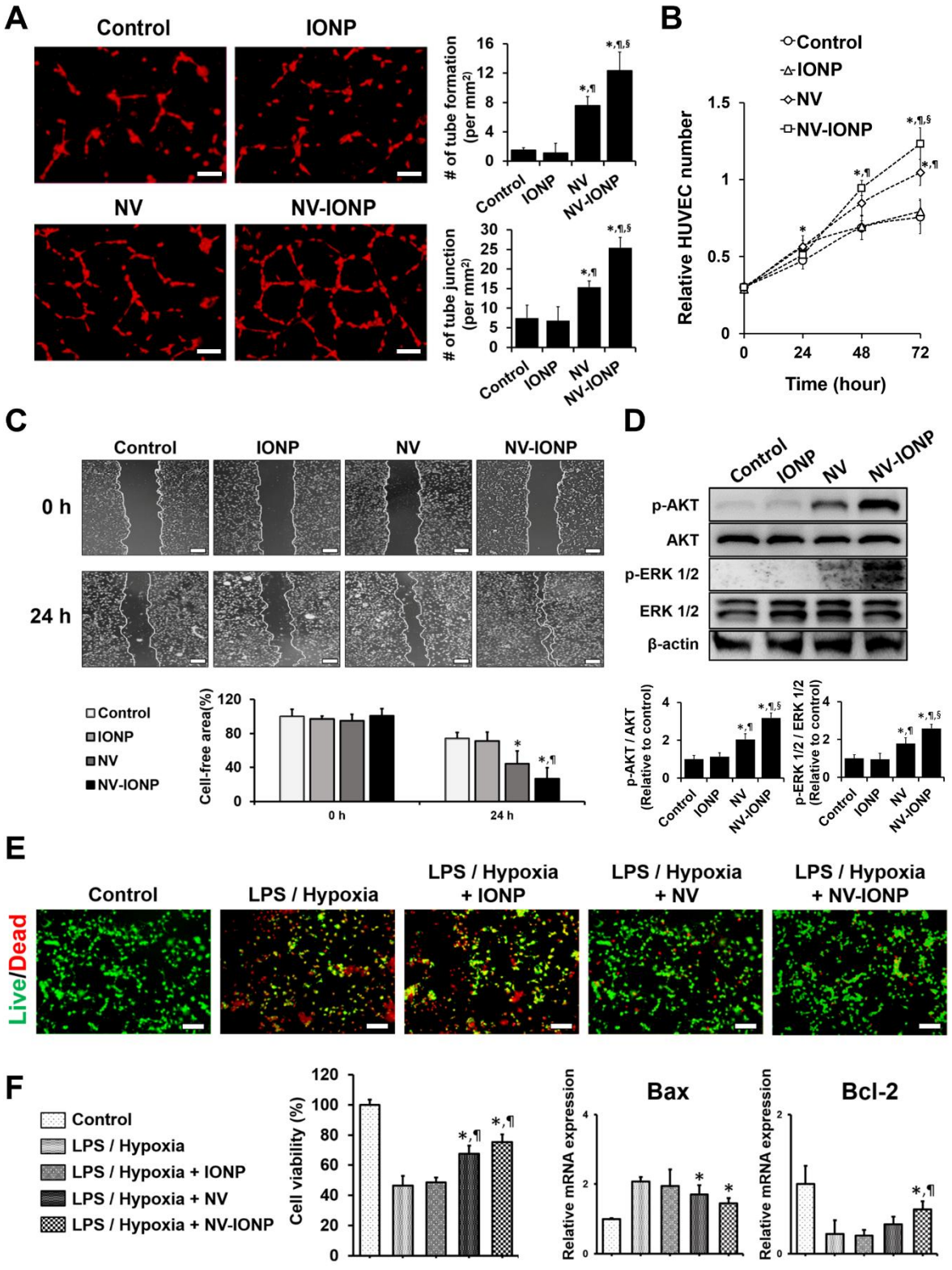

Figure 3.6. In vitro angiogenic effects of NV-IONP on human umbilical vein endothelial cells (HUVECs) and anti-apoptotic effects of NV-IONP on neuron-like PC12 cells. (A)

Tube formation assay of HUVECs after treatment with IONP, NV, or NV-IONP. HUVECs were cultured in matrigel-coated plates and visualized with DiI, a red fluorescent dye. The number of tubes and tube junctions formed were determined at 8 h. Bars = 100 μm. (B) The proliferative behavior of HUVECs with various treatments. The relative cell number was evaluated by the CCK-8 assay. (C) Migration of HUVECs with various treatments in serum-free medium for 24 h. The quantification shows the percentage of cell-free area at 24 h compared with the initial cell-free area. Bars = 200 μm. (D) Western blot analysis and quantification of the expression of cell signaling molecules in HUVECs after treatment of IONP, NV, or NV-IONP. (A, B, C, D) The control group received no treatment. n = 3, $^{*}p < 0.05$ versus control, $^{¶}p < 0.05$ versus IONP, and $^{§}p < 0.05$ versus NV. (E) Live/dead cell staining of PC12 cells 24 h after LPS treatment and culturing under hypoxic conditions (2% O_2). PC12 cells were treated with either IONP, NV, or NV-IONP prior to LPS treatment and hypoxic environment. Live cells and dead cells were stained with FDA (green) and EB (red), respectively. The control group was not treated with LPS, and was incubated under normoxic conditions (20% O_2). Bars = 100 μm. (F) Cell viability and the expression of apoptotic (Bax) and anti-apoptotic (BCl-2) genes at the mRNA level in PC12 cells treated with the same conditions of (E). n = 3, $^{*}p < 0.05$ versus LPS / Hypoxia, $^{¶}p < 0.05$ versus LPS / Hypoxia + IONP

3.2.3. Enhanced angiogenesis and anti-apoptotic effect of NV-IONP

Previous studies have reported that conditioned media or extracellular vesicles from MSCs stimulate proliferation, migration, and angiogenesis in endothelial cells[16, 105] and show neuro-protective effect against apoptosis in neuron-like cells.[18, 106, 107] As growth factors are major contributors in angiogenesis and anti-apoptosis,[108, 109] we investigated whether the higher level of growth factors in NV-IONP could enhance angiogenesis and anti-apoptotic activity in target cells. First, we carried out capillary tube formation assay using human umbilical vein endothelial cells (HUVECs) to examine the angiogenic activity of NV-IONP. Capillary tube formation of DiI-labeled HUVECs were analyzed 8 h after incubation in the matrigel-coated plates in the presence of IONP, NV, or NV-IONP (Figure 3.6A). The treatment of HUVECs with NV-IONP (40 μg/mL) markedly enhanced both tube formation and tube junction compared to the other treatments. The treatment with IONP at 0.68 μg/mL, which is the equal iron concentration of NV-IONP at 40 μg/mL, did not enhance the capillary formation. Furthermore, NV-IONP-treated HUVECs showed active proliferation compared to the other groups (Figure 3.6B). Next, the scratch assay was carried out to investigate the ability of NV-IONP to stimulate the migration of HUVECs (Figure 3.6C). To minimize the cell proliferation, HUVECs were incubated in a serum-free medium for 24 h. NV-IONP-treated HUVECs showed more active migration compared to the other groups. As a previous report revealed that exosomes derived from hMSCs enhanced proliferation and migration of fibroblasts by triggering AKT and $ERK_{1/2}$ pathway,[110] western blot analysis of signaling cascades in HUVECs was carried out (Figure 3.6D). As expected, NV-IONP-treated HUVECs showed significant up-regulation in the phosphorylated forms of both, AKT and $ERK_{1/2}$.

Next, we evaluated the anti-apoptotic effect of NV-IONP on neuron-like PC12 cells cultured in an inflammatory and ischemic environment. As SCI lesion shows strong

peripheral inflammation and ischemia, which exacerbate the tissue damage, PC12 cells were treated with lipopolysaccharide (LPS) and cultured under hypoxic condition (2% O_2) for 24 h (Figure 3.6E and F). PC12 cells showed poor survival under the LPS/hypoxic condition. Interestingly, the pre-treatment with NV or NV-IONP improved the cell viability (Figure 3.6E and F). Moreover, qRT-PCR assay indicated that the pre-treatment with NV or NV-IONP down-regulated Bax (apoptotic) and up-regulated Bcl-2 (anti-apoptotic) mRNA compared to the other groups (Figure 3.6F).

In the above-mentioned experiments, the IONP treatment at 0.68 μg/mL did not activate the pathways or cause the phenotypical changes in HUVECs and PC12 cells. These data indicate that contained therapeutic growth factors and their mRNAs are responsible for the angiogenic and anti-apoptotic effects of NV-IONP, rather than the contained IONPs. These results correspond with the results of previous studies that hMSC-derived extracellular vesicles exert therapeutic effects by delivering mRNA[85, 87] and proteins.[73, 86] Moreover, as the IONP concentration of 0.68 μg/mL is only 1.7% of the IONP concentration (40 μg/mL) that significantly up-regulated growth factor expression in the hMSC-IONP, the IONP concentration of 0.68 μg/mL is possibly insufficient amount to activate the angiogenesis or anti-apoptosis in HUVECs and PC12 cells.

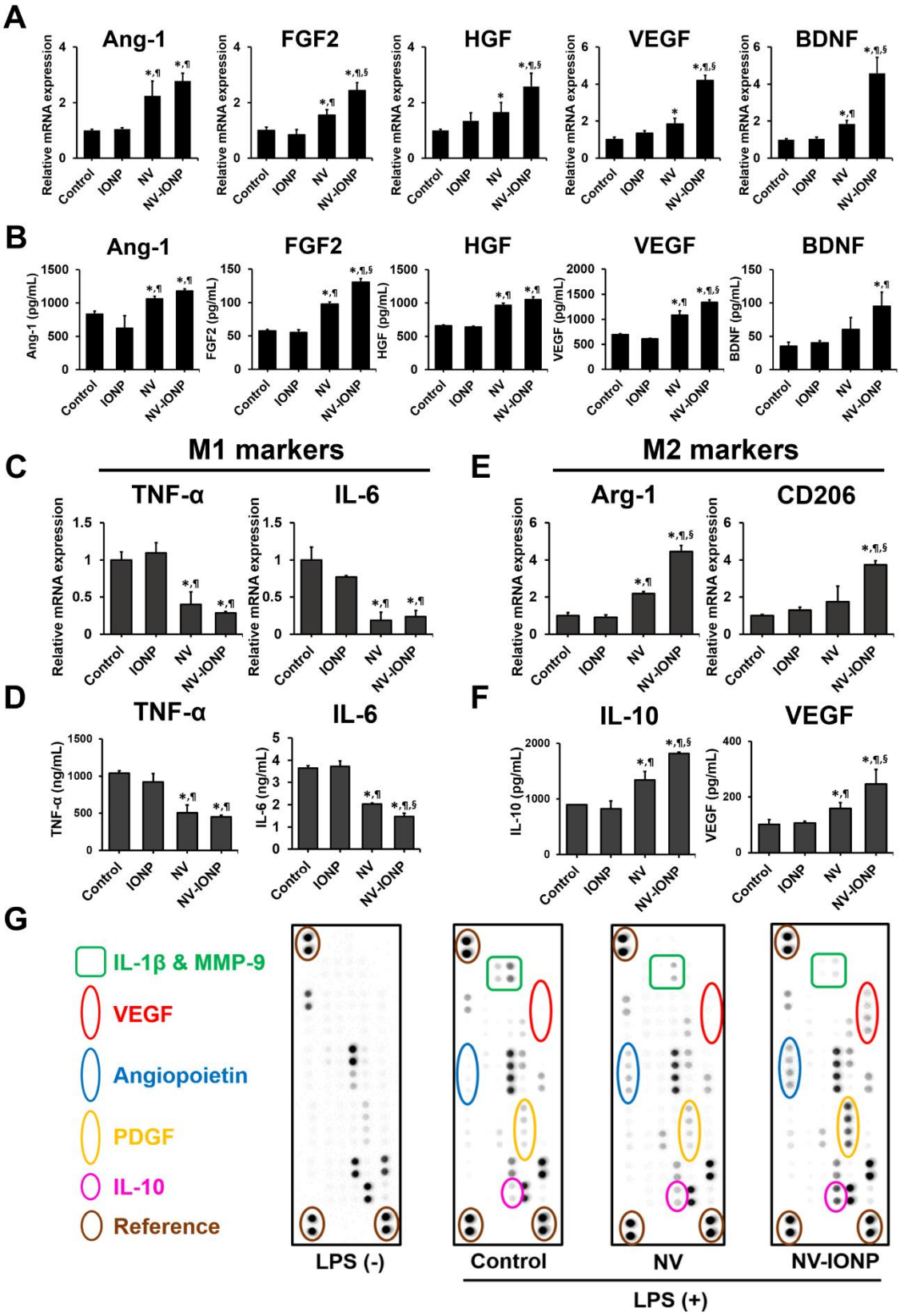

Figure 3.7. In vitro effects of NV-IONP on the expression of angiogenic, anti-apoptotic, and neurotrophic factors in astrocytes and on M2 polarization of LPS-stimulated

macrophages. (A) qRT-PCR analysis for mRNA expression and (B) ELISA analysis for secretion of angiogenic, anti-apoptotic, and neurotrophic factors in astrocytes at 48 h after IONP, NV, or NV-IONP treatment. (C, E) qRT-PCR analysis for mRNA expression and (D, F) ELISA analysis for secretion (C, D) of M1 macrophage phenotype cytokine markers and (E, F) M2 macrophage phenotype markers in LPS-stimulated Raw264.7 macrophages 48 h after IONP, NV, or NV-IONP treatment. (G) Angiogenic and inflammatory protein array of conditioned medium from cultures of unstimulated Raw264.7 (LPS (-)) and LPS-stimulated Raw264.7 cells (LPS (+)) 48 h after NV or NV-IONP treatment. Designated factors are significantly changed proteins among the groups. (A, B, C, D, E, and F) n = 3, $^{*}p < 0.05$ versus control, $^{¶}p < 0.05$ versus IONP, and $^{§}p < 0.05$ versus NV. The control group received no treatment.

3.2.4. Stimulation of therapeutic growth factor expression in astrocytes by NV-IONP

Astrocytes in CNS play a pivotal role in maintaining optimal microenvironment and homeostatic functions for neurons and endothelial cells.[111] Astrocytes modulate the tight junction integrity and angiogenesis of the gliovascular system and the survival of neurons by secreting various growth and neurotrophic factors.[112] As a previous study reported that co-culture of bone marrow-derived MSCs and astrocytes enhanced the expression of BDNF, FGF2, and VEGF gene in the astrocytes *via* AKT and $ERK_{1/2}$ signaling cascades,[113] in this study we hypothesized that NV and NV-IONP might stimulate the expression of therapeutic growth factors in astrocytes.

The treatment of NV and NV-IONP on astrocytes significantly increased the expression of Ang-1, FGF2, HGF, VEGF, and BDNF mRNA, which promote angiogenesis and neuronal survival[112] (Figure 3.7A). The NV-IONP treatment showed a significantly higher expression of growth factor mRNA, except for Ang-1 mRNA, compared to the NV treatment. ELISA analysis of the conditioned medium of astrocyte cultures indicated that the secretion of therapeutic growth factors was significantly increased in the NV- and NV-IONP-treated astrocytes (Figure 3.7B). The proliferation of astrocytes did not get affected by NV-IONP (data not shown). The secretion of FGF2 and VEGF was significantly higher in the NV-IONP-treated astrocytes than that in the NV-treated astrocytes. The treatment with IONP (0.68 μg/mL) at the equal iron amount to NV-IONP (40 μg/mL) did not increase the growth factor expression, excluding the effect of IONP inside NV-IONP on the enhanced therapeutic growth factor expression in astrocytes. These results suggest that when astrocytes in injured spinal cord were treated with NV or NV-IONP, the secretion of therapeutic growth factors from astrocytes can be stimulated, resulting in improved angiogenesis and neuronal survival in the injured spinal cord.

3.2.5. *In Vitro* attenuation of inflammatory responses and M2 polarization in macrophages

The various pathological events in SCI include significant infiltration and activity of macrophages in the spinal cord lesion.[114] Therefore, understanding and modulating the inflammatory responses of macrophages would be crucial in SCI repair. Macrophages, in terms of distinctive phenotypes and functions, can be classified to pro-inflammatory and cytotoxic state (M1) and anti-inflammatory and regenerative state (M2). During the early stage of SCI, M1 macrophages are the majority among the macrophage population in spinal cord lesion.[115] Previous studies have reported that conditioned medium and extracellular vesicles from MSCs exhibited anti-inflammatory effect *via* M2 polarization of macrophages.[22, 116] Thus, we investigated the effects of NV and NV-IONP on inflammatory cytokine expression and macrophage polarization. Raw 264.7 cells, a murine macrophage cell line, were activated to M1 state by LPS-treatment for 24 h.[117] Then the cells were treated with IONP, NV, or NV-IONP for 16 h. Forty-eight hours after removal of treatments, qRT-PCR and ELISA analysis indicated that the NV or NV-IONP treatment drastically reduced the expression of M1-related cytokines such as TNF-α and IL-6 (Figure 3.7C and D). The insignificant difference between the M1 marker expression in NV- and NV-IONP-treated macrophages may be possibly due to excessive M1-stimulation by LPS. The IONP treatment did not show any significant effect on the TNF-α and IL-6 expression. Meanwhile, the NV or NV-IONP treatment increased the expression of Arginase-1 (Arg-1) and CD206 mRNA, which are highly expressed in M2-polarized macrophages (Figure 3.7E). ELISA indicated that the secretion of IL-10, an anti-inflammatory M2 cytokine, was drastically increased in NV- and NV-IONP-treated macrophages (Figure 3.7F). The secretion of VEGF, which is also classified as an M2 marker,[118, 119] was increased in the NV and NV-IONP groups. The expression of M2 markers was significantly enhanced in the NV-IONP group than that in the

NV group. M2 polarization induced by NV-IONP may be attributed to the up-regulation of TGF-β1, which is known to induce M2 polarization.[120, 121]

Next, we performed angiogenic and inflammation-regulatory protein array assay on the conditioned media of the groups (Figure 3.7G). The NV and NV-IONP group showed decreased secretion of IL-1β and MMP-9, which are M1 markers. In agreement with the ELISA result, the secretion of VEGF and IL-10 in the NV-IONP group was increased in the protein array assay. The expression of angiogenic growth factors such as angiopoietin and platelet-derived growth factor (PDGF) was also increased in the NV-IONP-treated macrophages.

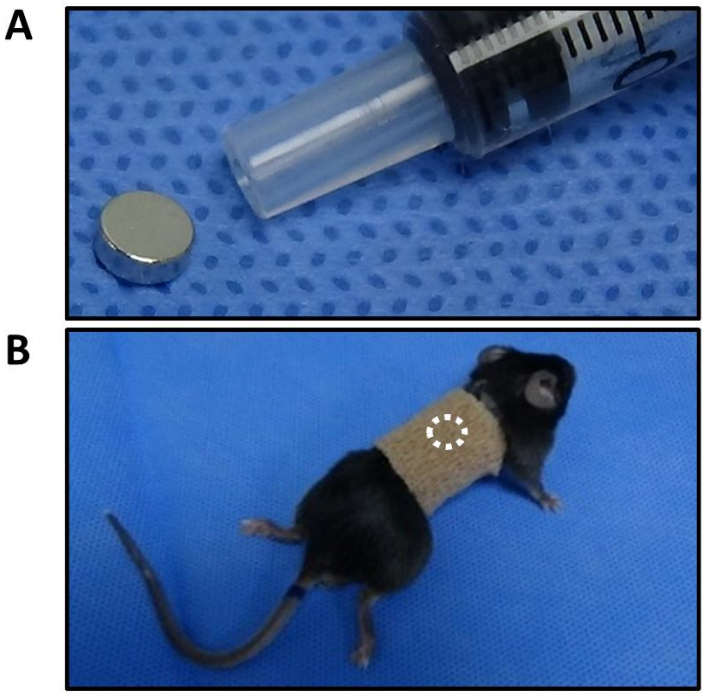

Figure 3.8. Photographs of a neodymium magnet and magnet strapping to SCI mouse model. (A) A neodymium magnet used for magnetic guidance. The size was compared with a 1 cc syringe. (B) A magnet was strapped on the skin above the injured spinal cord (dotted white circle) using Tegarderm® and self-adherent strap.

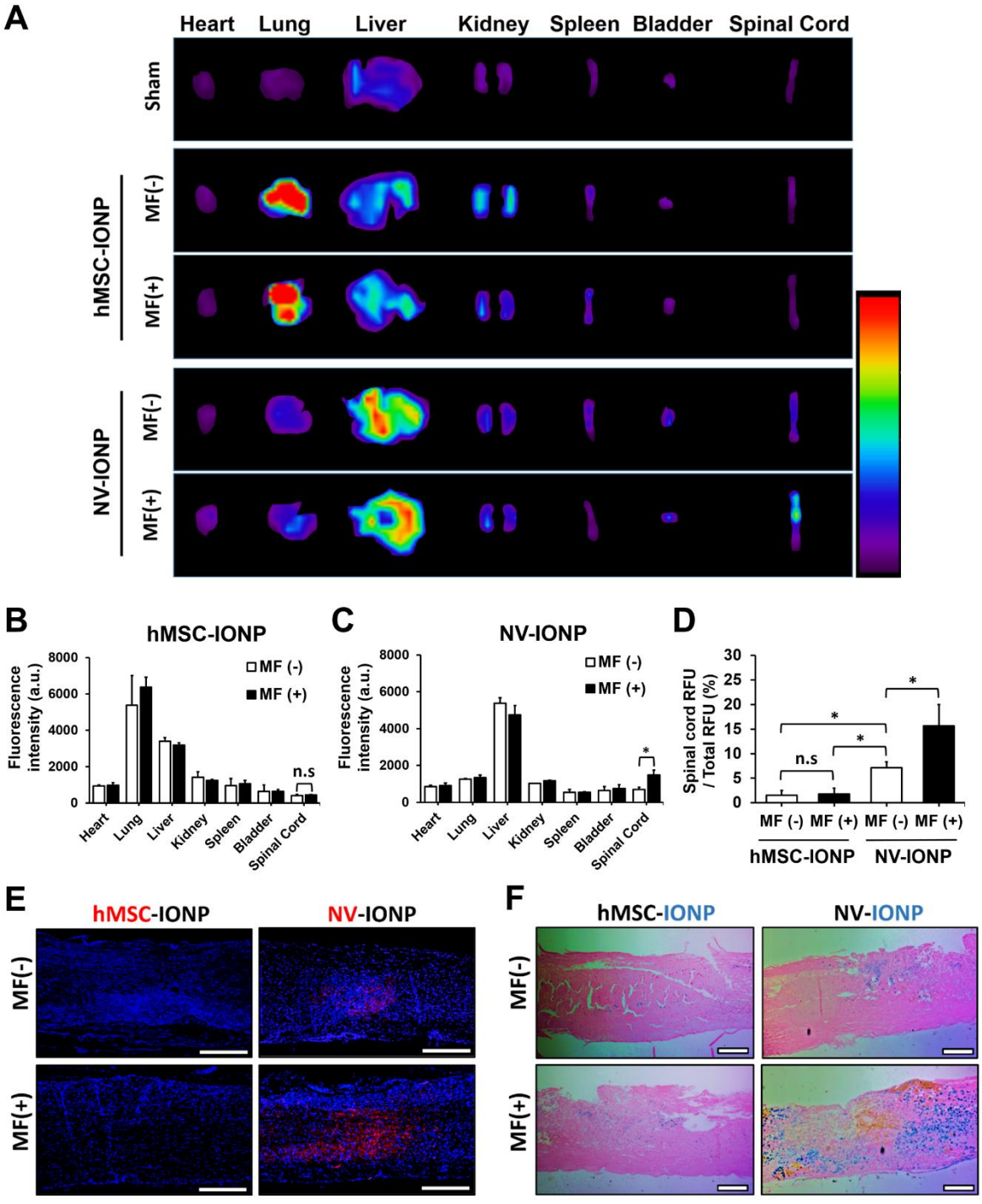

Figure 3.9. Biodistribution of systemically injected hMSC-IONP and NV-IONP in spinal cord-injured mice, in the presence or absence of an external magnetic field (MF) for 24 h. (A) *Ex vivo* fluorescence images of major organs and injured spinal cord at 24 h after injection of hMSC-IONP or NV-IONP, in the presence or absence of an applied MF on

injured spinal cord. VivoTrack 680, a lipophilic red fluorescent dye, was used for labeling hMSC-IONP and NV-IONP. The region-of-interest (ROI) quantification analysis of major organs from mice injected with (B) hMSC-IONP or (C) NV-IONP. (D) Spinal cord-targeting efficiency of hMSC-IONP and NV-IONP, with or without magnetic guidance. (B, C, and D) n = 3 animals per group, n.s. indicates no significance. *$p < 0.05$ (E) Confocal microscopy images of longitudinal sections of spinal cord of hMSC-IONP- or NV-IONP-injected mice in the presence or absence of an applied MF. VivoTrack 680 from hMSC-IONP or NV-IONP is visualized as red. Blue indicates DAPI (nuclei). Bars = 200 μm. (F) Prussian blue staining of longitudinal sections of spinal cord of hMSC-IONP- or NV-IONP-injected mice in the presence or absence of an applied MF. Blue pigment indicates IONP. Bars = 200 μm.

3.2.6. Spinal cord targeting of NV-IONP *via* external magnetic guidance

Systemic administration of hMSCs results in accumulation in pulmonary capillaries due to their relatively large size (15 ~ 50 μm).[122-124] Thus, we intravenously injected nano-sized NV-IONP to evade the entrapment in pulmonary capillaries, and therefore to improve the efficiency of targeting toward injured spinal cord *via* external magnetic guidance. To show the enhanced spinal cord-targeting ability of NV-IONP over hMSC-IONP, intravenous injection of hMSC-IONP served as the control in the biodistribution assay. NV-IONP and hMSC-IONP were fluorescently labeled with VivoTrack 680, a lipophilic red dye. A neodymium magnet was placed and fixed near the injured spinal cord (Figure 3.8). After 24 h post-injection, major organs (heart, lung, liver, kidney, spleen, bladder, and the spinal cord) were retrieved and examined using an optical imaging system (Figure 3.9A). The majority of injected hMSC-IONP accumulated in lung and liver (Figure 3.9A and B). hMSC-IONP were poorly accumulated in the injured spinal cord regardless of the magnetic field (MF+ or MF-). Due to entrapment in the pulmonary capillary, hMSC-IONP possibly did not have sufficient blood-circulation time to be navigated toward the MF-guided spinal cord. In contrast, administered NV-IONP showed a relatively high fluorescence intensity in the liver (Figure 3.9A and C), which is in agreement with the result of previous studies reporting that systemically injected extracellular vesicles are taken up mainly by liver due to mononuclear phagocyte system.[94, 95] However, we observed a relatively insignificant accumulation of NV-IONP in the lung, suggesting that the nano-sized NV-IONP successively passed through the pulmonary capillary. Importantly, injected and magnet-guided NV-IONP showed significantly enhanced accumulation in the spinal cord (Figure 3.9A and C), possibly due to increased blood-circulation time of NV-IONP and the external magnetic guidance. Next, we compared the spinal cord-targeting efficiency by percentage of relative fluorescence unit

(RFU) (Figure 3.9D). The fluorescence intensity in the spinal cord was divided with the sum of the fluorescence intensities from all major organs retrieved. The quantification analysis indicated that NV-IONP (MF-) showed 3.9 ~ 4.5-fold higher accumulation in the spinal cord compared to hMSC-IONP (MF+ or MF-) and the magnetic guidance increased the spinal cord-targeting efficiency of NV-IONP by 2.18-fold. Accordingly, NV-IONP (MF+) showed 8.5 ~ 10-fold higher accumulation in the spinal cord compared to hMSC-IONP (MF+ or MF-).

Next, spinal cord tissue sections were obtained, and the accumulation of fluorescently labeled hMSC-IONP and NV-IONP in the spinal cord was observed using confocal fluorescence microscopy (Figure 3.9E). No fluorescence signals were detected in the hMSC-IONP groups regardless of MF. Notable fluorescence signals were observed in the NV-IONP (MF-). The signals were further increased in the NV-IONP (MF+). Prussian blue staining, which stains accumulated IONP in the tissue, of the spinal cord tissue sections also revealed the improved targeting efficiency of NV-IONP (MF+) (Figure 3.9F).

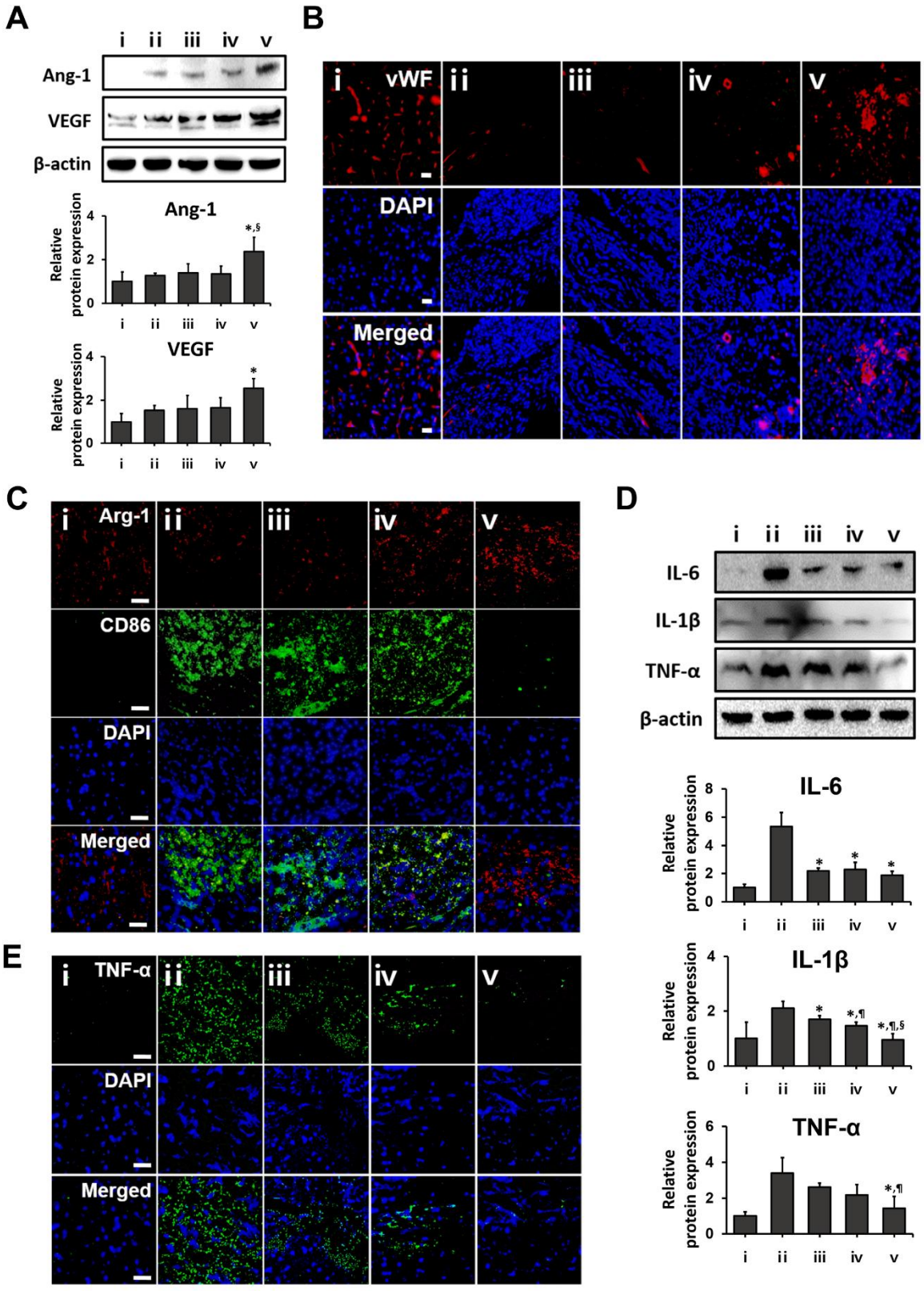

Figure 3.10. In vivo angiogenesis and M2 phenotype polarization of infiltrated macrophages in injured spinal cord after intravenous injection of NV or NV-IONP, with

or without magnetic guidance. Animals were assigned into five groups; (i) sham, (ii) injury + PBS injection, (iii) injury + NV injection, (iv) injury + NV-IONP injection, and (v) injury + NV-IONP injection + magnetic guidance for 24 h. (A) Western blot analysis and quantification of angiogenic factors (Ang-1 and VEGF) in spinal cord tissue at 14 days after injury. n = 3 animals per group. (B) Immunohistochemical (IHC) staining for blood vessels (vWF, red) at the lesion core at 28 days after injury. n = 3 animals per group. Bars = 20 μm. (C) IHC staining for M1 phenotype (CD86, green) and M2 phenotype (Arg-1, red) macrophages at the site of injury at 28 days after injury. n = 3 animals per group. Bars = 20 μm. (D) Western blot analysis and quantification of M1 phenotype-related inflammatory cytokines (IL-6, IL-1β, and TNF- α) in spinal cord tissue 1 day after injection. n = 3 animals per group. (E) IHC staining for TNF-α at the site of injury at 1 day after injury (green). Bars = 20 μm. (A and D) $*p < 0.05$ versus (ii), $^{¶}p < 0.05$ versus (iii), and $^{§}p < 0.05$ versus (iv).

3.2.7. Enhanced angiogenesis and M2 polarization in injured spinal cord by magnet-guided NV-IONP

It was previously demonstrated that angiogenic factors promote angiogenesis, neural regeneration, and functional recovery in SCI.[125] VEGF induce re-vascularization in the injured spinal cord.[126] VEGF is also a crucial neurotrophic factor, and it plays a significant role in neuron survival in the spinal cord.[127] Meanwhile, Ang-1 suppresses vascular leakage and inflammation and accelerates blood vessel formation during angiogenesis.[128] Exogenous administration of Ang-1 has favorable effects on both vascular integrity and functional recovery after SCI.[129, 130] In the present study, injection of NV-IONP and external magnetic guidance significantly increased protein expression of Ang-1 and VEGF in the injured spinal cord, evaluated by western blot analysis (Figure 3.10A). Immunohistochemical (IHC) staining of injured spinal cord with von Willebrand factor (vWF) at 28 days post-injury revealed vascular impairment after SCI (Figure 3.10B). Importantly, a markedly enhanced expression of vWF was observed in the NV-IONP (MF+) group as compared to the other groups.

Prolonged inflammation at the lesion site results in augmented tissue damage. Macrophage polarization is one of the cellular mechanisms involved in controlling the inflammation and tissue repair of injured spinal cord.[114] M1 and M2 are the two major subsets of macrophages at the injured site. Macrophage can switch from one phenotype to the other depending on the microenvironment following injury. To minimize tissue damage and maximize tissue repair after SCI, the tissue-reparative M2 macrophages should be induced and the number of pro-inflammatory M1 macrophages should be reduced.[119, 131] IHC staining of the injured spinal cord sections revealed a drastically increased expression of CD86, an M1 marker, in the injured spinal cord, indicating the M1 polarization of infiltrated

macrophages after SCI (Figure 3.10C). The injection of either NV or NV-IONP (MF-) did not significantly reduce inflammatory M1 macrophages in the injured spinal cord, however the injection of NV-IONP (MF+) showed significant effect. Also, the injection of NV-IONP (MF+ and MF-) significantly enhanced expression of Arg-1, an M2 marker, while the other groups did not. Moreover, as M1 macrophages secrete inflammatory cytokines, the expression of IL-6, IL-1β, and TNF-α was significantly elevated in the injured spinal cord at 1 day post injury, however, the injection of NV-IONP (MF+) significantly attenuated the SCI-induced expression of the inflammatory cytokines, as evaluated by western blot analysis (Figure 3.10D). IHC staining for TNF-α in the injured spinal cord sections also showed significantly decreased expression of inflammatory TNF-α in the injured spinal cord after injection of NV-IONP (MF+) (Figure 3.10E). These results demonstrated that the injection of NV-IONP along with external magnetic guidance is able to induce the phenotypic shift of macrophages from M1 to M2 for effective repair of injured spinal cord.

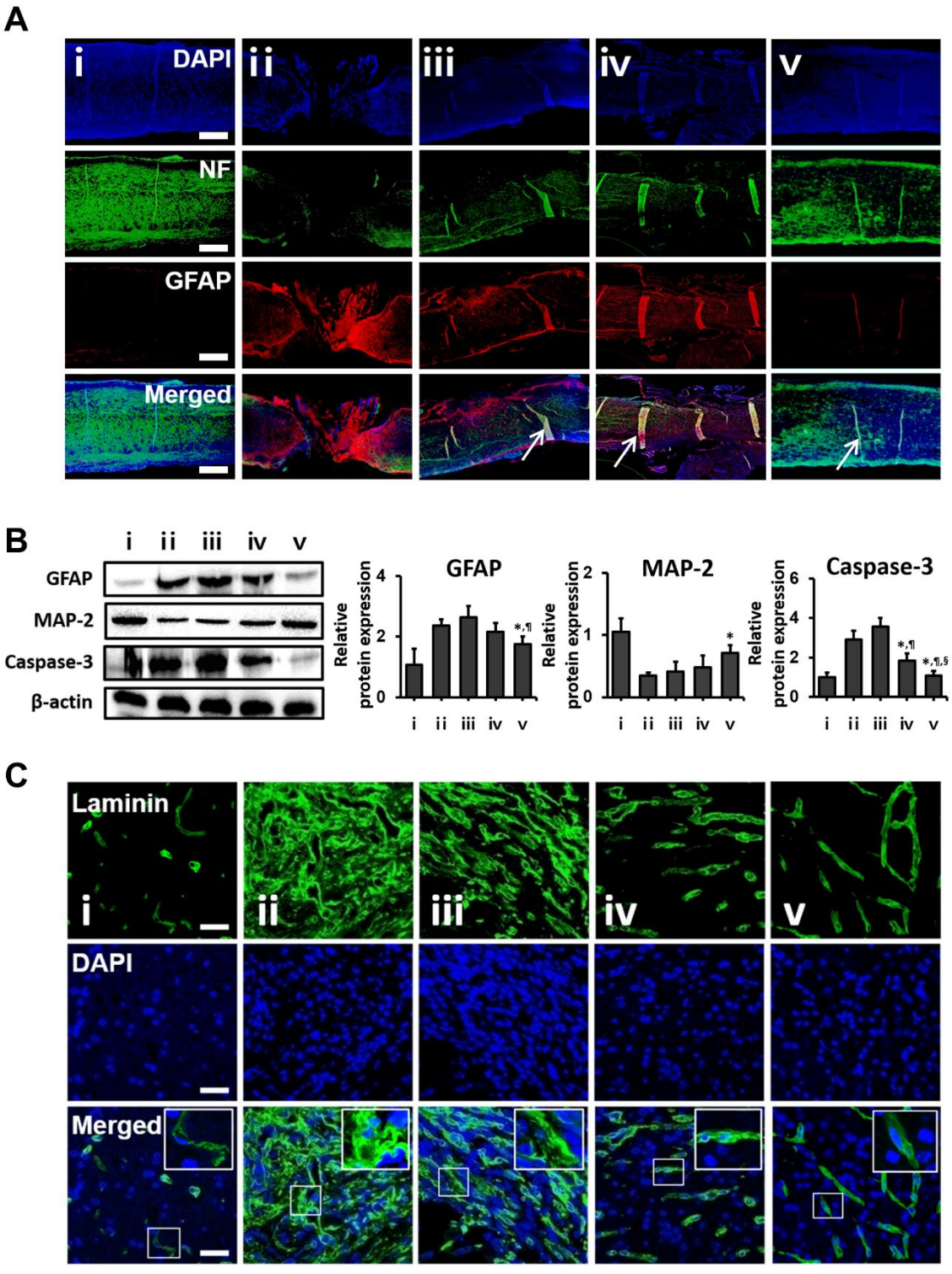
A
i
DAPI
ii
iii
iv
v
NF
GFAP
Merged
B
i ii iii iv v
GFAP
MAP-2
Caspase-3
β-actin
Relative protein expression
GFAP
MAP-2
Caspase-3
*,¶
*
*,¶
*,¶,§
C
Laminin
DAPI
Merged

D

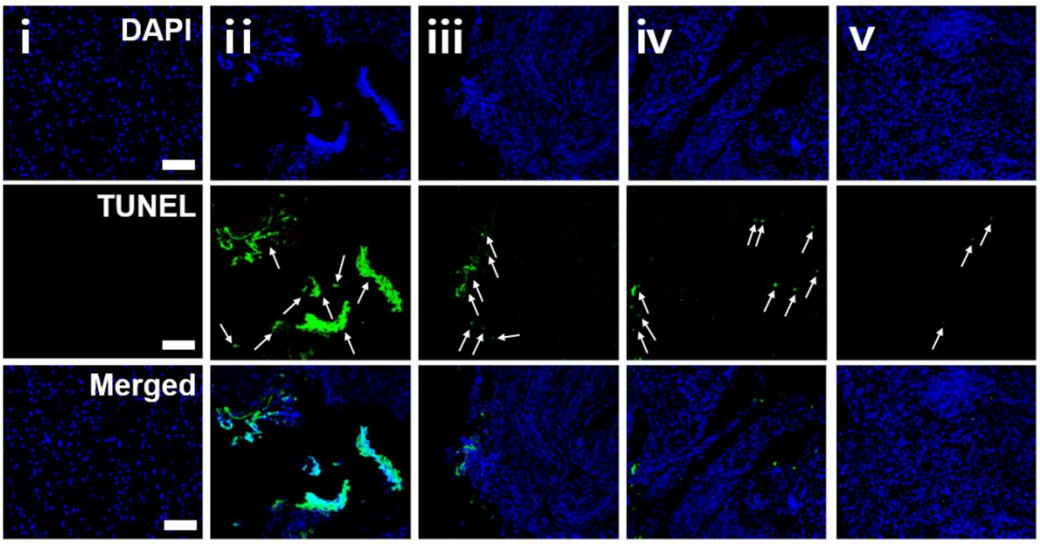
i
DAPI
ii
iii
iv
v
TUNEL
Merged

E

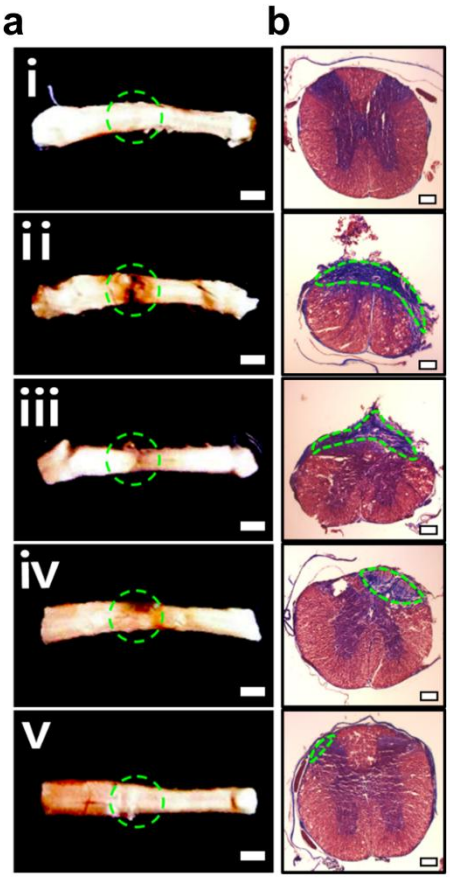
a
b
i
ii
iii
iv
v

F

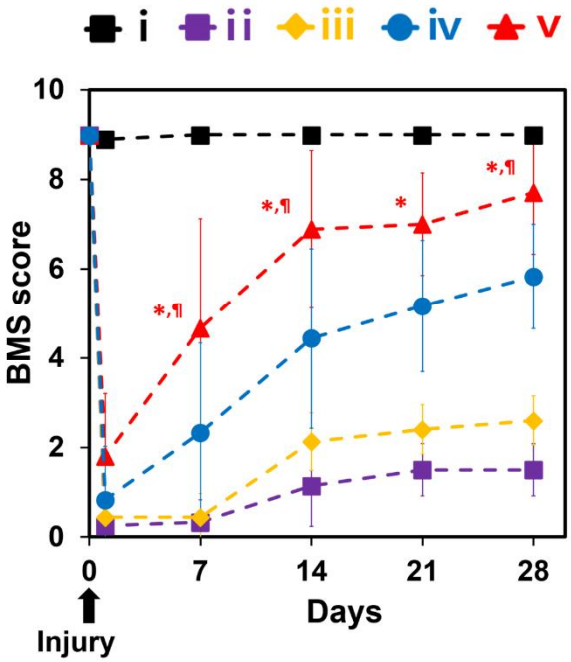
i
ii
iii
iv
v
BMS score
10
8
6
4
2
0
0
7
14
21
28
Days
Injury
*,¶
*,¶
*
*,¶

Figure 3.11. Attenuation of glia scar formation and enhancement in functional recovery in spinal cord-injured mice by intravenous injection of NV-IONP with magnetic guidance. Animals were assigned into five groups; (i) sham, (ii) injury + PBS injection, (iii) injury + NV injection, (iv) injury + NV-IONP injection, and (v) injury + NV-IONP injection + magnetic guidance for 24 h. (A) IHC analysis for neuron (NF, green) and astrogliosis (GFAP, red) in longitudinal sections of spinal cord at 28 days after injury. The white arrows indicate artifacts produced during the histological analysis processing. Bars = 100 μm. (B) Western blot analysis and quantification of astrogliosis (GFAP), neuron-specific (MAP-2), and apoptotic (C-Cas-3) proteins in spinal cord tissue at 14 days after injury. n = 3 animals per group. $^{*}p < 0.05$ versus (ii), $^{¶}p < 0.05$ versus (iii), and $^{§}p < 0.05$ versus (iv). (C) IHC analysis for fibrotic tissue (laminin, green) in spinal cord sections at 28 days after injury. Bars = 50 μm. (D) Fluorescence microscopy images of apoptotic TUNEL-positive cells (green, white arrows) at the injured spinal cord at 7 days after injury. n = 3 animals per group. Bars = 100 μm. (E) (a) Representative images of the spinal cord retrieved at 28 days after injury. The dotted green circles indicate the lesion core. Bars = 2 mm. (b) Masson's trichrome-stained transverse sections of lesion core tissues. The dotted area indicates fibrotic tissue area. Bars = 100 μm. (F) BMS score-based quantitative analysis of time-lapse functional recovery in spinal cord-injured mice for 28 days. n = 10 animals per group, $^{*}p < 0.05$ versus (ii), and $^{¶}p < 0.05$ versus (iii).

3.2.8. Attenuation of glial scar formation and enhanced functional recovery by magnet-guided NV-IONP

After SCI, the number of astrocytes increases and causes scar formation, which is called astrogliosis.[132] The glial scar formation acts as a substantial impediment inhibiting axonal regeneration after SCI.[133] At 28 days after the injury; neuronal disintegration and astrogliosis were evaluated by IHC staining for neurofilament (NF) and glial fibrillary acidic protein (GFAP), respectively (Figure 3.11A). Extensive recruitment of astrocytes and neuronal loss were evident in the PBS injection group. In contrast, the NV-IONP (MF+) group showed markedly attenuated astrogliosis and neuronal loss. Western blot analysis for GFAP also revealed the drastic attenuation of astrogliosis in the NV-IONP (MF+) group compared to that in the other groups (Figure 3.11B). Moreover, expression of microtubule-associated protein-2 (MAP-2), a neuron-specific protein that promotes assembly and stability of the microtubule network, was significantly increased in the NV-IONP (MF+) group, indicating the prevention of SCI-induced neuronal loss. Another essential feature of the glial scar is the increased expression of extracellular matrix (ECM) proteins. Fibrotic scar tissue is rich in fibronectin and laminin at the lesion site after SCI.[134] The compression injury caused a drastic increase in laminin at the injury site after 28 days post-injury (Figure 3.11C). The injection of NV-IONP (MF+) significantly reduced the laminin at the lesion site. As previous studies have reported that acidic FGF[135] and HGF[136] reduced the astrocytic scar formation in injured spinal cord, we speculate that the attenuated glial scar is possibly due to greater amounts of FGF2 and HGF in NV-IONP. Furthermore, as one of the functions of glial scar formation is preventing the spread of inflammation,[137] the anti-inflammatory effect of NV-IONP may have induced the attenuation of astrogliosis.

The increased apoptosis that occurs after SCI is also detrimental to functional recovery. To evaluate apoptosis at the lesion site after SCI, terminal deoxynucleotidyl transferase dUTP nick end labeling (TUNEL) staining was performed at 7 days post-injury (Figure 3.11D). The number of TUNEL-positive cells in the spinal cord was increased after SCI. The injection of NV-IONP (MF+) remarkably reduced the number of apoptotic cells, Moreover, western blot assay for cleaved caspase-3 (C-Cas-3), an apoptotic marker, showed a strong inhibition of apoptosis in the NV-IONP (MF+) group (Figure 3.11B). The reduced apoptosis in the NV-IONP (MF+) group is likely due to targeted delivery of NV-IONP that contain large amounts of anti-apoptotic factors including VEGF, FGF2, and HGF.

The injured spinal cord retrieved at 28 days post-injury revealed the efficient preservation of its structure after injection of NV-IONP (MF+) (Figure 3.11E). The morphological observation revealed that the width of the lesion (dotted green circle) was constant after injection of NV-IONP (MF+). Furthermore, Masson's trichrome staining of the lesion site showed significantly reduced fibrotic area (dotted green area) and efficient preservation of both, white and grey matter in the spinal cord after injection of NV-IONP (MF+).

Functional recovery after SCI was assessed in open-field testing by the Basso Mouse Scale (BMS) score until 28 days post-injury (Figure 3.11F). Animals that develop paraplegia after SCI exhibit a low BMS score, and functional recovery after SCI is indicated by the gradual increase in the score. The result revealed that, although the NV and NV-IONP (MF-) groups showed a higher BMS score compared to PBS group at 28 days post-injury, there was no significant difference among the scores, possibly due to insufficient targeting efficiency of NV and NV-IONP in absence of magnetic field. In contrast, the injection of NV-IONP and their subsequent magnetic guidance showed a significant improvement in functional recovery after SCI.

Chapter 4. Stem Cell-derived Magnetic Nanovesicles Target and Attenuate Ischemic Stroke

4.1. Introduction

Ischemic stroke is one of the most lethal diseases and leading cause of long-term disability.[138] Main pathological event of ischemic stroke is temporary brain ischemia occurred by blood vessel occlusion, resulting a neuronal damage of brain tissue.[139] Severe inflammation in microenvironment of damaged brain tissue also contributes to exacerbation of neuronal injury and brain dysfunction.[140] Oxidative stress caused by ischemia and reperfusion in brain tissue activates macrophages to release pro-inflammatory cytokines, leading to detrimental outcomes in brain microenvironment.[141, 142]

As a promising neuronal regenerative strategy, administration of mesenchymal stem cells (MSC) has gained widespread attention for treatment of cerebral ischemic stroke.[143, 144] MSC are one of the most promising tools in cell-based therapeutics and regenerative medicine. Due to its unique properties, MSC have generated considerable interest in various clinical applications.[1, 145, 146] MSC release therapeutic biomolecules that promote angiogenesis,[147] anti-apoptotis,[148] immunomodulation,[149] and therefore have a great potential in the treatment of ischemic stroke. However, in spite of those advantages, there are still few considerations about delivering the MSC *in vivo*. Direct intra-cerebral implantation of stem cells in ischemic brain is invasive operation that can cause an additional damage of normal brain tissues, thus can be more concerned in clinical trials.[150] Furthermore, administered MSC show poor survival rate in inflammatory and ischemic lesion.[151] Indeed, intravenous administration is simpler and less invasive route compared to direct implantation, therefore a highly preferred route for patients suffering from severe clinical condition. However, systemic delivery of MSC poses a problem such as lung entrapment causing the poor accumulation of administered MSC in ischemic brain. Due to the large diameter of MSC (15 ~ 40 μm), pulmonary capillary acts as a barrier which captures the intravenously infused

MSC and cause decreased blood flow velocity.[5, 123, 124] Consequently, systemically administered MSC lack their targeting ability *in vivo*. Because the size of MSC causes lung accumulation, there has been increased demand of nano-sized therapeutic agent with similar therapeutic functions to those of MSC.

Exosomes, recently emerged as preferable option for cell-free therapeutics, are nano-sized extracellular vesicles which contain various genes and proteins produced from donor cells.[73] Once reached to target cells, exosome deliver various mRNAs and proteins inducing biological process and signaling pathways, thereby elicit the physiological changes in target cells. Moreover, nanoscopic size and surface proteins enable exosomes to penetrate interstitial space among the organs and to accumulate in target tissue.[52] Based on compelling evidences of therapeutic effects from MSC, exosomes derived from MSC have been studied as a therapeutic agent for treatment of various CNS injuries,[82, 91] including ischemic stroke.[41, 152-154] These reports support an evidence that the MSC-derived exosomes exert similar or equivalent therapeutic functions to those of MSC in treatment of ischemic stroke. Furthermore, exosomes provide several benefits over the MSC that exosomes are independent from cell viability, can pass the pulmonary capillaries after intravenous administration, and have a lower possibility of immune-rejection.[76] However, as well as from other mammalian cells, very small quantities of exosomes are released from MSC. Less than 4 μg of exosomes per day are produced from one million MSC,[51] indicating that collecting sufficient amount of naturally secreted exosomes for pre-clinical or clinical studies is impractical and highly laborious. Furthermore, repetitive cell culture can cause poor expression of growth factors in MSC, which would significantly reduce the therapeutic efficacy of exosomes released from those MSC.[93] Importantly, poor *in vivo* targeting ability of systemically administered exosomes toward the target tissue still remain as critical

challenge for further therapeutic application.[94-96] Surface modification of exosome with peptide can enhance accumulation of MSC-exosomes in ischemic brain,[154] however, conjugation of targeting moieties require multiple chemical reaction steps which may affect the function of exosomal proteins. Moreover, therapeutic agent such as curcumin, was additionally loaded on MSC-exosomes to improve their therapeutic efficacy.

In this context, rather than integration of additional targeting moieties or therapeutic agent in natural exosomes, we synthesized therapeutic efficacy-potentiated magnetic nanovesicles (MNV) by simple utilization of iron oxide nanoparticles (IONP). According to our previous studies that the treatment of IONP activates the phosphorylation of c-Jun and JNK molecules,[24, 101] signaling cascades associated with growth factor expressions,[102, 155] we discovered that the expressions of therapeutic growth factors in MSC were markedly upregulated in time-dependent manner after the treatment of IONP (MSC-IONP). Fabricated by serial extrusion of MSC-IONP, MNV contained significantly larger amount of therapeutic growth factors compared to control nanovesicle (NV) isolated from untreated MSC. In addition to growth factors, MNV also contained IONP which act as a navigator of MNV to target ischemic brain with assistance of external magnetic field (Figure 4.1). Together, we demonstrate that the simple treatment of IONP to MSC can provide not only magnetic properties but also potentiated therapeutic efficacy of MSC-derived nanovesicles.

4.2. Result and discussion

4.2.1. IONP uptake and enhanced therapeutic growth factors in MSC

We first investigated the physiological properties of iron oxide nanoparticles (IONP), and its biological effects including therapeutic growth factor up-regulation in MSC. PEG-ylated superparamagnetic IONP with size of 12 nm were fabricated, and treated to human bone marrow-derived MSC. Transmission electron microscopy (TEM) showed the shape and size of IONP, and internalization to MSC (Figure 4.1A). Agglomerated IONP clusters (red arrows) were observed in endosomes of MSC-IONP. To determine the cytotoxicity, IONP were treated to MSC with increasing concentration from 5 to 160 μg/mL, and incubated for 16 h (Figure 4.1B). Measured by CCK-8 assay, IONP did not show significant cytotoxicity up to concentration of 80 μg/mL. MSC-IONP with increasing dose of IONP, were investigated by Prussian blue staining (Figure 4.1C). Blue pigments which indicate internalized IONP, were distributed in cytoplasm of MSC. Next, we investigated whether the treatment of IONP induce cell proliferation of MSC (Figure 4.1D). Measured until 72 h after removal of IONP-containing cell medium, MSC proliferation was significantly increased in dose-dependent manner, indicating internalized IONP influenced the biological process of MSC. Thus, we evaluated the expressions of various therapeutic growth factors and cytokines associated with angiogenesis (Ang-1, FGF2, HGF, VEGF, PDGF, TGF-β1, TGF-β3), anti-apoptosis (FGF2, HGF, VEGF, PDGF, TGF-β1, TGF-β3), neurotrophic (NGF, BDNF, GDNF, NT3, NT4), and anti-inflammation (TGF-β1, TGF-β3), in MSC-IONP at 2, 24, 48 h after treatment of 40 μg/mL IONP (Figure 4.1E). Those respective genes were markedly up-regulated in a time-dependent manner until 48 h, as compared to untreated MSC. We

discovered that low pH in intracellular endosome partially ionize IONP into iron ions, and stimulate the JNK and c-Jun signaling pathways (Figure 4.1F). Whole cell lysate of MSC-IONP was collected 48 h after IONP treatment, and analyzed by western blot and corresponding quantification. Expressions of Ang-1, FGF2, HGF, VEGF, BDNF, and TGF-β3 were significantly increased in MSC-IONP compared to untreated MSC. Enhanced expressions of therapeutic growth factors were attributed to phosphorylation of JNK and c-Jun signaling molecules.

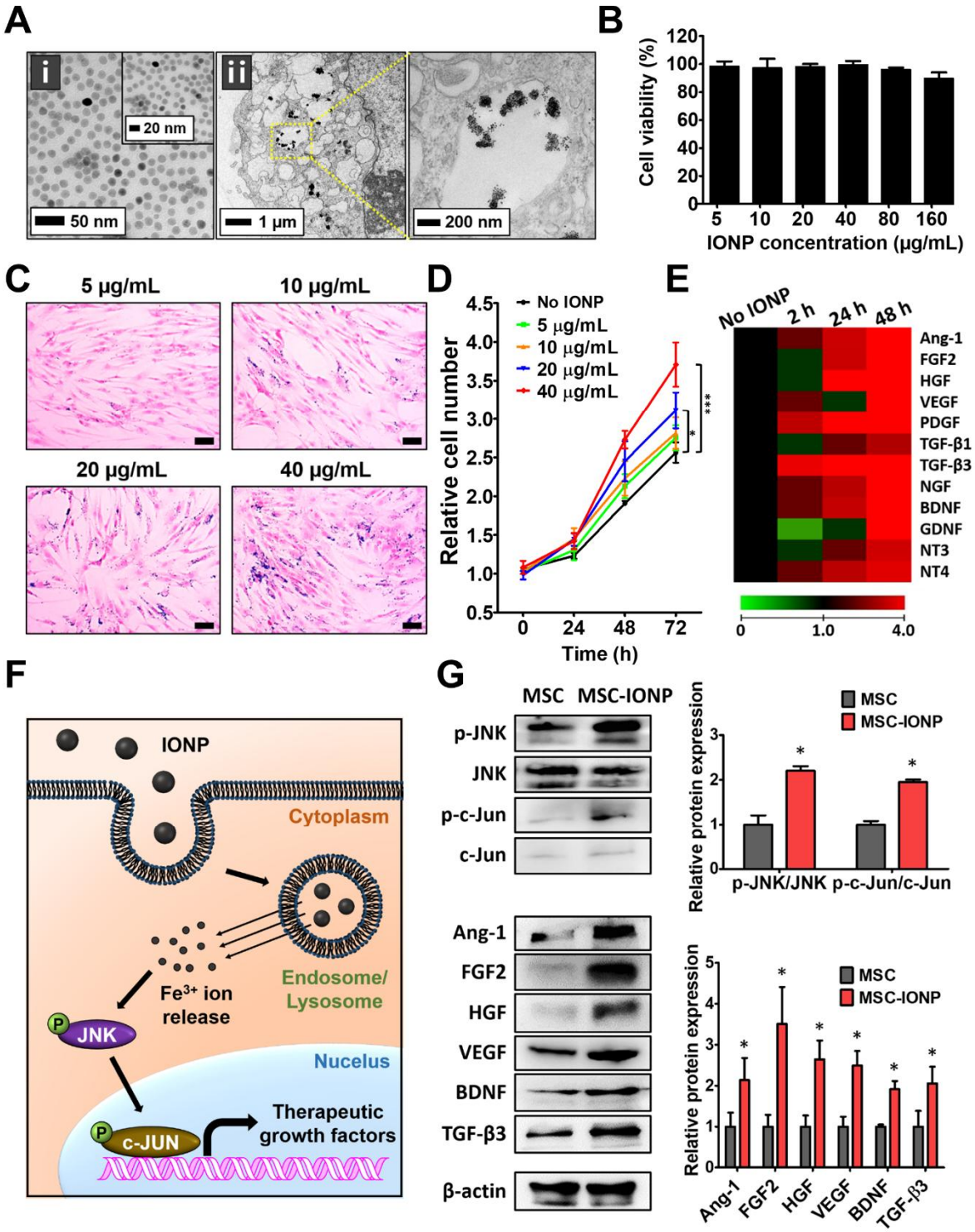

Figure 4.1. Enhanced expression of angiogenic, neuroprotective, and anti-inflammatory factors in MSC by IONP. (A) Transmission electron microscopy of (i) IONP and (ii)

MSC-IONP. The dotted yellow box indicates cell endosome in MSC-IONP. (B) Cell viability of MSCs at 16 h after incubation with various concentrations of IONP. (C) Dose-dependent uptake of IONP by MSC, as evaluated by Prussian blue staining. Blue pigments indicate internalized IONP. Bars = 100μm. (D) The proliferative behavior of MSC-IONP until 72 h after treatment of various concentrations of IONP. *P<0.05, ***P<0.001. (E) Relative mRNA expressions of angiogenic, neuroprotective, and anti-inflammatory factors in MSC-IONP, as evaluated by qRT-PCR analysis. (F) Schematic illustration of intracellular mechanism underlying the growth factor up-regulations in MSC-IONP. (G) Western blotting and quantification of Ang-1, FGF2, HGF, VEGF, BDNF, and TGF-β3 expressions in MSC and MSC-IONP. *P<0.05 versus MSC.

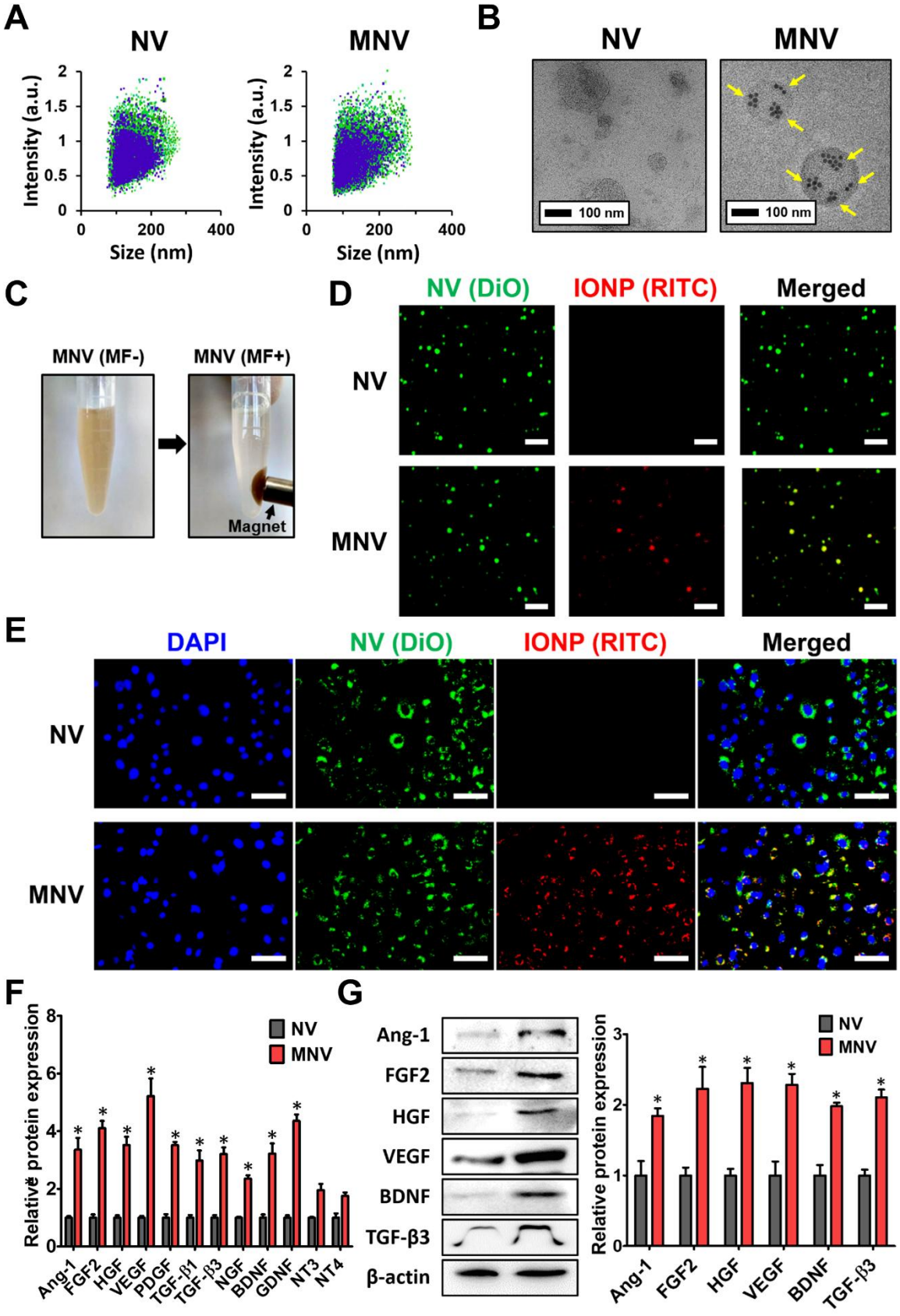
A
NV
MNV
Intensity (a.u.)
Size (nm)
B
NV
MNV
100 nm
C
MNV (MF-)
MNV (MF+)
Magnet
D
NV (DiO)
IONP (RITC)
Merged
NV
MNV
E
DAPI
NV (DiO)
IONP (RITC)
Merged
NV
MNV
F
Relative protein expression
NV
MNV
Ang-1
FGF2
HGF
VEGF
PDGF
TGF-β1
TGF-β3
NGF
BDNF
GDNF
NT3
NT4
G
Ang-1
FGF2
HGF
VEGF
BDNF
TGF-β3
β-actin
Relative protein expression
NV
MNV
Ang-1
FGF2
HGF
VEGF
BDNF
TGF-β3

Figure 4.2. Characterization of NV and MNV. (A) Size distribution of NV and MNV. (B) Transmission electron microscopy of NV and MNV. Yellow arrows indicated IONP. (C) Magnetization of MNV by application of external magnetic field (MF). (D) Fluorescence observation of NV and MNV. Lipid bilayer of NV and MNV was stained with DiO (green) lipophilic dye, and RITC-labeled IONP was used for synthesis of MNV. Scale bar = 2 μm. (E) PC12 cells treated with NV or MNV. Blue indicates cell nuclei (DAPI). Scale bar = 50 μm. (F) qRT-PCR and (G) western blot analysis of various therapeutic factors in NV and MNV. *$P<0.05$ versus NV.

4.2.2. IONP and higher level of therapeutic growth factors in MNV

According to qRT-PCR and western blot analysis that gene and protein expressions of therapeutic growth factors are significantly enhanced in MSC-IONP at 48 h after IONP treatment, MSC-IONP were harvested at 48 h post-treatment of IONP and serially extruded to 10, 5, 1, and 0.4 μm pore-sized membrane filters to fabricate MNV. Non-encapsulated IONP were removed during the synthesis. NV isolated from untreated MSC were served as control. Hydrodynamic size of NV and MNV was measured using dynamic light scattering (DLS) analysis (Figure 4.2A). NV and MNV showed the average size of 168.3 ± 48.3 and 194.2 ± 44.5 nm, respectively. Next, TEM observation of NV and MNV revealed their spherical formation (Figure 4.2B). Importantly, it demonstrated that IONP were successfully encapsulated in MNV (yellow arrows indicate IONP). To determine the magnetic properties of MNV, external magnetic field (MF) was applied to MNV (Figure 4.2C). Neodymium magnet was placed on side of MNV-containing tube, and the MNV pellet was observed near the magnet after 10 min of magnetization. Encapsulation of IONP in MNV was further confirmed with confocal microscopy (Figure 4.2D and 4.2E). MNV were fabricated using IONP labeled with Rhodamine-B-Isothiocyanate (RITC, red), and their surface lipid bilayer was stained with 3,3′-dioctadecyloxacarbocyanine perchlorate (DiO, green). Confocal microscopy observation of MNV revealed the overlapped locations of green and red fluorescence signals, indicating the successful encapsulation of IONP inside MNV (Figure 4.2D). To evaluate their stable incorporation during the cellular internalization, PC12 cells were treated with MNV (Figure 4.2E). At 4 h after treatment of MNV, cells showed both green and red fluorescence signal with their overlapped locations. In contrast, cells treated with NV showed only green fluorescence signals due to the absence of IONP. We next determined whether the enhanced expressions of therapeutic growth factors in MSC-IONP

can be transferred to MNV. qRT-PCR analysis showed that MNV contain significantly larger amounts of mRNAs encoding those growth factors, as compared to NV (Figure 4.2F). Western blotting also revealed that increased protein level of therapeutic growth factors was contained in MNV than NV (Figure 4.2G). These results demonstrate that MNV encapsulate not only IONP as magnet navigating tool, but also significantly larger amount of therapeutic factors to treat ischemic stroke.

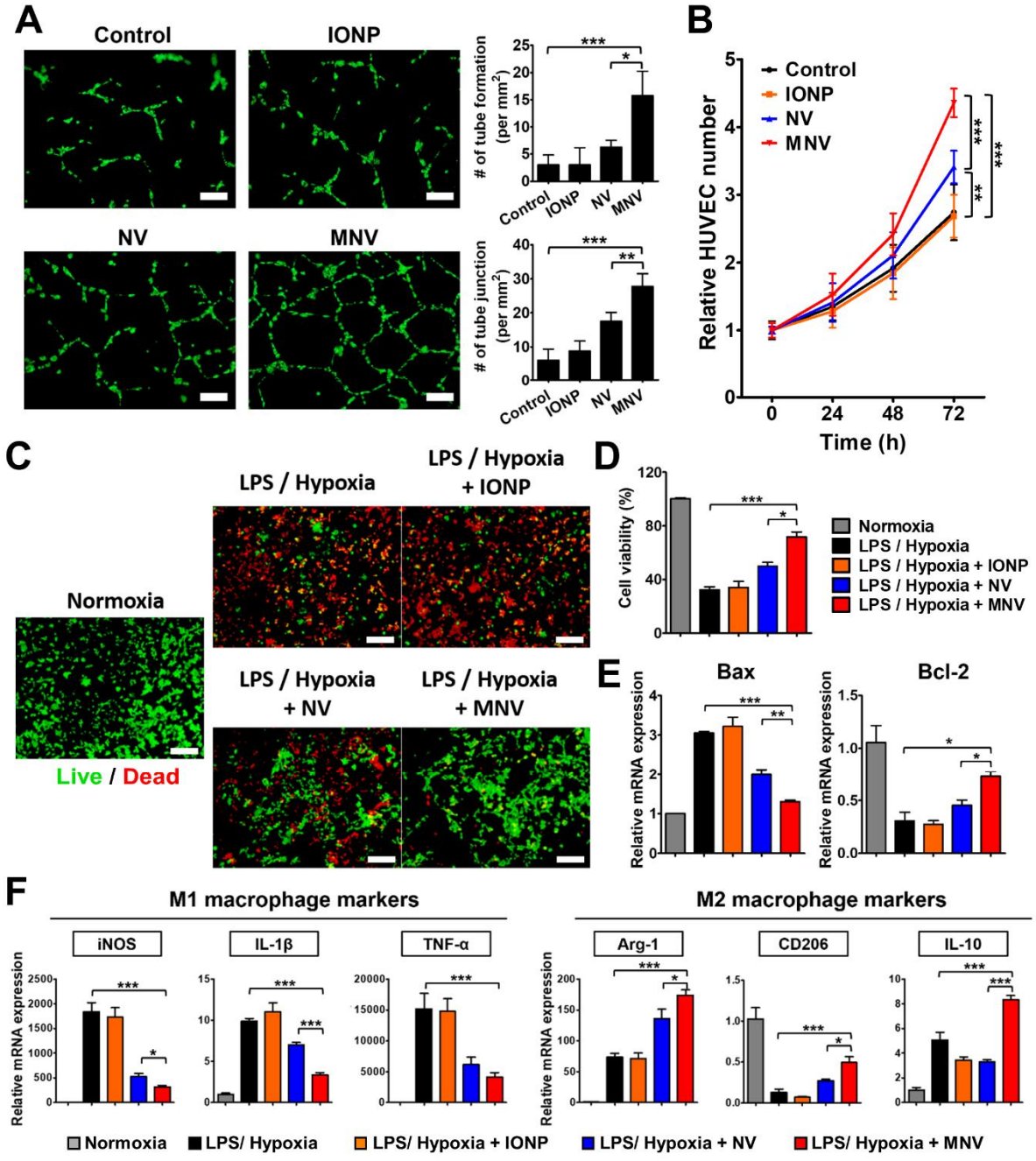

Figure 4.3. In vitro angiogenic, neuroprotective, and anti-inflammatory effects of NV and MNV on endothelial cells (HUVEC), neuronal cells (PC12 cells), and rat bone marrow-derived macrophages (rBMDM) (a) Angiogenic behavior of HUVEC after treatment with IONP, NV, or MNV, as determined by tube formation assay. HUVEC were stained with DiO, a green fluorescent dye. Bars = 100 μm. Number of tubes and tube junctions were quantified. *P<0.05, **P<0.01, ***P<0.001. (b) Increased proliferation of

HUVEC after various treatments. Relative cell number was determined by CCK-8 assay. **P<0.01, ***P<0.001. (c) Cell viability of PC12 cells treated with IONP, NV, or MNV, followed by incubation under inflammatory (LPS) and hypoxic condition (1% O2). For visualization of live and dead cells, PC12 cells were stained with FDA (green) and EB (red), respectively. (d) Viability of PC12 cells was quantified by CCK-8 assay. (e) Relative values of Bax (apoptotic) and Bcl-2 (anti-apoptotic) were evaluated by qRT-PCR analysis. The normoxia group did not receive LPS treatment and hypoxia. *P<0.05, **P<0.01, ***P<0.001. (f) Relative mRNA expressions of M1 (iNOS, IL-1β, and TNF-α) and M2 (Arg-1, CD206, and IL-10) macrophage markers in rBMDM after various treatments. rBMDM were pre-activated to M1 state by LPS treatment and hypoxia. The normoxia group did not receive LPS treatment and hypoxia. *P<0.05, ***P<0.001.

4.2.3. *In vitro* therapeutic effects of MNV

Next we investigated whether the increased growth factors in MNV exert enhanced angiogenic, anti-apoptotic, and anti-inflammatory effect. Human umbilical vein endothelial cells (HUVEC), neuron-like PC12 cells, and rat bone marrow-derived macrophages (rBMDM) were treated with IONP (0.68 μg/mL), NV, and MNV (40 μg/mL). IONP with concentration of 0.68 μg/mL, an equal concentration of IONP inside 40 μg/mL of MNV (17 ng of IONP in 1 μg of MNV), were served as a control to determine whether the function of MNV is an effect from therapeutic growth factors or IONP inside MNV.

First, angiogenic activity of HUVEC was determined by tube formation assay. HUVEC fluorescently labeled with 3,3´-dioctadecyloxacarbocyanine perchlorate (DiO), were seeded on matrigel-coated well and incubated in presence of IONP, NV, or MNV (Figure 4.3A). After 8 h, capillary tube formation of HUVEC was prominent in MNV-treated group. By quantified analysis, number of tube formation and tube junctions were significantly increased in HUVEC treated with MNV, as compared to IONP- or NV-treated HUVEC. Proliferation behavior of HUVEC after various treatment revealed the similar tendency (Figure 4.3B). Measured until 72 h after treatment, HUVEC incubated with MNV showed the most active proliferation. This result may attribute to larger amounts of therapeutic growth factors inside MNV which contribute to angiogenesis of endothelial cells.[108, 156] Next, we investigated whether MNV show anti-apoptotic and neuroprotective effect on neuron-like PC12 cells in inflammatory and hypoxic condition, which are representative pathological events in brain microenvironment after ischemic stroke.[157] To induce apoptosis, PC12 cells were treated with lipopolysaccharide (LPS, 5 μg/mL) and incubated under hypoxic (1% O_2) condition.[158, 159] Cells were pre-treated with IONP, NV, or MNV before inducing apoptosis. After 24 h, survival of PC12 cells was evaluated by live (green) and dead (red) staining

(Figure 4.3C), and quantified by CCK-8 assay (Figure 4.3D). Pre-treatment of MNV significantly alleviated the apoptosis of PC12 cells, as compared to IONP or NV. The expressions of pro-apoptotic Bax, and anti-apoptotic Bcl-2 were measured by qRT-PCR (Figure 4.3E). Compared to other groups, Bax was significantly down-regulated and Bcl-2 was up-regulated in MNV-treated group.

Next, we investigated the anti-inflammatory effect of MNV. Macrophages, in terms of distinctive phenotypes and functions, can be classified to pro-inflammatory and cytotoxic state (M1) and anti-inflammatory and regenerative state (M2).[160] During the progression of stroke, the M1 phenotype drastically increases in peri-infarct regions, and release pro-inflammatory cytokines that exacerbate neuronal injury.[161] Phenotypic transition of M1 macrophages toward M2 subtype can prevent further brain damage.[162] To determine whether MNV elicit M2 polarization of M1 macrophages, we first activated rBMDM to M1 state by LPS and culturing them under hypoxic condition. Then, M1-induced rBMDM were treated with IONP, NV, or MNV. After 48 h, mRNA expressions of M1 markers (iNOS, IL-1β, and TNF-α) and M2 markers (Arg-1, CD206, and IL-10) were evaluated (Figure 4.3F). In contrast to non-activated rBMDM (normoxia), M1-induced rBMDM showed up-regulated M1 markers. However, treatment of MNV resulted in significant down-regulation of those M1 markers. Meanwhile, M2 markers were markedly up-regulated after the treatment of MNV. In the above *in vitro* experiments, treatment of IONP did not showed significant differences compared to control group. This demonstrates that the potentiated biological effect of MNV is an effect of larger amount of therapeutic growth factors rather than the incorporated IONP.

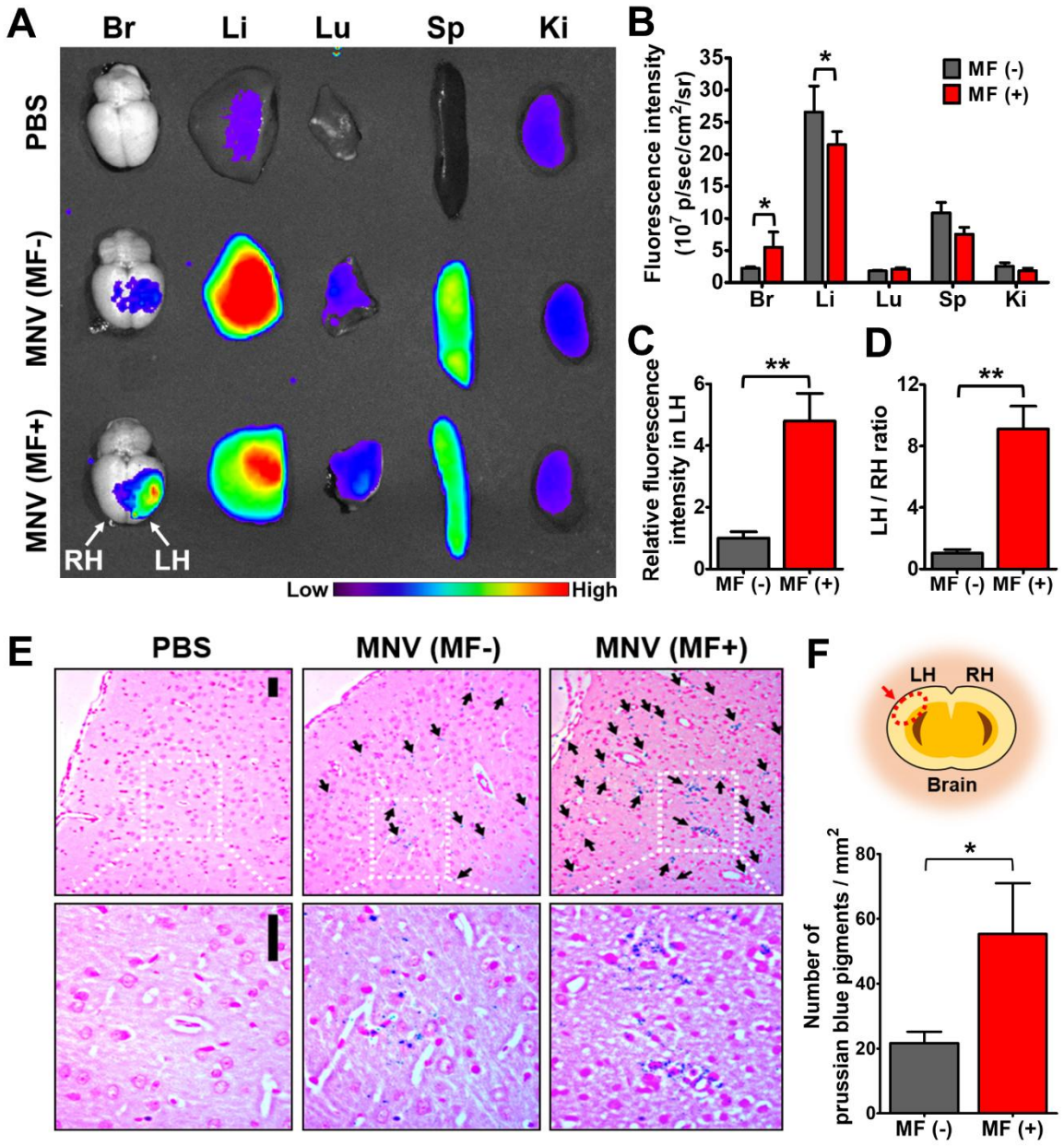

Figure 4.4. In vivo targeting of ischemic stroke lesion of MCAO rats by systemic injection of MNV with application of external magnetic field (MF). (A) Biodistribution of intravenously injected MNV with or without MF, as evaluated by IVIS imaging of major organs. (Br: brain, Li: liver, Lu: lung, Sp: spleen, Ki: kidney), LH: left hemisphere (ischemic lesion), RH: right hemisphere (non-ischemic region) (B) Quantitative fluorescence

measurement of major organs collected from rats injected with MNV, with or without MF. **P<0.05. (C) Comparison of fluorescence intensity in ischemic lesion between MNV (MF-) and MNV (MF+). **P<0.01. (D) Normalized ratio of fluorescence intensity in LH versus RH, indicating ischemic lesion-specific accumulation of MNV in presence of MF. **P<0.01. (E) Prussian blue staining of ischemic stroke lesion of rats injected with MNV with or without MF. Blue pigments (black arrows) indicate IONP inside MNV. Bars = 50 μm. (F) Number of blue pigments were quantified. *P<0.05.

4.2.4. Magnet-assisted ischemic lesion targeting of MNV

To evaluate the feasibility of MNV for magnet-guided targeting toward ischemic stroke lesion, we next performed fluorescence imaging to track the intravenously injected MNV in transient middle cerebral artery occlusion (MCAO)-induced rats. After reperfusion, MNV were injected *via* the lateral tail vein. MNV were fluorescently labeled with a lipophilic dye VivoTrack 680 before injection. As an external magnetic field (MF), magnet helmet was applied to MCAO rats. After 24 h of post-injection, major organs including brain, liver, lung, spleen, and kidney were obtained from MCAO rats, and fluorescently visualized with IVIS fluorescence imaging system (Figure 4.4A). The fluorescence imaging revealed that MNV are partially accumulated in brain without MF, however, a majority of injected MNV were accumulated in liver and spleen. This result corresponds to previous reports that systemically administered extracellular vesicles rapidly accumulate in organs of the reticuloendothelial system, such as liver and spleen.[94, 96, 154] Nevertheless, fluorescence signals in ischemic brain was markedly increased in MNV (MF+) group, notably in the left hemisphere (LH, ischemic lesion) where the magnet was placed above. Region-of-interest analysis of major organs collected from MNV (MF+) group also revealed that MNV were significantly less accumulated in liver, thereby targeted the ischemic brain 2.9-fold higher than MNV (MF-) group (Figure 4.4B). Narrowing down the scope to LH of brain (Figure 4.4C), MNV (MF+) showed 5.1-fold increased fluorescence intensity compared to MNV (MF-). Moreover, the fluorescence ratio of LH to right hemisphere (RH) showed as high as 9.2-fold following application of external MF (Figure 4.4D). Next, brain tissue sections were obtained, and the accumulation of MNV in ischemic lesion was observed by Prussian blue staining. LH of cerebral cortex was observed with optical microscopy (Figure 4.4E). Quantification of blue

pigments which indicates IONP inside MNV, demonstrated that significantly larger amount of MNV were accumulated in ischemic lesion in presence of MF (Figure 4.4F).

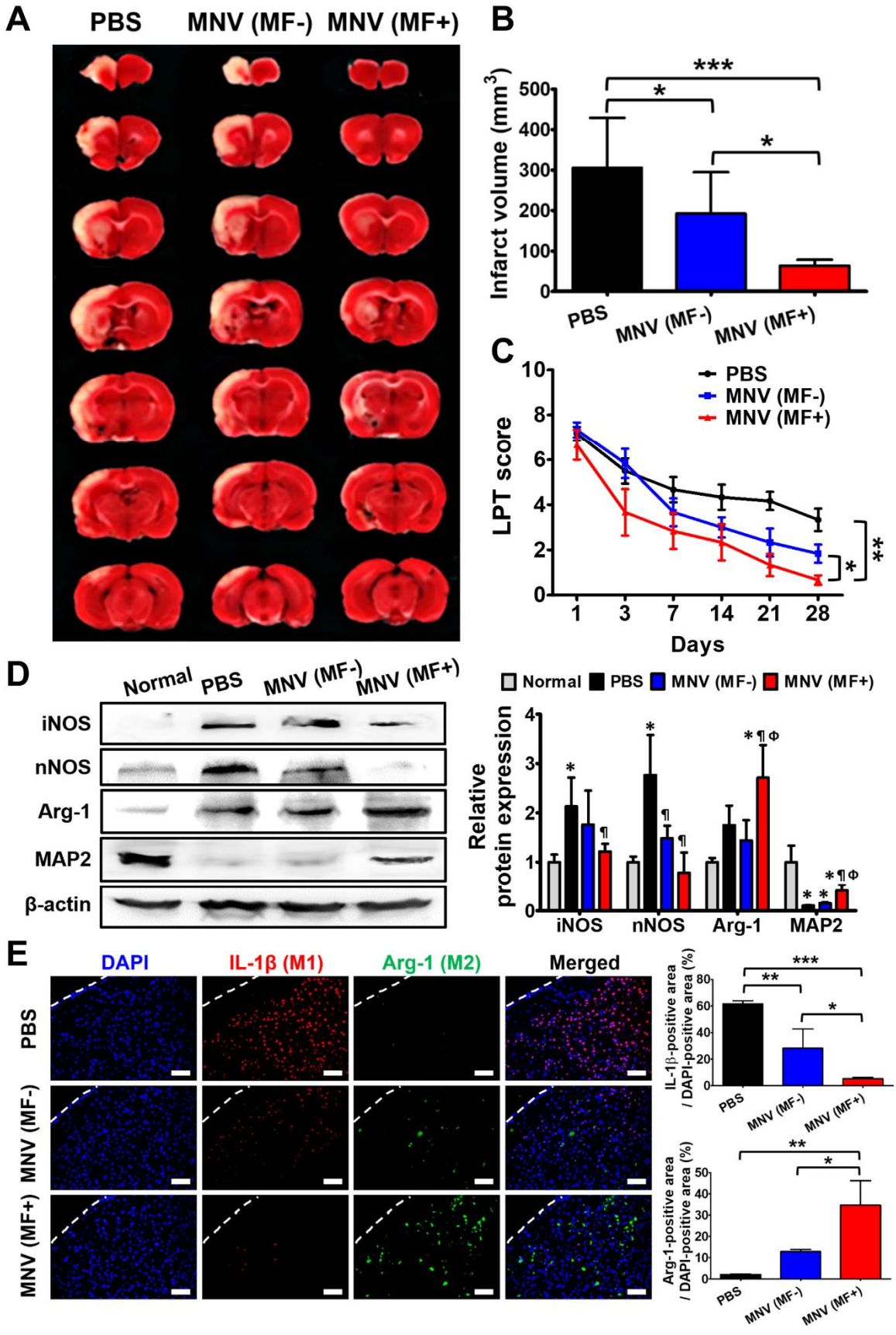
A
PBS
MNV (MF-)
MNV (MF+)
B
Infarct volume (mm3)
500
400
300
200
100
0
***
*
*
PBS
MNV (MF-)
MNV (MF+)
C
LPT score
10
8
6
4
2
0
PBS
MNV (MF-)
MNV (MF+)
*
**
1
3
7
14
21
28
Days
D
Normal
PBS
MNV (MF-)
MNV (MF+)
iNOS
nNOS
Arg-1
MAP2
β-actin
Normal
PBS
MNV (MF-)
MNV (MF+)
Relative protein expression
4
3
2
1
0
iNOS
nNOS
Arg-1
MAP2
E
DAPI
IL-1β (M1)
Arg-1 (M2)
Merged
PBS
MNV (MF-)
MNV (MF+)
IL-1β-positive area / DAPI-positive area (%)
80
60
40
20
0
***
**
*
PBS
MNV (MF-)
MNV (MF+)
Arg-1-positive area / DAPI-positive area (%)
50
40
30
20
10
0
**
*
PBS
MNV (MF-)
MNV (MF+)

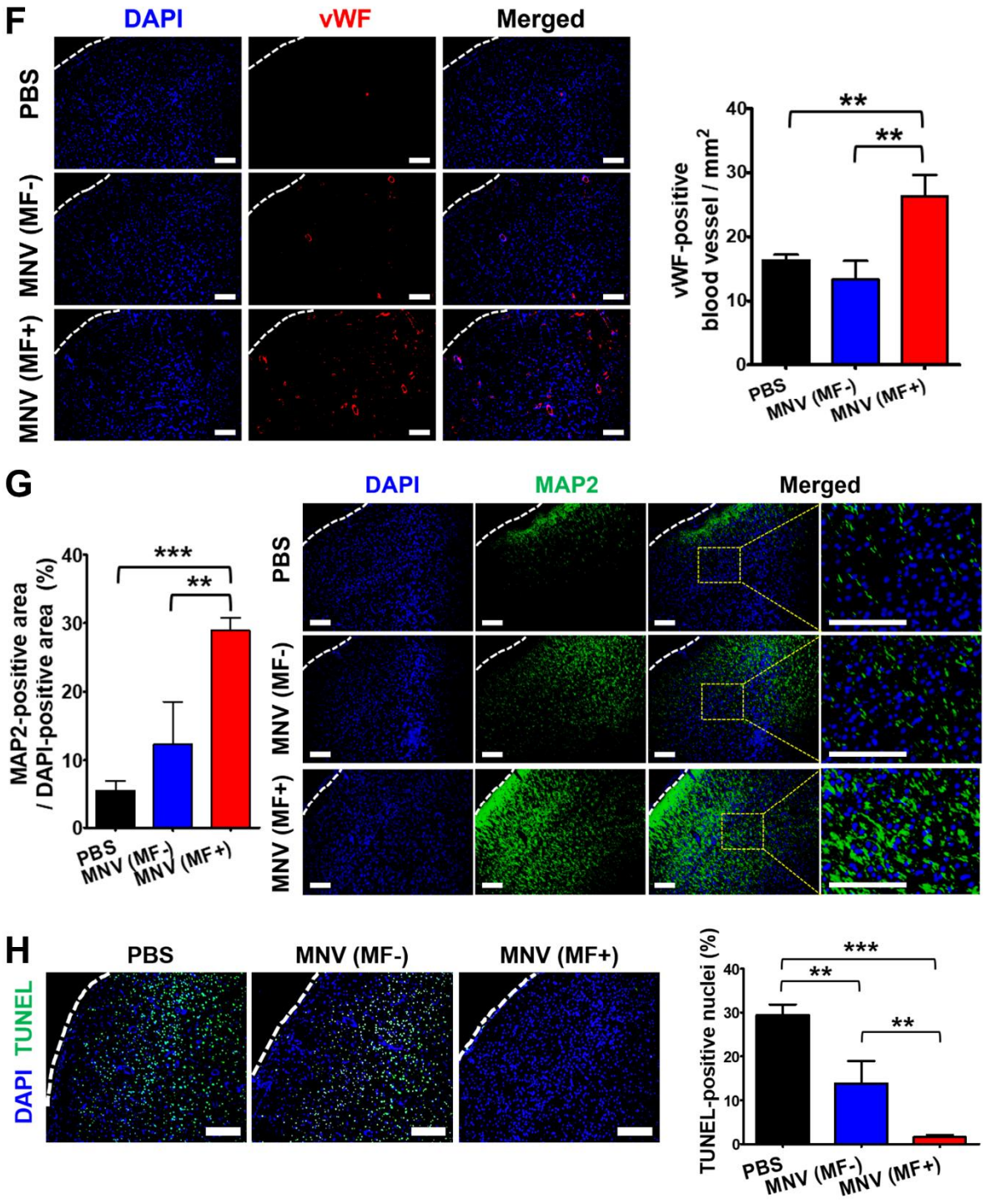

Figure 4.5. In vivo therapeutic effect of MNV in ischemic stroke. (A) TTC staining of serial sections of brain tissues and quantification of the cerebral infarction volume in MCAO rats systemically administered with PBS, MNV (MF-) or, MNV (MF+) (n = 11 per group). (B) Infarct volume of rat MCAO models after different treatments. *P<0.05, ***P<0.001. (C)

LPT score-based quantitative analysis of functional recovery until 28 days after MCAO (n = 6). *P<0.05, **P<0.01. (D) Western blot and corresponding quantification of M1 (iNOS and nNOS) and M2 (Arg-1) macrophage markers, and neuronal marker (MAP2) in brain tissue lysate of MCAO rats. The normal group did not receive MCAO. *, ¶, and Φ indicate significant differences in comparison with the normal, PBS, and MNV (MF-) groups, respectively. (E) Macrophage polarization in ischemic brain tissues obtained from different groups, evaluated by IHC staining against M1 (IL-1β, red) and M2 (Arg-1, green) markers. Bars = 50 μm. *P<0.05, **P<0.01, ***P<0.001. (F) IHC staining for blood vessels (vWF, red) in ischemic brain tissues obtained from different groups, **P<0.01. Bars = 50 μm. (G) Evaluation of neuronal survival in ischemic brain by IHC staining of MAP2 (green), followed by quantitative analysis. Bars = 100μm. **P<0.01, ***P<0.001. (H) Fluorescence microscopy images and quantification of apoptotic TUNEL-positive cells (green) in ischemic stroke lesion. Bars = 100 μm. **P<0.01, ***P<0.001.

4.2.5. *In vivo* therapeutic effect and mechanism of MNV for treatment of ischemic stroke

To investigate the therapeutic effect of MNV in ischemic stroke, we measured and compared the infarct volume at 3 days after MCAO and injection of MNV. The infarct volume in brain of MNV (MF+) group was significantly reduced compared to that in the brain of MNV (MF-) and PBS groups (75.48 ± 28.62 mm^3 in MNV (MF+) vs. 168.50 ± 105.70 mm^3 in MNV (MF-) vs. 272.6 ± 132.4 mm^3 in PBS) (Figure 4.5A and 4.5B). Possibly due to partial accumulation in ischemic lesion, MNV (MF-) also decreased the infarction volume, as compared to PBS control group (Figure 4.5B). These results showed that MNV administration decreased the infarct volume, especially the application of external magnet noted to effectively reduce infarct volume. The delivery of MNV (MF+) improved functional recovery after transient MCAO, compared to that in the MNV (MF-) and PBS groups (Figure 4.5C). It caused an amelioration of neurological deterioration during the monitoring period, and the functional recovery was significant at 28 days.

We next determined the therapeutic mechanism of MNV. On the basis of *in vitro* findings, anti-inflammatory, angiogenic, and neuroprotective events were assessed. Evaluated by western blot analysis of brain tissue lysate collected from different groups (Figure 4.5D), pro-inflammatory M1 markers such as iNOS and nNOS were significantly attenuated in MNV (MF+) group, as compared to PBS and MNV (MF-) groups. Meanwhile, expression of Arg-1 (M2 marker) and MAP2 (neuronal marker) in MNV (MF+) group were significantly higher than others. Furthermore, as evaluated by immunohistochemical (IHC) staining (Figure 4.5E), MNV (MF+) group exhibited markedly attenuated IL-1β (M1) and increased Arg-1 (M2) expressions, as compared to PBS and MNV (MF-) groups. These result indicate that increased amount of MNV accumulated in ischemic lesion successfully polarized the

brain-resident macrophages (microglia) toward M2 subtype. We next stained the Von Willebrand factor (vWF), an endothelial cell marker to observe the angiogenesis in each group (Figure 4.5F). Although blood vessels were disrupted after ischemic stroke as shown in PBS injected group, MNV (MF+) injected group showed enhanced reconstruction of vascular system. Moreover, as determined by IHC staining of MAP2 (Figure 4.5G), MNV accumulated in ischemic lesion showed an excellent neuroprotection. As compared to ischemic lesion of PBS group in which severe neuronal loss was observed, population of neurons was notably higher in MNV (MF+) group. This was confirmed by TUNEL staining of ischemic lesion (Figure 4.5H). Highly increased number of TUNEL-positive cells in the brain tissue after MCAO was remarkably reduced by administration of MNV (MF+).

Chapter 5. Conclusion

This thesis presents the studies on systemic administration of IONP-incorporated exosome-mimetic nanovesicles in presence of external MF to specifically target and treat two representative CNS injuries, SCI and ischemic stroke.

Chapter 3 demonstrates the effective systemic targeting ability of NV-IONP. Furthermore, we discovered that IONP not only served as a navigating tool for systemic targeting, but also up-regulated the therapeutic growth factors in hMSC. Accordingly, NV-IONP successfully delivered large amounts of therapeutic growth factors to the injured spinal cord in the presence of a magnetic field. NV-IONP induced angiogenesis, anti-apoptosis, neuro-protection, and anti-inflammation by M2 polarization which are involved in repair of injured spinal cord. Systemic injection of NV-IONP, which were magnetically guided, in spinal cord-injured mice markedly enhanced the targeting efficacy toward injured spinal cord, alleviated spinal cord damage, and improved neuronal function.

Chapter 4 show the fabrication of MSC-derived nanovesicles with magnetic properties and their application for treatment of ischemic stroke. MSC treated with IONP showed enhanced expressions of therapeutic growth factors which are major contributors in angiogenesis, anti-apoptosis, and anti-inflammation. Moreover, those enhanced growth factors were stably incorporated in isolated MNV. Magnetic properties of MNV enabled MNV to specifically target ischemic brain with the help of external magnetic field. Accumulated MNV elicited polarization of macrophages in ischemic lesion from cytotoxic M1 to anti-inflammatory M2 subtype. MNV also improved the blood vessel formation of infarcted lesion, and consequently attenuated the neuronal damage. Due to those therapeutic functions, MCAO-induced rats showed significant functional recovery after the systemic administration of MNV in presence of external MF.

The results described in this thesis collectively demonstrate that IONP-incorporated exosome-mimetic nanovesicles can be served as nano-sized therapeutic agent capable of precise targeting the injured neuronal tissues such as spinal cord and cerebral lesion with help of external magnet. Their application may be a potential new therapy for CNS injuries, and can be expanded to treat various diseases including myocardial infarction that involve the sequence of tissue damage, inflammation, and tissue repair. The injured CNS-targeting efficacy of these IONP-incorporated nanovesicles can be further fortified by magnetic resonance imaging (MRI), because IONP are widely used as a contrast agent for MRI.[163] IONP-incorporated nanovesicles accumulated in injured tissues can be imaged *in vivo* or *ex vivo* by MRI. Therefore, these nanovesicles can be served as theranostic (therapy + diagnosis) agent for CNS injuries.

Furthermore, this cell-derived nanovesicle technology can be further expanded to other types of stem cells such as embryonic stem cells, hematopoietic stem cells, or induced pluripotent stem cells. In addition to stem cells, various types of immune cells such as macrophages, dendritic cells, or T cells can be subjected to extrusion to fabricate nanovesicles. Those immune cell-derived nanovesicles can be utilized in immuno-therapeutic studies.

References

1. Squillaro, T.; Peluso, G.; Galderisi, U., Clinical Trials With Mesenchymal Stem Cells: An Update. *Cell Transplant* **2016,** *25* (5), 829-48.

2. Crivelli, B.; Chlapanidas, T.; Perteghella, S.; Lucarelli, E.; Pascucci, L.; Brini, A. T.; Ferrero, I.; Marazzi, M.; Pessina, A.; Torre, M. L.; Italian Mesenchymal Stem Cell, G., Mesenchymal stem/stromal cell extracellular vesicles: From active principle to next generation drug delivery system. *J Control Release* **2017,** *262*, 104-117.

3. Dimmeler, S.; Burchfield, J.; Zeiher, A. M., Cell-based therapy of myocardial infarction. *Arterioscler Thromb Vasc Biol* **2008,** *28* (2), 208-16.

4. Moll, G.; Rasmusson-Duprez, I.; von Bahr, L.; Connolly-Andersen, A. M.; Elgue, G.; Funke, L.; Hamad, O. A.; Lonnies, H.; Magnusson, P. U.; Sanchez, J.; Teramura, Y.; Nilsson-Ekdahl, K.; Ringden, O.; Korsgren, O.; Nilsson, B.; Le Blanc, K., Are therapeutic human mesenchymal stromal cells compatible with human blood? *Stem Cells* **2012,** *30* (7), 1565-74.

5. Fischer, U. M.; Harting, M. T.; Jimenez, F.; Monzon-Posadas, W. O.; Xue, H.; Savitz, S. I.; Laine, G. A.; Cox, C. S., Jr., Pulmonary passage is a major obstacle for intravenous stem cell delivery: the pulmonary first-pass effect. *Stem Cells Dev* **2009,** *18* (5), 683-92.

6. Lukomska, B.; Stanaszek, L.; Zuba-Surma, E.; Legosz, P.; Sarzynska, S.; Drela, K., Challenges and Controversies in Human Mesenchymal Stem Cell Therapy. *Stem Cells Int* **2019,** *2019*, 9628536.

7. van Niel, G.; D'Angelo, G.; Raposo, G., Shedding light on the cell biology of extracellular vesicles. *Nat Rev Mol Cell Biol* **2018,** *19* (4), 213-228.

8. Colombo, M.; Raposo, G.; Thery, C., Biogenesis, secretion, and intercellular interactions of exosomes and other extracellular vesicles. *Annu Rev Cell Dev Biol* **2014,** *30*, 255-89.

9. Lo Cicero, A.; Stahl, P. D.; Raposo, G., Extracellular vesicles shuffling intercellular messages: for good or for bad. *Curr Opin Cell Biol* **2015,** *35*, 69-77.

10. Zha, Q. B.; Yao, Y. F.; Ren, Z. J.; Li, X. J.; Tang, J. H., Extracellular vesicles: An overview of biogenesis, function, and role in breast cancer. *Tumour Biol* **2017,** *39* (2), 1010428317691182.

11. Pisitkun, T.; Shen, R. F.; Knepper, M. A., Identification and proteomic profiling of exosomes in human urine. *Proc Natl Acad Sci U S A* **2004,** *101* (36), 13368-73.

12. Alvarez-Erviti, L.; Seow, Y.; Yin, H.; Betts, C.; Lakhal, S.; Wood, M. J., Delivery of siRNA to the mouse brain by systemic injection of targeted exosomes. *Nat Biotechnol* **2011,** *29* (4), 341-5.

13. Tricarico, C.; Clancy, J.; D'Souza-Schorey, C., Biology and biogenesis of shed microvesicles. *Small GTPases* **2017,** *8* (4), 220-232.

14. Mentkowski, K. I.; Snitzer, J. D.; Rusnak, S.; Lang, J. K., Therapeutic Potential of Engineered Extracellular Vesicles. *AAPS J* **2018,** *20* (3), 50.

15. Borger, V.; Bremer, M.; Ferrer-Tur, R.; Gockeln, L.; Stambouli, O.; Becic, A.; Giebel, B., Mesenchymal Stem/Stromal Cell-Derived Extracellular Vesicles and Their Potential as Novel Immunomodulatory Therapeutic Agents. *Int J Mol Sci* **2017,** *18* (7).

16. Liang, X. L.; Zhang, L. N.; Wang, S. H.; Han, Q.; Zhao, R. C., Exosomes secreted by mesenchymal stem cells promote endothelial cell angiogenesis by transferring miR-125a. *J Cell Sci* **2016,** *129* (11), 2182-2189.

17. Zhang, B.; Wu, X.; Zhang, X.; Sun, Y.; Yan, Y.; Shi, H.; Zhu, Y.; Wu, L.; Pan, Z.; Zhu, W.; Qian, H.; Xu, W., Human umbilical cord mesenchymal stem cell

exosomes enhance angiogenesis through the Wnt4/beta-catenin pathway. *Stem Cells Transl Med* **2015,** *4* (5), 513-22.

18. Lin, S. S.; Zhu, B.; Guo, Z. K.; Huang, G. Z.; Wang, Z.; Chen, J.; Wei, X. J.; Li, Q., Bone marrow mesenchymal stem cell-derived microvesicles protect rat pheochromocytoma PC12 cells from glutamate-induced injury via a PI3K/Akt dependent pathway. *Neurochem Res* **2014,** *39* (5), 922-31.

19. Liu, Z.; Xu, Y.; Wan, Y.; Gao, J.; Chu, Y.; Li, J., Exosomes from adipose-derived mesenchymal stem cells prevent cardiomyocyte apoptosis induced by oxidative stress. *Cell Death Discov* **2019,** *5*, 79.

20. Wang, Y.; Ma, W. Q.; Zhu, Y.; Han, X. Q.; Liu, N., Exosomes Derived From Mesenchymal Stromal Cells Pretreated With Advanced Glycation End Product-Bovine Serum Albumin Inhibit Calcification of Vascular Smooth Muscle Cells. *Front Endocrinol (Lausanne)* **2018,** *9*, 524.

21. Liu, W.; Wang, Y.; Gong, F.; Rong, Y.; Luo, Y.; Tang, P.; Zhou, Z.; Zhou, Z.; Xu, T.; Jiang, T.; Yang, S.; Yin, G.; Chen, J.; Fan, J.; Cai, W., Exosomes Derived from Bone Mesenchymal Stem Cells Repair Traumatic Spinal Cord Injury by Suppressing the Activation of A1 Neurotoxic Reactive Astrocytes. *J Neurotrauma* **2019,** *36* (3), 469-484.

22. Lo Sicco, C.; Reverberi, D.; Balbi, C.; Ulivi, V.; Principi, E.; Pascucci, L.; Becherini, P.; Bosco, M. C.; Varesio, L.; Franzin, C.; Pozzobon, M.; Cancedda, R.; Tasso, R., Mesenchymal Stem Cell-Derived Extracellular Vesicles as Mediators of Anti-Inflammatory Effects: Endorsement of Macrophage Polarization. *Stem Cells Transl Med* **2017,** *6* (3), 1018-1028.

23. Zhao, J.; Li, X.; Hu, J.; Chen, F.; Qiao, S.; Sun, X.; Gao, L.; Xie, J.; Xu, B., Mesenchymal stromal cell-derived exosomes attenuate myocardial ischaemia-reperfusion

injury through miR-182-regulated macrophage polarization. *Cardiovasc Res* **2019,** *115* (7), 1205-1216.

24. Kim, H. Y.; Kumar, H.; Jo, M. J.; Kim, J.; Yoon, J. K.; Lee, J. R.; Kang, M.; Choo, Y. W.; Song, S. Y.; Kwon, S. P.; Hyeon, T.; Han, I. B.; Kim, B. S., Therapeutic Efficacy-Potentiated and Diseased Organ-Targeting Nanovesicles Derived from Mesenchymal Stem Cells for Spinal Cord Injury Treatment. *Nano Lett* **2018,** *18* (8), 4965-4975.

25. Reis, M.; Mavin, E.; Nicholson, L.; Green, K.; Dickinson, A. M.; Wang, X. N., Mesenchymal Stromal Cell-Derived Extracellular Vesicles Attenuate Dendritic Cell Maturation and Function. *Front Immunol* **2018,** *9*, 2538.

26. Zhang, B.; Yeo, R. W. Y.; Lai, R. C.; Sim, E. W. K.; Chin, K. C.; Lim, S. K., Mesenchymal stromal cell exosome-enhanced regulatory T-cell production through an antigen-presenting cell-mediated pathway. *Cytotherapy* **2018,** *20* (5), 687-696.

27. Lai, R. C.; Arslan, F.; Lee, M. M.; Sze, N. S.; Choo, A.; Chen, T. S.; Salto-Tellez, M.; Timmers, L.; Lee, C. N.; El Oakley, R. M.; Pasterkamp, G.; de Kleijn, D. P.; Lim, S. K., Exosome secreted by MSC reduces myocardial ischemia/reperfusion injury. *Stem Cell Res* **2010,** *4* (3), 214-22.

28. Teng, X.; Chen, L.; Chen, W.; Yang, J.; Yang, Z.; Shen, Z., Mesenchymal Stem Cell-Derived Exosomes Improve the Microenvironment of Infarcted Myocardium Contributing to Angiogenesis and Anti-Inflammation. *Cell Physiol Biochem* **2015,** *37* (6), 2415-24.

29. Tsao, C. R.; Liao, M. F.; Wang, M. H.; Cheng, C. M.; Chen, C. H., Mesenchymal Stem Cell Derived Exosomes: A New Hope for the Treatment of Cardiovascular Disease? *Acta Cardiol Sin* **2014,** *30* (5), 395-400.

30. Shafei, A. E.; Ali, M. A.; Ghanem, H. G.; Shehata, A. I.; Abdelgawad, A. A.;

Handal, H. R.; Talaat, K. A.; Ashaal, A. E.; El-Shal, A. S., Mesenchymal stem cell therapy: A promising cell-based therapy for treatment of myocardial infarction. *J Gene Med* **2017,** *19* (12).

31. Hu, G. W.; Li, Q.; Niu, X.; Hu, B.; Liu, J.; Zhou, S. M.; Guo, S. C.; Lang, H. L.; Zhang, C. Q.; Wang, Y.; Deng, Z. F., Exosomes secreted by human-induced pluripotent stem cell-derived mesenchymal stem cells attenuate limb ischemia by promoting angiogenesis in mice. *Stem Cell Res Ther* **2015,** *6*, 10.

32. Li, T.; Yan, Y.; Wang, B.; Qian, H.; Zhang, X.; Shen, L.; Wang, M.; Zhou, Y.; Zhu, W.; Li, W.; Xu, W., Exosomes derived from human umbilical cord mesenchymal stem cells alleviate liver fibrosis. *Stem Cells Dev* **2013,** *22* (6), 845-54.

33. Tan, C. Y.; Lai, R. C.; Wong, W.; Dan, Y. Y.; Lim, S. K.; Ho, H. K., Mesenchymal stem cell-derived exosomes promote hepatic regeneration in drug-induced liver injury models. *Stem Cell Res Ther* **2014,** *5* (3), 76.

34. Lee, C.; Mitsialis, S. A.; Aslam, M.; Vitali, S. H.; Vergadi, E.; Konstantinou, G.; Sdrimas, K.; Fernandez-Gonzalez, A.; Kourembanas, S., Exosomes mediate the cytoprotective action of mesenchymal stromal cells on hypoxia-induced pulmonary hypertension. *Circulation* **2012,** *126* (22), 2601-11.

35. Zhu, Y. G.; Feng, X. M.; Abbott, J.; Fang, X. H.; Hao, Q.; Monsel, A.; Qu, J. M.; Matthay, M. A.; Lee, J. W., Human mesenchymal stem cell microvesicles for treatment of Escherichia coli endotoxin-induced acute lung injury in mice. *Stem Cells* **2014,** *32* (1), 116-25.

36. Nakamura, Y.; Miyaki, S.; Ishitobi, H.; Matsuyama, S.; Nakasa, T.; Kamei, N.; Akimoto, T.; Higashi, Y.; Ochi, M., Mesenchymal-stem-cell-derived exosomes accelerate skeletal muscle regeneration. *FEBS Lett* **2015,** *589* (11), 1257-65.

37. Cosenza, S.; Toupet, K.; Maumus, M.; Luz-Crawford, P.; Blanc-Brude, O.;

Jorgensen, C.; Noel, D., Mesenchymal stem cells-derived exosomes are more immunosuppressive than microparticles in inflammatory arthritis. *Theranostics* **2018,** *8* (5), 1399-1410.

38. Cosenza, S.; Ruiz, M.; Toupet, K.; Jorgensen, C.; Noel, D., Mesenchymal stem cells derived exosomes and microparticles protect cartilage and bone from degradation in osteoarthritis. *Sci Rep* **2017,** *7* (1), 16214.

39. Lankford, K. L.; Arroyo, E. J.; Nazimek, K.; Bryniarski, K.; Askenase, P. W.; Kocsis, J. D., Intravenously delivered mesenchymal stem cell-derived exosomes target M2-type macrophages in the injured spinal cord. *PLoS One* **2018,** *13* (1), e0190358.

40. Li, D.; Zhang, P.; Yao, X.; Li, H.; Shen, H.; Li, X.; Wu, J.; Lu, X., Exosomes Derived From miR-133b-Modified Mesenchymal Stem Cells Promote Recovery After Spinal Cord Injury. *Front Neurosci* **2018,** *12*, 845.

41. Xin, H.; Li, Y.; Cui, Y.; Yang, J. J.; Zhang, Z. G.; Chopp, M., Systemic administration of exosomes released from mesenchymal stromal cells promote functional recovery and neurovascular plasticity after stroke in rats. *J Cereb Blood Flow Metab* **2013,** *33* (11), 1711-5.

42. Otero-Ortega, L.; Laso-Garcia, F.; Gomez-de Frutos, M. D.; Rodriguez-Frutos, B.; Pascual-Guerra, J.; Fuentes, B.; Diez-Tejedor, E.; Gutierrez-Fernandez, M., White Matter Repair After Extracellular Vesicles Administration in an Experimental Animal Model of Subcortical Stroke. *Sci Rep* **2017,** *7*, 44433.

43. Xin, H.; Wang, F.; Li, Y.; Lu, Q. E.; Cheung, W. L.; Zhang, Y.; Zhang, Z. G.; Chopp, M., Secondary Release of Exosomes From Astrocytes Contributes to the Increase in Neural Plasticity and Improvement of Functional Recovery After Stroke in Rats Treated With Exosomes Harvested From MicroRNA 133b-Overexpressing Multipotent Mesenchymal Stromal Cells. *Cell Transplant* **2017,** *26* (2), 243-257.

44. Zhang, Y.; Chopp, M.; Zhang, Z. G.; Katakowski, M.; Xin, H.; Qu, C.; Ali, M.; Mahmood, A.; Xiong, Y., Systemic administration of cell-free exosomes generated by human bone marrow derived mesenchymal stem cells cultured under 2D and 3D conditions improves functional recovery in rats after traumatic brain injury. *Neurochem Int* **2017,** *111*, 69-81.

45. Zhang, Y.; Chopp, M.; Meng, Y.; Katakowski, M.; Xin, H.; Mahmood, A.; Xiong, Y., Effect of exosomes derived from multipluripotent mesenchymal stromal cells on functional recovery and neurovascular plasticity in rats after traumatic brain injury. *J Neurosurg* **2015,** *122* (4), 856-67.

46. de Godoy, M. A.; Saraiva, L. M.; de Carvalho, L. R. P.; Vasconcelos-Dos-Santos, A.; Beiral, H. J. V.; Ramos, A. B.; Silva, L. R. P.; Leal, R. B.; Monteiro, V. H. S.; Braga, C. V.; de Araujo-Silva, C. A.; Sinis, L. C.; Bodart-Santos, V.; Kasai-Brunswick, T. H.; Alcantara, C. L.; Lima, A.; da Cunha, E. S. N. L.; Galina, A.; Vieyra, A.; De Felice, F. G.; Mendez-Otero, R.; Ferreira, S. T., Mesenchymal stem cells and cell-derived extracellular vesicles protect hippocampal neurons from oxidative stress and synapse damage induced by amyloid-beta oligomers. *J Biol Chem* **2018,** *293* (6), 1957-1975.

47. Reza-Zaldivar, E. E.; Hernandez-Sapiens, M. A.; Minjarez, B.; Gutierrez-Mercado, Y. K.; Marquez-Aguirre, A. L.; Canales-Aguirre, A. A., Potential Effects of MSC-Derived Exosomes in Neuroplasticity in Alzheimer's Disease. *Front Cell Neurosci* **2018,** *12*, 317.

48. Vilaca-Faria, H.; Salgado, A. J.; Teixeira, F. G., Mesenchymal Stem Cells-derived Exosomes: A New Possible Therapeutic Strategy for Parkinson's Disease? *Cells* **2019,** *8* (2).

49. van Dommelen, S. M.; Vader, P.; Lakhal, S.; Kooijmans, S. A. A.; van Solinge, W. W.; Wood, M. J. A.; Schiffelers, R. M., Microvesicles and exosomes: Opportunities for cell-derived membrane vesicles in drug delivery. *J Control Release* **2012,**

161 (2), 635-644.

50. Lakhal, S.; Wood, M. J. A., Exosome nanotechnology: An emerging paradigm shift in drug delivery Exploitation of exosome nanovesicles for systemic in vivo delivery of RNAi heralds new horizons for drug delivery across biological barriers. *Bioessays* **2011,** *33* (10), 737-741.

51. Katsuda, T.; Tsuchiya, R.; Kosaka, N.; Yoshioka, Y.; Takagaki, K.; Oki, K.; Takeshita, F.; Sakai, Y.; Kuroda, M.; Ochiya, T., Human adipose tissue-derived mesenchymal stem cells secrete functional neprilysin-bound exosomes. *Sci Rep* **2013,** *3*, 1197.

52. Jang, S. C.; Kim, O. Y.; Yoon, C. M.; Choi, D. S.; Roh, T. Y.; Park, J.; Nilsson, J.; Lotvall, J.; Kim, Y. K.; Gho, Y. S., Bioinspired exosome-mimetic nanovesicles for targeted delivery of chemotherapeutics to malignant tumors. *ACS Nano* **2013,** *7* (9), 7698-710.

53. Jo, W.; Kim, J.; Yoon, J.; Jeong, D.; Cho, S.; Jeong, H.; Yoon, Y. J.; Kim, S. C.; Gho, Y. S.; Park, J., Large-scale generation of cell-derived nanovesicles. *Nanoscale* **2014,** *6* (20), 12056-64.

54. Wu, J. Y.; Ji, A. L.; Wang, Z. X.; Qiang, G. H.; Qu, Z.; Wu, J. H.; Jiang, C. P., Exosome-Mimetic Nanovesicles from Hepatocytes promote hepatocyte proliferation in vitro and liver regeneration in vivo. *Sci Rep-Uk* **2018,** *8*.

55. Tao, S. C.; Rui, B. Y.; Wang, Q. Y.; Zhou, D.; Zhang, Y.; Guo, S. C., Extracellular vesicle-mimetic nanovesicles transport LncRNA-H19 as competing endogenous RNA for the treatment of diabetic wounds. *Drug Deliv* **2018,** *25* (1), 241-255.

56. Li, S. D.; Huang, L., Nanoparticles evading the reticuloendothelial system: role of the supported bilayer. *Biochim Biophys Acta* **2009,** *1788* (10), 2259-66.

57. Lu, C. W.; Hung, Y.; Hsiao, J. K.; Yao, M.; Chung, T. H.; Lin, Y. S.; Wu, S. H.; Hsu, S. C.; Liu, H. M.; Mou, C. Y.; Yang, C. S.; Huang, D. M.; Chen, Y. C.,

Bifunctional magnetic silica nanoparticles for highly efficient human stem cell labeling. *Nano Lett* **2007,** *7* (1), 149-54.

58. Shirvalilou, S.; Khoei, S.; Khoee, S.; Raoufi, N. J.; Karimi, M. R.; Shakeri-Zadeh, A., Development of a magnetic nano-graphene oxide carrier for improved glioma-targeted drug delivery and imaging: In vitro and in vivo evaluations. *Chem Biol Interact* **2018,** *295*, 97-108.

59. Cho, H. Y.; Lee, T.; Yoon, J.; Han, Z.; Rabie, H.; Lee, K. B.; Su, W. W.; Choi, J. W., Magnetic Oleosome as a Functional Lipophilic Drug Carrier for Cancer Therapy. *Acs Appl Mater Inter* **2018,** *10* (11), 9301-9309.

60. Wang, C.; Sun, X. Q.; Cheng, L.; Yin, S. N.; Yang, G. B.; Li, Y. G.; Liu, Z., Multifunctional Theranostic Red Blood Cells For Magnetic-Field-Enhanced in vivo Combination Therapy of Cancer. *Advanced Materials* **2014,** *26* (28), 4794-+.

61. Qi, H.; Liu, C.; Long, L.; Ren, Y.; Zhang, S.; Chang, X.; Qian, X.; Jia, H.; Zhao, J.; Sun, J.; Hou, X.; Yuan, X.; Kang, C., Blood Exosomes Endowed with Magnetic and Targeting Properties for Cancer Therapy. *ACS Nano* **2016,** *10* (3), 3323-33.

62. Chen, P. J.; Kang, Y. D.; Lin, C. H.; Chen, S. Y.; Hsieh, C. H.; Chen, Y. Y.; Chiang, C. W.; Lee, W.; Hsu, C. Y.; Liao, L. D.; Fan, C. T.; Li, M. L.; Shyu, W. C., Multitheragnostic Multi-GNRs Crystal-Seeded Magnetic Nanoseaurchin for Enhanced In Vivo Mesenchymal-Stem-Cell Homing, Multimodal Imaging, and Stroke Therapy. *Adv Mater* **2015,** *27* (41), 6488-95.

63. Boltznitulescu, G.; Wiltschke, C.; Holzinger, C.; Fellinger, A.; Scheiner, O.; Gessl, A.; Forster, O., Differentiation of Rat Bone-Marrow Cells into Macrophages under the Influence of Mouse L929 Cell Supernatant. *J. Leukoc. Biol.* **1987,** *41* (1), 83-91.

64. Kim, C. K.; Yang, X.-L.; Kim, Y.-J.; Choi, I.-Y.; Jeong, H.-G.; Park, H.-K.; Kim, D.; Kim, T. J.; Jang, H.; Ko, S.-B. J. B. r. i., Effect of long-term treatment with

fimasartan on transient focal ischemia in rat brain. **2015,** *2015*.

65. Longa, E. Z.; Weinstein, P. R.; Carlson, S.; Cummins, R. J. s., Reversible middle cerebral artery occlusion without craniectomy in rats. **1989,** *20* (1), 84-91.

66. Song, M.; Kim, Y.-J.; Kim, Y.-h.; Roh, J.; Kim, E.-C.; Lee, H. J.; Kim, S. U.; Yoon, B.-W. J. C. t., Long-term effects of magnetically targeted ferumoxide-labeled human neural stem cells in focal cerebral ischemia. **2015,** *24* (2), 183-190.

67. Song, M.; Kim, Y.-J.; Kim, Y.-h.; Roh, J.; Kim, S. U.; Yoon, B.-W. J. H. g. t., Using a neodymium magnet to target delivery of ferumoxide-labeled human neural stem cells in a rat model of focal cerebral ischemia. **2010,** *21* (5), 603-610.

68. De Ryck, M.; Van Reempts, J.; Borgers, M.; Wauquier, A.; Janssen, P. J. S., Photochemical stroke model: flunarizine prevents sensorimotor deficits after neocortical infarcts in rats. **1989,** *20* (10), 1383-1390.

69. Linero, I.; Chaparro, O., Paracrine effect of mesenchymal stem cells derived from human adipose tissue in bone regeneration. *PLoS One* **2014,** *9* (9), e107001.

70. Yao, Y.; Huang, J.; Geng, Y.; Qian, H.; Wang, F.; Liu, X.; Shang, M.; Nie, S.; Liu, N.; Du, X.; Dong, J.; Ma, C., Paracrine action of mesenchymal stem cells revealed by single cell gene profiling in infarcted murine hearts. *PLoS One* **2015,** *10* (6), e0129164.

71. Vizoso, F. J.; Eiro, N.; Cid, S.; Schneider, J.; Perez-Fernandez, R., Mesenchymal Stem Cell Secretome: Toward Cell-Free Therapeutic Strategies in Regenerative Medicine. *Int J Mol Sci* **2017,** *18* (9).

72. Han, C.; Sun, X.; Liu, L.; Jiang, H. Y.; Shen, Y.; Xu, X. Y.; Li, J.; Zhang, G. X.; Huang, J. S.; Lin, Z. C.; Xiong, N.; Wang, T., Exosomes and Their Therapeutic Potentials of Stem Cells. *Stem Cells International* **2016**.

73. Raposo, G.; Stoorvogel, W., Extracellular vesicles: exosomes, microvesicles, and

friends. *J Cell Biol* **2013,** *200* (4), 373-83.

74. Bang, C.; Thum, T., Exosomes: new players in cell-cell communication. *Int J Biochem Cell Biol* **2012,** *44* (11), 2060-4.

75. Yu, B.; Zhang, X.; Li, X., Exosomes derived from mesenchymal stem cells. *Int J Mol Sci* **2014,** *15* (3), 4142-57.

76. Katsuda, T.; Kosaka, N.; Takeshita, F.; Ochiya, T., The therapeutic potential of mesenchymal stem cell-derived extracellular vesicles. *Proteomics* **2013,** *13* (10-11), 1637-53.

77. Lener, T.; Gimona, M.; Aigner, L.; Borger, V.; Buzas, E.; Camussi, G.; Chaput, N.; Chatterjee, D.; Court, F. A.; Del Portillo, H. A.; O'Driscoll, L.; Fais, S.; Falcon-Perez, J. M.; Felderhoff-Mueser, U.; Fraile, L.; Gho, Y. S.; Gorgens, A.; Gupta, R. C.; Hendrix, A.; Hermann, D. M.; Hill, A. F.; Hochberg, F.; Horn, P. A.; de Kleijn, D.; Kordelas, L.; Kramer, B. W.; Kramer-Albers, E. M.; Laner-Plamberger, S.; Laitinen, S.; Leonardi, T.; Lorenowicz, M. J.; Lim, S. K.; Lotvall, J.; Maguire, C. A.; Marcilla, A.; Nazarenko, I.; Ochiya, T.; Patel, T.; Pedersen, S.; Pocsfalvi, G.; Pluchino, S.; Quesenberry, P.; Reischl, I. G.; Rivera, F. J.; Sanzenbacher, R.; Schallmoser, K.; Slaper-Cortenbach, I.; Strunk, D.; Tonn, T.; Vader, P.; van Balkom, B. W.; Wauben, M.; Andaloussi, S. E.; Thery, C.; Rohde, E.; Giebel, B., Applying extracellular vesicles based therapeutics in clinical trials - an ISEV position paper. *J Extracell Vesicles* **2015,** *4*, 30087.

78. Arslan, F.; Lai, R. C.; Smeets, M. B.; Akeroyd, L.; Choo, A.; Aguor, E. N.; Timmers, L.; van Rijen, H. V.; Doevendans, P. A.; Pasterkamp, G.; Lim, S. K.; de Kleijn, D. P., Mesenchymal stem cell-derived exosomes increase ATP levels, decrease oxidative stress and activate PI3K/Akt pathway to enhance myocardial viability and prevent adverse remodeling after myocardial ischemia/reperfusion injury. *Stem Cell Res* **2013,** *10* (3), 301-12.

79. Norenberg, M. D.; Smith, J.; Marcillo, A., The pathology of human spinal cord injury: defining the problems. *J Neurotrauma* **2004,** *21* (4), 429-40.

80. Oyinbo, C. A., Secondary injury mechanisms in traumatic spinal cord injury: a nugget of this multiply cascade. *Acta Neurobiol Exp (Wars)* **2011,** *71* (2), 281-99.

81. Dasari, V. R.; Veeravalli, K. K.; Dinh, D. H., Mesenchymal stem cells in the treatment of spinal cord injuries: A review. *World J Stem Cells* **2014,** *6* (2), 120-33.

82. Qu, J.; Zhang, H., Roles of Mesenchymal Stem Cells in Spinal Cord Injury. *Stem Cells Int* **2017,** *2017*, 5251313.

83. Willerth, S. M.; Sakiyama-Elbert, S. E., Cell therapy for spinal cord regeneration. *Adv Drug Deliv Rev* **2008,** *60* (2), 263-76.

84. Zhou, Z.; Chen, Y.; Zhang, H.; Min, S.; Yu, B.; He, B.; Jin, A., Comparison of mesenchymal stromal cells from human bone marrow and adipose tissue for the treatment of spinal cord injury. *Cytotherapy* **2013,** *15* (4), 434-48.

85. Tomasoni, S.; Longaretti, L.; Rota, C.; Morigi, M.; Conti, S.; Gotti, E.; Capelli, C.; Introna, M.; Remuzzi, G.; Benigni, A., Transfer of growth factor receptor mRNA via exosomes unravels the regenerative effect of mesenchymal stem cells. *Stem Cells Dev* **2013,** *22* (5), 772-80.

86. Anderson, J. D.; Johansson, H. J.; Graham, C. S.; Vesterlund, M.; Pham, M. T.; Bramlett, C. S.; Montgomery, E. N.; Mellema, M. S.; Bardini, R. L.; Contreras, Z.; Hoon, M.; Bauer, G.; Fink, K. D.; Fury, B.; Hendrix, K. J.; Chedin, F.; El-Andaloussi, S.; Hwang, B.; Mulligan, M. S.; Lehtio, J.; Nolta, J. A., Comprehensive Proteomic Analysis of Mesenchymal Stem Cell Exosomes Reveals Modulation of Angiogenesis via Nuclear Factor-KappaB Signaling. *Stem Cells* **2016,** *34* (3), 601-13.

87. Ragni, E.; Banfi, F.; Barilani, M.; Cherubini, A.; Parazzi, V.; Larghi, P.; Dolo, V.; Bollati, V.; Lazzari, L., Extracellular Vesicle-Shuttled mRNA in Mesenchymal

Stem Cell Communication. *Stem Cells* **2017,** *35* (4), 1093-1105.

88. Bai, L.; Shao, H.; Wang, H.; Zhang, Z.; Su, C.; Dong, L.; Yu, B.; Chen, X.; Li, X.; Zhang, X., Effects of Mesenchymal Stem Cell-Derived Exosomes on Experimental Autoimmune Uveitis. *Sci Rep* **2017,** *7* (1), 4323.

89. Yu, B.; Shao, H.; Su, C.; Jiang, Y.; Chen, X.; Bai, L.; Zhang, Y.; Li, Q.; Zhang, X.; Li, X., Exosomes derived from MSCs ameliorate retinal laser injury partially by inhibition of MCP-1. *Sci Rep* **2016,** *6*, 34562.

90. Luarte, A.; Batiz, L. F.; Wyneken, U.; Lafourcade, C., Potential Therapies by Stem Cell-Derived Exosomes in CNS Diseases: Focusing on the Neurogenic Niche. *Stem Cells Int* **2016,** *2016*, 5736059.

91. Yang, Y.; Ye, Y.; Su, X.; He, J.; Bai, W.; He, X., MSCs-Derived Exosomes and Neuroinflammation, Neurogenesis and Therapy of Traumatic Brain Injury. *Front Cell Neurosci* **2017,** *11*, 55.

92. Huang, J. H.; Yin, X. M.; Xu, Y.; Xu, C. C.; Lin, X.; Ye, F. B.; Cao, Y.; Lin, F. Y., Systemic Administration of Exosomes Released from Mesenchymal Stromal Cells Attenuates Apoptosis, Inflammation, and Promotes Angiogenesis after Spinal Cord Injury in Rats. *J Neurotrauma* **2017**.

93. Mastri, M.; Lin, H.; Lee, T., Enhancing the efficacy of mesenchymal stem cell therapy. *World J Stem Cells* **2014,** *6* (2), 82-93.

94. Wiklander, O. P.; Nordin, J. Z.; O'Loughlin, A.; Gustafsson, Y.; Corso, G.; Mager, I.; Vader, P.; Lee, Y.; Sork, H.; Seow, Y.; Heldring, N.; Alvarez-Erviti, L.; Smith, C. I.; Le Blanc, K.; Macchiarini, P.; Jungebluth, P.; Wood, M. J.; Andaloussi, S. E., Extracellular vesicle in vivo biodistribution is determined by cell source, route of administration and targeting. *J Extracell Vesicles* **2015,** *4*, 26316.

95. Hwang, D. W.; Choi, H.; Jang, S. C.; Yoo, M. Y.; Park, J. Y.; Choi, N. E.;

Oh, H. J.; Ha, S.; Lee, Y. S.; Jeong, J. M.; Gho, Y. S.; Lee, D. S., Noninvasive imaging of radiolabeled exosome-mimetic nanovesicle using Tc-99m-HMPAO. *Sci Rep-Uk* **2015,** *5*.

96. Lai, C. P.; Mardini, O.; Ericsson, M.; Prabhakar, S.; Maguire, C.; Chen, J. W.; Tannous, B. A.; Breakefield, X. O., Dynamic biodistribution of extracellular vesicles in vivo using a multimodal imaging reporter. *ACS Nano* **2014,** *8* (1), 483-494.

97. Ruiz, A.; Gutierrez, L.; Caceres-Velez, P. R.; Santos, D.; Chaves, S. B.; Fascineli, M. L.; Garcia, M. P.; Azevedo, R. B.; Morales, M. P., Biotransformation of magnetic nanoparticles as a function of coating in a rat model. *Nanoscale* **2015,** *7* (39), 16321-16329.

98. Kolosnjaj-Tabi, J.; Lartigue, L.; Javed, Y.; Luciani, N.; Pellegrino, T.; Wilhelm, C.; Alloyeau, D.; Gazeau, F., Biotransformations of magnetic nanoparticles in the body. *Nano Today* **2016,** *11* (3), 280-284.

99. Lee, N.; Hyeon, T., Designed synthesis of uniformly sized iron oxide nanoparticles for efficient magnetic resonance imaging contrast agents. *Chem Soc Rev* **2012,** *41* (7), 2575-2589.

100. Zhang, S. L.; Gao, H. J.; Bao, G., Physical Principles of Nanoparticle Cellular Endocytosis. *Acs Nano* **2015,** *9* (9), 8655-8671.

101. Han, J.; Kim, B.; Shin, J. Y.; Ryu, S.; Noh, M.; Woo, J.; Park, J. S.; Lee, Y.; Lee, N.; Hyeon, T.; Choi, D.; Kim, B. S., Iron oxide nanoparticle-mediated development of cellular gap junction crosstalk to improve mesenchymal stem cells' therapeutic efficacy for myocardial infarction. *ACS Nano* **2015,** *9* (3), 2805-19.

102. Vleugel, M. M.; Greijer, A. E.; Bos, R.; van der Wall, E.; van Diest, P. J., c-Jun activation is associated with proliferation and angiogenesis in invasive breast cancer. *Hum Pathol* **2006,** *37* (6), 668-74.

103. Folkman, J., Angiogenesis and c-Jun. *JNCI Journal of the National Cancer Institute* **2004,** *96* (9), 644-644.

104. Zhang, E.; Feng, X.; Liu, F.; Zhang, P.; Liang, J.; Tang, X., Roles of PI3K/Akt and c-Jun signaling pathways in human papillomavirus type 16 oncoprotein-induced HIF-1alpha, VEGF, and IL-8 expression and in vitro angiogenesis in non-small cell lung cancer cells. *PLoS One* **2014,** *9* (7), e103440.

105. Shen, C. Y.; Lie, P. C.; Miao, T. Y.; Yu, M. X.; Lu, Q.; Feng, T.; Li, J. R.; Zu, T. T.; Liu, X. H.; Li, H., Conditioned medium from umbilical cord mesenchymal stem cells induces migration and angiogenesis. *Molecular Medicine Reports* **2015,** *12* (1), 20-30.

106. Li, S. Y.; Qi, Y.; Hu, S. H.; Piao, F. Y.; Guan, H.; Wang, Z. M.; Chen, R. L.; Liu, S., Mesenchymal stem cells-conditioned medium protects PC12 cells against 2,5-hexanedione-induced apoptosis via inhibiting mitochondria-dependent caspase 3 pathway. *Toxicol Ind Health* **2017,** *33* (2), 107-118.

107. Kim, Y. J.; Park, H. J.; Lee, G.; Bang, O. Y.; Ahn, Y. H.; Joe, E.; Kim, H. O.; Lee, P. H., Neuroprotective Effects of Human Mesenchymal Stem Cells on Dopaminergic Neurons Through Anti-Inflammatory Action. *Glia* **2009,** *57* (1), 13-23.

108. Nor, J. E.; Christensen, J.; Mooney, D. J.; Polverini, P. J., Vascular endothelial growth factor (VEGF)-mediated angiogenesis is associated with enhanced endothelial cell survival and induction of Bcl-2 expression. *Am J Pathol* **1999,** *154* (2), 375-384.

109. Hemalatha, T.; Tiwari, M.; Balachandran, C.; Manohar, B. M.; Puvanakrishnan, R., Platelet-derived endothelial cell growth factor mediates angiogenesis and antiapoptosis in rat aortic endothelial cells. *Biochem Cell Biol* **2009,** *87* (6), 883-893.

110. Shabbir, A.; Cox, A.; Rodriguez-Menocal, L.; Salgado, M.; Van Badiavas, E., Mesenchymal Stem Cell Exosomes Induce Proliferation and Migration of Normal and Chronic Wound Fibroblasts, and Enhance Angiogenesis In Vitro. *Stem Cells and*

Development **2015,** *24* (14), 1635-1647.

111. Barreto, G.; White, R. E.; Ouyang, Y.; Xu, L.; Giffard, R. G., Astrocytes: targets for neuroprotection in stroke. *Cent Nerv Syst Agents Med Chem* **2011,** *11* (2), 164-73.

112. Becerra-Calixto, A.; Cardona-Gomez, G. P., The Role of Astrocytes in Neuroprotection after Brain Stroke: Potential in Cell Therapy. *Front Mol Neurosci* **2017,** *10*.

113. Gao, Q.; Li, Y.; Chopp, M., Bone marrow stromal cells increase astrocyte survival via upregulation of phosphoinositide 3-kinase/threonine protein kinase and mitogen-activated protein kinase kinase/extracellular signal-regulated kinase pathways and stimulate astrocyte trophic factor gene expression after anaerobic insult. *Neuroscience* **2005,** *136* (1), 123-34.

114. Kong, X.; Gao, J., Macrophage polarization: a key event in the secondary phase of acute spinal cord injury. *J Cell Mol Med* **2017,** *21* (5), 941-954.

115. Kigerl, K. A.; Gensel, J. C.; Ankeny, D. P.; Alexander, J. K.; Donnelly, D. J.; Popovich, P. G., Identification of two distinct macrophage subsets with divergent effects causing either neurotoxicity or regeneration in the injured mouse spinal cord. *J Neurosci* **2009,** *29* (43), 13435-44.

116. Cho, D. I.; Kim, M. R.; Jeong, H. Y.; Jeong, H. C.; Jeong, M. H.; Yoon, S. H.; Kim, Y. S.; Ahn, Y., Mesenchymal stem cells reciprocally regulate the M1/M2 balance in mouse bone marrow-derived macrophages. *Exp Mol Med* **2014,** *46*, e70.

117. He, Z. S.; Zhang, H.; Yang, C. X.; Zhou, Y. J.; Zhou, Y.; Han, G.; Xia, L.; Wen, O. Y.; Zhou, F. X.; Zhou, Y. F.; Xie, C. H., The interaction between different types of activated RAW 264.7 cells and macrophage inflammatory protein-1 alpha. *Radiat Oncol* **2011,** *6*.

118. Jetten, N.; Verbruggen, S.; Gijbels, M. J.; Post, M. J.; De Winther, M. P.; Donners, M. M., Anti-inflammatory M2, but not pro-inflammatory M1 macrophages promote angiogenesis in vivo. *Angiogenesis* **2014,** *17* (1), 109-18.

119. Gensel, J. C.; Zhang, B., Macrophage activation and its role in repair and pathology after spinal cord injury. *Brain Research* **2015,** *1619*, 1-11.

120. Zhang, F.; Wang, H.; Wang, X.; Jiang, G.; Liu, H.; Zhang, G.; Wang, H.; Fang, R.; Bu, X.; Cai, S.; Du, J., TGF-beta induces M2-like macrophage polarization via SNAIL-mediated suppression of a pro-inflammatory phenotype. *Oncotarget* **2016,** *7* (32), 52294-52306.

121. Gong, D.; Shi, W.; Yi, S. J.; Chen, H.; Groffen, J.; Heisterkamp, N., TGFbeta signaling plays a critical role in promoting alternative macrophage activation. *BMC Immunol* **2012,** *13*, 31.

122. Walczak, P.; Zhang, J.; Gilad, A. A.; Kedziorek, D. A.; Ruiz-Cabello, J.; Young, R. G.; Pittenger, M. F.; Van Zijl, P. C. M.; Huang, J.; Bulte, J. W. M., Dual-modality monitoring of targeted intraarterial delivery of mesenchymal stem cells after transient ischemia. *Stroke* **2008,** *39* (5), 1569-1574.

123. Boltze, J.; Arnold, A.; Walczak, P.; Jolkkonen, J.; Cui, L.; Wagner, D. C., The Dark Side of the Force - Constraints and Complications of Cell Therapies for Stroke. *Front Neurol* **2015,** *6*, 155.

124. Lee, R. H.; Pulin, A. A.; Seo, M. J.; Kota, D. J.; Ylostalo, J.; Larson, B. L.; Semprun-Prieto, L.; Delafontaine, P.; Prockop, D. J., Intravenous hMSCs improve myocardial infarction in mice because cells embolized in lung are activated to secrete the anti-inflammatory protein TSG-6. *Cell Stem Cell* **2009,** *5* (1), 54-63.

125. Kundi, S.; Bicknell, R.; Ahmed, Z., The role of angiogenic and wound-healing factors after spinal cord injury in mammals. *Neurosci Res* **2013,** *76* (1-2), 1-9.

126. Widenfalk, J.; Lipson, A.; Jubran, M.; Hofstetter, C.; Ebendal, T.; Cao, Y.; Olson, L., Vascular endothelial growth factor improves functional outcome and decreases secondary degeneration in experimental spinal cord contusion injury. *Neuroscience* **2003,** *120*

(4), 951-60.

127. Park, H. W.; Jeon, H. J.; Chang, M. S., Vascular endothelial growth factor enhances axonal outgrowth in organotypic spinal cord slices via vascular endothelial growth factor receptor 1 and 2. *Tissue Eng Regen Med* **2016,** *13* (5), 601-609.

128. Lee, H. S.; Han, J.; Bai, H. J.; Kim, K. W., Brain angiogenesis in developmental and pathological processes: regulation, molecular and cellular communication at the neurovascular interface. *The FEBS journal* **2009,** *276* (17), 4622-35.

129. Han, S.; Arnold, S. A.; Sithu, S. D.; Mahoney, E. T.; Geralds, J. T.; Tran, P.; Benton, R. L.; Maddie, M. A.; D'Souza, S. E.; Whittemore, S. R.; Hagg, T., Rescuing vasculature with intravenous angiopoietin-1 and alpha v beta 3 integrin peptide is protective after spinal cord injury. *Brain : a journal of neurology* **2010,** *133* (Pt 4), 1026-42.

130. Herrera, J. J.; Sundberg, L. M.; Zentilin, L.; Giacca, M.; Narayana, P. A., Sustained expression of vascular endothelial growth factor and angiopoietin-1 improves blood-spinal cord barrier integrity and functional recovery after spinal cord injury. *J Neurotrauma* **2010,** *27* (11), 2067-76.

131. Gensel, J. C.; Kopper, T. J.; Zhang, B.; Orr, M. B.; Bailey, W. M., Predictive screening of M1 and M2 macrophages reveals the immunomodulatory effectiveness of post spinal cord injury azithromycin treatment. *Sci Rep-Uk* **2017,** *7*.

132. Okada, S.; Hara, M.; Kobayakawa, K.; Matsumoto, Y.; Nakashima, Y., Astrocyte reactivity and astrogliosis after spinal cord injury. *Neurosci Res* **2017**.

133. Zhao, Y. Y.; Yuan, Y.; Chen, Y.; Jiang, L.; Liao, R. J.; Wang, L.; Zhang, X. N.; Ohtsu, H.; Hu, W. W.; Chen, Z., Histamine Promotes Locomotion Recovery After Spinal Cord Hemisection via Inhibiting Astrocytic Scar Formation. *Cns Neurosci Ther* **2015,** *21* (5), 454-462.

134. Zhu, Y.; Soderblom, C.; Trojanowsky, M.; Lee, D. H.; Lee, J. K., Fibronectin

Matrix Assembly after Spinal Cord Injury. *J Neurotrauma* **2015,** *32* (15), 1158-67.

135. Wang, Q. Q.; He, Y.; Zhao, Y. Z.; Xie, H. X.; Lin, Q.; He, Z. L.; Wang, X. Y.; Li, J. W.; Zhang, H. Y.; Wang, C. G.; Gong, F. H.; Li, X. K.; Xu, H. Z.; Ye, Q. S.; Xiao, J., A Thermosensitive Heparin-Poloxamer Hydrogel Bridges aFGF to Treat Spinal Cord Injury. *Acs Appl Mater Inter* **2017,** *9* (8), 6725-6745.

136. Jeong, S. R.; Kwon, M. J.; Lee, H. G.; Joe, E. H.; Lee, J. H.; Kim, S. S.; Suh-Kim, H.; Kim, B. G., Hepatocyte growth factor reduces astrocytic scar formation and promotes axonal growth beyond glial scars after spinal cord injury. *Exp Neurol* **2012,** *233* (1), 312-22.

137. Hamby, M. E.; Sofroniew, M. V., Reactive Astrocytes As Therapeutic Targets for CNS Disorders. *Neurotherapeutics* **2010,** *7* (4), 494-506.

138. Chen, L. K.; Zhang, G. L.; Khan, A. A.; Guo, X. Y.; Gu, Y. C., Clinical Efficacy and Meta-Analysis of Stem Cell Therapies for Patients with Brain Ischemia. *Stem Cells Int* **2016**.

139. Moustafa, R. R.; Baron, J. C., Pathophysiology of ischaemic stroke: insights from imaging, and implications for therapy and drug discovery. *Brit J Pharmacol* **2008,** *153*, S44-S54.

140. Jin, R.; Yang, G. J.; Li, G. H., Inflammatory mechanisms in ischemic stroke: role of inflammatory cells. *J Leukocyte Biol* **2010,** *87* (5), 779-789.

141. Iadecola, C.; Anrather, J., The immunology of stroke: from mechanisms to translation. *Nat Med* **2011,** *17* (7), 796-808.

142. Becher, B.; Spath, S.; Goverman, J., Cytokine networks in neuroinflammation. *Nat Rev Immunol* **2017,** *17* (1), 49-59.

143. Li, G. H.; Yu, F. B.; Lei, T.; Gao, H. J.; Li, P. W.; Sun, Y. X.; Huang, H. Y.; Mu, Q. C., Bone marrow mesenchymal stem cell therapy in ischemic stroke: mechanisms of

action and treatment optimization strategies. *Neural Regen Res* **2016,** *11* (6), 1015-1024.

144. Bang, O. Y.; Kim, E. H.; Cha, J. M.; Moon, G. J., Adult Stem Cell Therapy for Stroke: Challenges and Progress. *J Stroke* **2016,** *18* (3), 256-266.

145. Trounson, A.; McDonald, C., Stem Cell Therapies in Clinical Trials: Progress and Challenges. *Cell Stem Cell* **2015,** *17* (1), 11-22.

146. Wang, S.; Qu, X.; Zhao, R. C., Clinical applications of mesenchymal stem cells. *J Hematol Oncol* **2012,** *5*, 19.

147. Zhang, T.; Lee, Y. W.; Rui, Y. F.; Cheng, T. Y.; Li, G., Bone Marrow-Derived Mesenchymal Stem Cells Promote Angiogenesis and Growth of Breast and Prostate Tumors. *Cytotherapy* **2013,** *15* (4), S15-S15.

148. Gu, Y.; Zhang, Y.; Bi, Y.; Liu, J. J.; Tan, B.; Gong, M.; Li, T. Y.; Chen, J., Mesenchymal stem cells suppress neuronal apoptosis and decrease IL-10 release via the TLR2/NF kappa B pathway in rats with hypoxic-ischemic brain damage. *Mol Brain* **2015,** *8*.

149. Zhang, R.; Liu, Y.; Yan, K.; Chen, L.; Chen, X. R.; Li, P.; Chen, F. F.; Jiang, X. D., Anti-inflammatory and immunomodulatory mechanisms of mesenchymal stem cell transplantation in experimental traumatic brain injury. *J Neuroinflamm* **2013,** *10*.

150. Shyu, W. C.; Lin, S. Z.; Chiang, M. F.; Su, C. Y.; Li, H., Intracerebral peripheral blood stem cell (CD34(+)) implantation induces neuroplasticity by enhancing beta 1 integrin-mediated angiogenesis in chronic stroke rats. *J Neurosci* **2006,** *26* (13), 3444-3453.

151. Eggenhofer, E.; Luk, F.; Dahlke, M. H.; Hoogduijn, M. J., The life and fate of mesenchymal stem cells. *Front Immunol* **2014,** *5*, 148.

152. Manuel, G. E.; Johnson, T.; Liu, D., Therapeutic angiogenesis of exosomes for ischemic stroke. *Int J Physiol Pathophysiol Pharmacol* **2017,** *9* (6), 188-191.

153. Correction to: MicroRNA-17-92 Cluster in Exosomes Enhance Neuroplasticity and Functional Recovery After Stroke in Rats. *Stroke* **2017,** *48* (5), e137.

154. Tian, T.; Zhang, H. X.; He, C. P.; Fan, S.; Zhu, Y. L.; Qi, C.; Huang, N. P.; Xiao, Z. D.; Lu, Z. H.; Tannous, B. A.; Gao, J., Surface functionalized exosomes as targeted drug delivery vehicles for cerebral ischemia therapy. *Biomaterials* **2018,** *150*, 137-149.

155. Shi, L.; Chang, Y.; Yang, Y.; Zhang, Y.; Yu, F. S.; Wu, X., Activation of JNK signaling mediates connective tissue growth factor expression and scar formation in corneal wound healing. *PLoS One* **2012,** *7* (2), e32128.

156. Saito, M.; Hamasaki, M.; Shibuya, M., Induction of tube formation by angiopoietin-1 in endothelial cell/fibroblast co-culture is dependent on endogenous VEGF. *Cancer Sci* **2003,** *94* (9), 782-90.

157. Wang, Q.; Tang, X. N.; Yenari, M. A., The inflammatory response in stroke. *J Neuroimmunol* **2007,** *184* (1-2), 53-68.

158. Dholakiya, S. L.; Benzeroual, K. E., Protective effect of diosmin on LPS-induced apoptosis in PC12 cells and inhibition of TNF-alpha expression. *Toxicol In Vitro* **2011,** *25* (5), 1039-44.

159. He, M.; Sun, H.; Pang, J.; Guo, X.; Huo, Y.; Wu, X.; Liu, Y.; Ma, J., Propofol alleviates hypoxia-induced nerve injury in PC-12 cells by up-regulation of microRNA-153. *BMC Anesthesiol* **2018,** *18* (1), 197.

160. Martinez, F. O.; Gordon, S., The M1 and M2 paradigm of macrophage activation: time for reassessment. *F1000Prime Rep* **2014,** *6*, 13.

161. Hu, X.; Li, P.; Guo, Y.; Wang, H.; Leak, R. K.; Chen, S.; Gao, Y.; Chen, J., Microglia/macrophage polarization dynamics reveal novel mechanism of injury expansion after focal cerebral ischemia. *Stroke* **2012,** *43* (11), 3063-70.

162. Zheng, Y.; He, R.; Wang, P.; Shi, Y.; Zhao, L.; Liang, J., Exosomes from LPS-stimulated macrophages induce neuroprotection and functional improvement after ischemic

stroke by modulating microglial polarization. *Biomater Sci* **2019,** *7* (5), 2037-2049.

163. Hilger, I.; Kaiser, W. A., Iron oxide-based nanostructures for MRI and magnetic hyperthermia. *Nanomedicine (Lond)* **2012,** *7* (9), 1443-59.

요약 (국문 초록)

뇌졸중, 뇌출혈, 외상성 뇌 손상, 그리고 척수 손상과 같은 중추신경계 손상 질환은 장기적인 신체 장애, 더 나아가 죽음까지 이르게 하는 원인이다. 새로운 조직 재생 치료 전략으로서, 중간엽줄기세포 유래 엑소좀을 이용한 중추신경계 손상 치료는 최근 각광을 받고 있다. 중간엽줄기세포 유래 엑소좀은 그 만의 독특한 성질 때문에 중추 신경계 손상을 비롯한 다양한 질병에서 활발히 연구되어 왔다. 그러나 중추신경계 손상 치료를 위해 엑소좀을 사용하는 방식에는 여전히 한계가 남아 있다. 극소량의 엑소좀만이 중간엽줄기세포에서 분비되며, 엑소좀을 전신 주사 (정맥 주사) 하여도 표적 조직에 잘 도달하지 않는다. 따라서 본 주제에서는 산화철 나노입자를 중간엽줄기세포에 처리하였고 해당 세포로부터 엑소좀-모방 나노베지클을 분리하였다. 산화철 나노입자는 중간엽 줄기세포 내에서 철 이온으로 이온화 되며, 해당 이온들은 세포의 JNK/c-JUN 세포 신호전달 체계를 자극하여 다양한 성장 인자의 발현을 촉진시킨다. 따라서 해당 세포로부터 분리한 나노베지클은 자성을 띄는 산화철 나노입자 뿐만 아니라 고용량의 성장 인자가 탑재되어 있다. 본 연구에서는,

산화철 나노입자가 탑재된 나노베지클을 중추 신경계 병변으로 체내 전달하였고 그에 따른 치료효과를 제시한다.

먼저, 제 3 장에서는 철나노입자가 처리된 중간엽줄기세포에서 철나노입자가 탑재된 철-나노베지클을 분리하였고, 이를 마우스 척수손상 모델에 전신 주사하여 외부 자장의 도움으로 손상된 척수에 전달되었다. 철나노입자가 처리된 중간엽줄기세포는 세포 자체의 큰 직경 때문에 대부분 폐에 걸렸지만, 나노미터 크기의 철-나노베지클은 폐 모세혈관을 통과하여 자기장이 있는 상태에서 손상된 척수에 상당 부분 축적되었다. 척수 병변에 축적 된 철-나노베시클은 혈관 재건에 기여하였고, 염증성 대식세포를 항염증성 아형으로 분화시켰으며, 성상교세포증을 감쇠하고 신경 세포 사멸을 억제 하였다. 결과적으로 동물 행동 검사에 의해 평가 된 바와 같이, 손상된 척수에 축적된 철-나노베지클은 치료 효과를 발휘하였고 척수 기능을 개선시켰다.

제 4 장에서는 중간엽줄기세포에서 유래하였고 철나노입자가 함유 된 자성 철-나노베지클을 랫드 허혈성 뇌졸중 모델에 정맥 주사 하였다. 동물 모델은 과도 중간 대뇌 동맥 폐색 수술을 통해 허혈성 뇌졸중을 유발했다. 세포 실험을 통해, 철-나노베지클은 대조군 나노베지클과 비교하여 다양한 유형의 세포에서 증진된 혈관 생성 효과, 세포 사멸 억제 효과, 그리고 항염증 효과를 나타내었다. 동물 실험에서는, 철-나노베지클의 정맥 주사 직후에 외부 자기장으로 작용하는 자석 헬멧을 동물 모델에 씌웠다. 그리고 동물 형광 촬영을 통해 좌뇌 반구 (뇌졸중 병변)에 철-나노베지클이 축적됨을 관찰하였다. 주사 후 3 일째에 경색 부위 크기를 정량화 한 결과, 외부 자기장 존재 아래 철-나노베지클을 투여 한 실험군에서 경색 부위가 대조군에 비하여 현저하게

감소되었다. 또한, 동물 행동 실험을 통하여 철-나노베지클 (자기장 O) 의 주입 및 치료가 동물 모델의 운동 기능을 향상 시킨다는 것을 입증하였다.

따라서 본 연구에서는 산화철 나노입자가 처리된 중간엽줄기세포로부터 분리한 나노베지클은 고용량의 성장 인자뿐만 자석 항법 도구로 쓰일 수 있는 산화철 나노입자를 함유하며, 외부 자기장을 통해 손상된 척수 또는 대뇌 병변에 표적 전달되는 것을 확인했다. 이러한 철-나노베지클은 중추신경계 손상 치료를 위한 우수한 치료제로서 활용될 수 있으며, 통상적인 중간엽줄기세포 기반 또는 중간엽줄기세포 유래 엑소좀 기반의 치료 기법을 대체할 수 있다. 본 연구의 기술은 미래에 중추신경계 손상의 성공적인 치료를 위해 사용 될 수 있을 것이다.

주요어: 중간엽줄기세포, 엑소좀, 나노베지클, 산화철 나노입자, 척수 손상, 뇌졸중, 중추신경계 손상

학번: 2015-31024